25

NASA CONTRACTOR REPORT

NASA CR-66659

NASA CR-66659

GPO PRICE $ ______

CFSTI PRICE(S) $ ______

Hard copy (HC) 3-00

Microfiche (MF) .65

ff 653 July 65

FACILITY FORM 602

N68-31831	
(ACCESSION NUMBER)	(THRU)
85	1
(PAGES)	(CODE)
CR-66659	30
(NASA CR OR TMX OR AD NUMBER)	(CATEGORY)

FINAL REPORT

STUDY OF DIRECT VERSUS ORBITAL ENTRY FOR MARS MISSIONS

Volume I - Summary

AUG 1968
RECEIVED
NASA STI FACILITY
INPUT BRANCH

Prepared by

MARTIN MARIETTA CORPORATION
DENVER, COLORADO

for

Langley Research Center

NATIONAL AERONATUICS AND SPACE ADMINISTRATION • WASHINGTON, D.C. • AUGUST 1968

NASA CR-66659

FINAL REPORT

STUDY OF DIRECT VERSUS ORBITAL ENTRY FOR MARS MISSIONS

VOLUME I: SUMMARY

By Raymond S. Wiltshire and Hugh E. Craig

Distribution of this report is provided in the interest of information exchange. Responsibility for the contents resides in the author or organization that prepared it.

Prepared under Contract No. NAS1-7976 by
MARTIN MARIETTA CORPORATION
Denver, Colorado

for

NATIONAL AERONATUTICS AND SPACE ADMINISTRATION

FOREWORD

This Final Report for the "Study of Direct Versus Orbital Entry for Mars Missions" (NASA Contract NAS1-7976) is provided in accordance with Part III A.4 of the contract schedule as amended. The report is in six volumes as follows:

NASA CR-66659 - Volume I - Summary;

NASA CR-66660 - Volume II - Parametric Studies, Final Analyses, and Conceptual Designs;

NASA CR-66661 - Volume III - Appendix A - Launch Vehicle Performance and Flight Mechanics;

NASA CR-66662 - Volume IV - Appendix B - Entry and Terminal Phase Performance Analysis;

NASA CR-66663 - Volume V - Appendix C - Entry Configuration Analysis;

NASA CR-66664 - Volume VI - Appendix D - Subsystem Studies and Parametric Data.

CONTENTS

Page

FOREWORD ii
CONTENTS . . . . iii thru v
SUMMARY 1
INTRODUCTION 1
SYMBOLS AND ABBREVIATIONS 2
MISSION ANALYSIS 5
  1. TARGETING AND ERROR ANALYSIS 5
  2. ENTRY ENVIRONMENT 18
  3. TERMINAL PHASE SYSTEM AND LAUNCH VEHICLES 22
  4. CONCLUSIONS 27
CONFIGURATION STUDIES 28
  1. PREFERRED APPROACH 28
  2. ALTERNATIVE CONFIGURATIONS CONSIDERED 32
  3. CONCLUSIONS 35
SUBSYSTEM STUDIES 39
  1. SCIENCE SUBSYSTEM 39
  2. STRUCTURES AND MECHANISMS 49
  3. PROPULSION SUBSYSTEM 59
  4. GUIDANCE AND CONTROL SUBSYSTEM 64
  5. TELECOMMUNICATIONS SUBSYSTEM 70
  6. POWER SUBSYSTEM 76
  7. THERMAL CONTROL SUBSYSTEM 82
CONCLUSIONS . . . . 89 thru 91

Figure

1 Geometry at Entry 6
2 Targeting Boundary, Direct Mode 7
3 Entry Location, Direct Mode 8
4 Targeting Boundary, Orbit Mode 10
5 Approach Trajectory Geometry 11
6 Possible V_{HE} Vector Positions 12
7 Possible Landing Area, Direct Mode 13
8 Launch Date/Encounter Date 15
9 Entry and Touchdown Dispersions, Direct Mode . . . 16
10 Entry and Touchdown Dispersions, Orbit Mode 17
11 Peak Load Factor Limits, Orbit and Direct Modes . . 19
12 Maximum Heating Rate Comparison, B = 0.30, Diameter = 15 ft, Cone Edge 20

Page
13 Total Heating Load Comparison, B - 0.30, Diameter = 15 ft, Cone Edge 21
14 Terminal Phase System Comparison, Maximum W_{LE} per Diameter 23
15 Terminal Phase System Comparison, Maximum W_{LE} per Pound Entry 24
16 Required Aeroshell Diameter, Maximum W_{LE} per Pound Entry 25
17 Aerodecelerator Capsule System Weight Summary . . . 26
18 Configuration 1B 29
19 Space Vehicle Integration, Configuration 1B 31
20 Science Subsystem 40
21 Results of Entry Error Analysis, VM-8 Atmopshere . 43
22 Humidity on Mars 45
23 Opportunities for Relay of Surface Images 47
24 Leg Stowage and Engine Installation 50
25 Landed Configuration 1B 53
26 Ratio of Aeroshell Structure to Entry Weight as a Function of Ballistic Coefficient 55
27 SLA 561 Ablator Weight Variations, Orbit Mode . . . 56
28 SLA 561 Ablator Weight Variations, Direct Mode . . 57
29 Landing Propulsion System 60
30 Summary of Trade Studies 61
31 Propulsion System Weight versus Total Impulse . . . 63
32 Guidance and Control Subsystem Block Diagram . . . 65
33 Terminal Descent Profile and Propellant Utilization (Configuration 1B) 66
34 Position Error (1σ) versus Time 69
35 Telecommunications Subsystem 71
36 Postland Relay Link Performance 73
37 Direct Link Performance 74
38 Energy Densities of Sterilizable Batteries 77
39 Weight Comparison of RTG and Solar Array Power Subsystems 79
40 Solar Array Performance Data 80
41 Preferred Mars Surface Thermal Design 83
42 Environmental Models 85
43 Insulation System Conductivity 87
44 Energy Sources 88

Table

1 Part II Point Designs 33
2 Mission, Sequential Weight, and Subsystem Parameters, Configurations 1A, 1B, and 2A 36
3 Summary Weight Comparison 38

Page
4 Summary of Science Data Return 42
5 Scope of Parametric Propulsion Study 62
6 Guidance and Control Subsystem Characteristics . . 67
7 Comparison of RTG and Solar Array Power Subsystem Characteristics 79
8 Scope of Parametric Thermal Control Study 84

FINAL REPORT

STUDY OF DIRECT VERSUS ORBITAL ENTRY FOR MARS MISSIONS

VOLUME I: SUMMARY

By Raymond S. Wiltshire and Hugh E. Craig
Martin Marietta Corporation

SUMMARY

This volume summarizes the work accomplished by the Martin Marietta Corporation for the Langley Research Center under the Contract: "Study of Direct versus Orbital Entry for Mars Missions." This effort was conducted during the period from March 26, 1968 to July 1, 1968.

The objectives of the study were twofold:

1) To obtain the net science payload for the direct entry mode;
2) To evaluate the direct and out-of-orbit entry modes for soft landing capsules.

To fulfill these objectives, three main tasks were defined:

1) Conduct mission and subsystem parametric analyses;
2) Establish mission design for each capsule mode;
3) Provide conceptual design for three capsule systems.

The initial effort concerned itself exclusively with the first of these tasks, that is, the parametric analyses. The analyses were completed and reported to Langley Research Center at the end of April 1968. As a result of these studies, a number of point designs were selected for more detailed evaluation.

INTRODUCTION

This summary volume is presented in four major sections. The first section covers the mission analysis studies, i.e., launch vehicle capability, transfer trajectories, targeting, aerothermodynamics, entry trajectories, and terminal phase systems. It is in this area of mission planning and mission operation that the out-of-orbit mode shows a distinct advantage over the direct entry mode. The out-of-orbit mode permits a greater mission flexibility.

The second section describes and compares the specific capsule configurations investigated. It is clear that the 8½-ft diameter aeroshell is marginal from a packaging viewpoint; the 10½-ft diameter examined is preferred. However, the potential for saving the development of a bulbous shroud is great enough to warrant further investigation of the maximum aeroshell diameter that can be accommodated in the Titan III/Centaur shroud.

Individual subsystems are discussed in the third section; parametric analyses are presented, the point designs are described with a preferred design identified, and the long-lead items are listed for these designs. The mission mode selection has little effect on the capsule subsystems. There is no effect on electronic subsystems. More tracking accuracy by the Deep Space Instrument Facility (DSIF) or a sun and planet tracker on the orbiter is required for the direct mode. The energy absorption subsystems are affected by mission mode selection in that the direct entry is a higher energy mode. However, the increase in subsystem capability is not large and is well within the state of the art.

The fourth section presents the study conclusions and identifies areas that merit further study.

SYMBOLS AND ABBREVIATIONS

ACS	attitude control system
AMR	altitude measuring radar
B_E	entry ballistic coefficient, M/C_DA, slugs/foot^2
bps	bits per second
C_3	Earth departure energy, (kilometers/second)^2
DSIF	Deep Space Instrument Facility
FSK	frequency shift keying
g	gravitational acceleration

GCC	guidance and control computer
h_p	periapsis altitude of orbiter, kilometers
IMU	inertial measurement unit
I_{sp}	specific impulse, seconds
M_D	deployment Mach number
PRIME	Precision Recovery including Maneuvering Entry
Q	total heat, $\int \dot{q}\, dt$, Btu/foot^2
$\dot{q}$	heating rate, Btu/foot^2-second
RTG	radioisotope thermoelectric generator
$R_{\text{♂}}$	radius of Mars (3393 km)
TDLR	terminal descent and landing radar
TWTA	traveling wave tube amplifier
TIIIC	Titan IIIC
TIIIF	Titan IIIF
V_E	entry velocity (inertial), kilometers/second
V_{HE}	Mars approach energy (asymptotic velocity), kilometers/second
W_{CS}	total capsule weight, pounds
W_E	entry weight, pounds
W_{LE}	landed equipment weight, pounds
α_{CE}	capsule antenna aspect angle at entry (see fig. 1), degrees

$\alpha_{C_{TD}}$	capsule antenna aspect angle at touchdown, degrees
β	targeting parameter (see fig. 1), degrees
γ_E	inertial entry flightpath angle, degrees
ΔV	velocity increment, meters/second
ΔV_D	deorbit velocity, meters/second
θ_{FM}	fading margin angle (between reflected signal from capsule to surface to orbiter and local vertical at reflection point), degrees
λ	orbiter lead angle (see fig. 1), degrees
ρ_{CE}	communication range: capsule to orbiter, kilometers
σ	standard deviation
τ'	approach trajectory periapsis location (see fig. 5), degrees

Subscripts:

Lam	laminar
Rad	radiative
Turb	turbulent
$\oplus$	Earth
♂	Mars

MISSION ANALYSIS

The mission analysis parametric study includes the definition of launch periods and targeting capability, entry and landing error analysis, launch vehicle capability, entry trajectory, aerothermodynamics, and terminal phase system analysis. The results of these parametric analyses are summarized in this section in three groupings. The first covers launch period, targeting, and error analysis; the second covers the entry environment; and the third covers the terminal phase system comparisons and launch vehicle capability.

1. TARGETING AND ERROR ANALYSIS

The targeting capability and launch period selection are shown below to be directly related. Before discussing the implications of launch period selection, the general targeting capability relative to the approach trajectory (direct mode) or orbit (orbit mode) will be summarized.

The parameters used to define targeting capability are the targeting parameter, β, and orbiter lead angle, λ. These two parameters, as well as the relay communication link geometry parameters, are illustrated in figure 1. The combination of communication link geometry and deorbit/ejection ΔV and maneuver strategy are used to evaluate the range of landing areas that can be achieved relative to orbit.

The communication link constraints impose the β versus λ boundaries shown in figure 2 for the direct mode. The boundaries illustrated guarantee good capsule antenna aspect angles $\left(\alpha_c < 50°\right)$, short communication range $\left(\rho_c < 5000 \text{ km}\right)$, good link time after touchdown and before losing relay contact $\left(t_{TD} > 5 \text{ min}\right)$, and avoidance of geometry that can lead to multipath losses $\left(\theta_{FM}\right)$. The data in figure 2 show that all of these constraints can be satisfied as long as the lead angle is approximately $\lambda = -16°$. For the direct mode, the achievable β is directly related to entry flightpath angle, γ_E. This relationship is shown in figure 3. The β is restricted at the low end by the skipout limit (γ_E approximately -16°) and on the high end by landed payload margin, which, as is shown below, is sensitive to γ_E. The nominal γ_E considered here is -21°, resulting in a nominal β of 27°. This really defines the minimum β that can be considered (in terms of preflight targeting) for the entry corridors defined below.

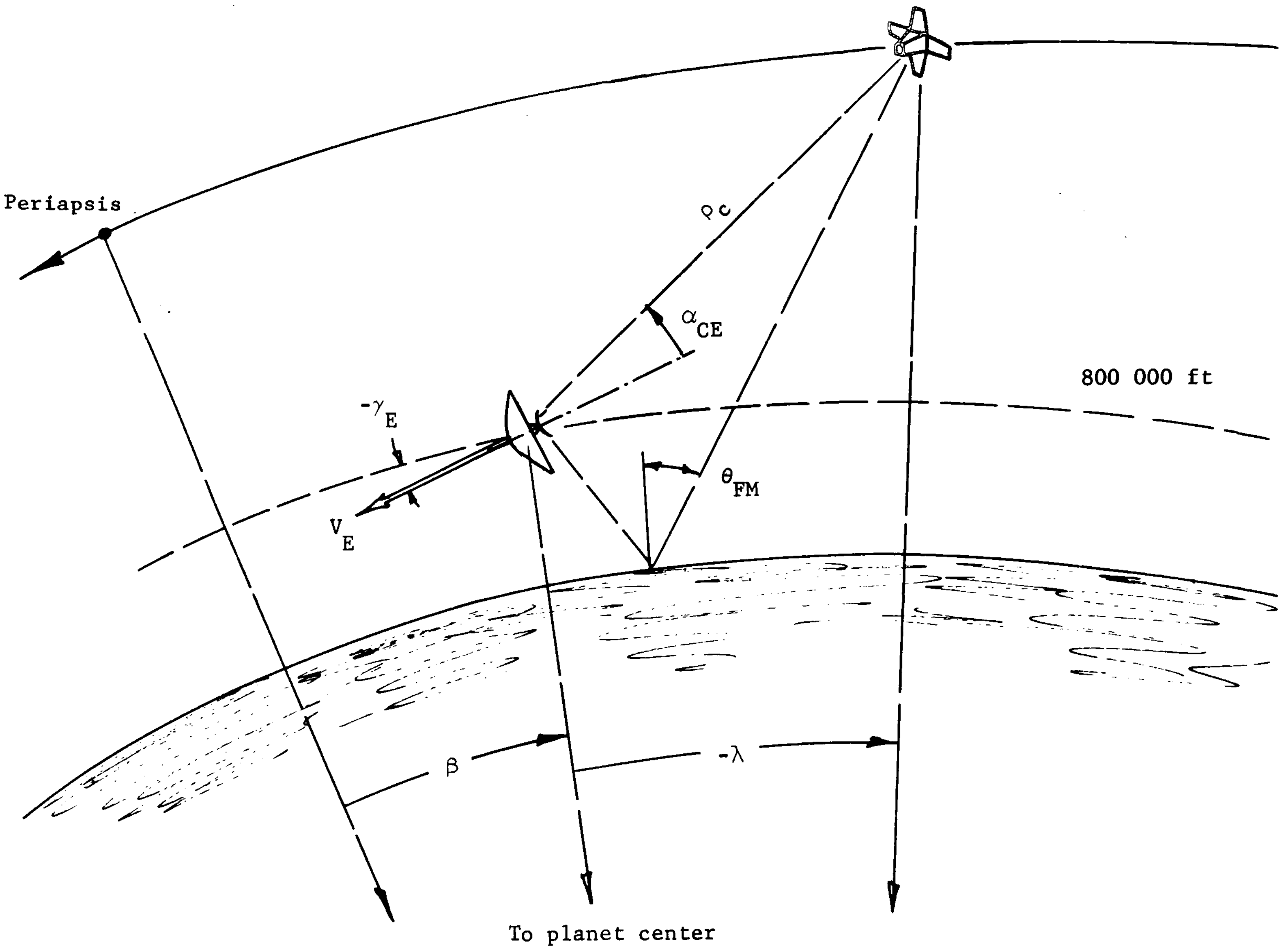
Periapsis
ρc
α_{CE}
800 000 ft
$-\gamma_E$
V_E
θ_{FM}
β
-λ
To planet center

Figure 1.- Geometry at Entry

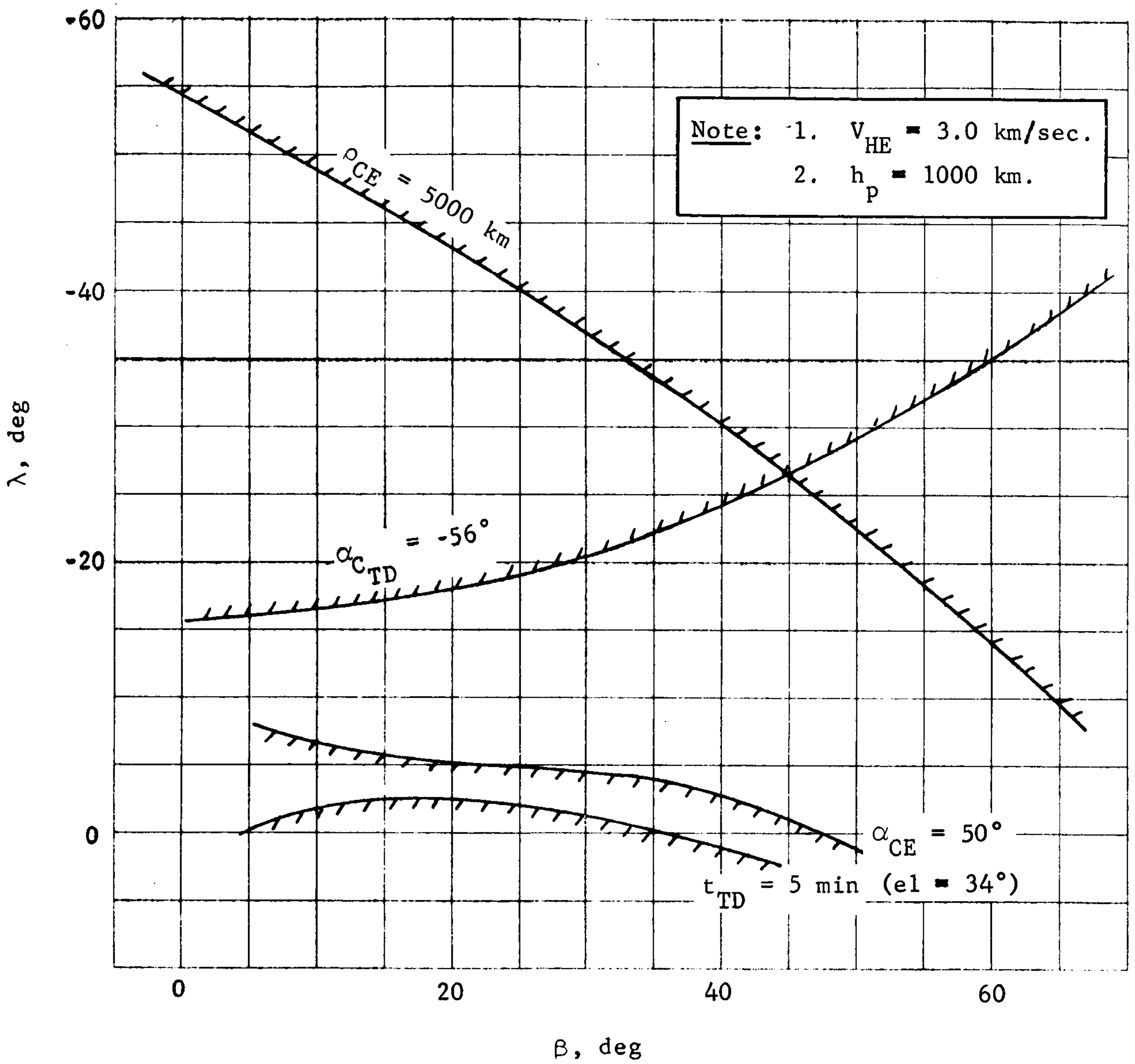

Figure 2.- Targeting Boundary, Direct Mode

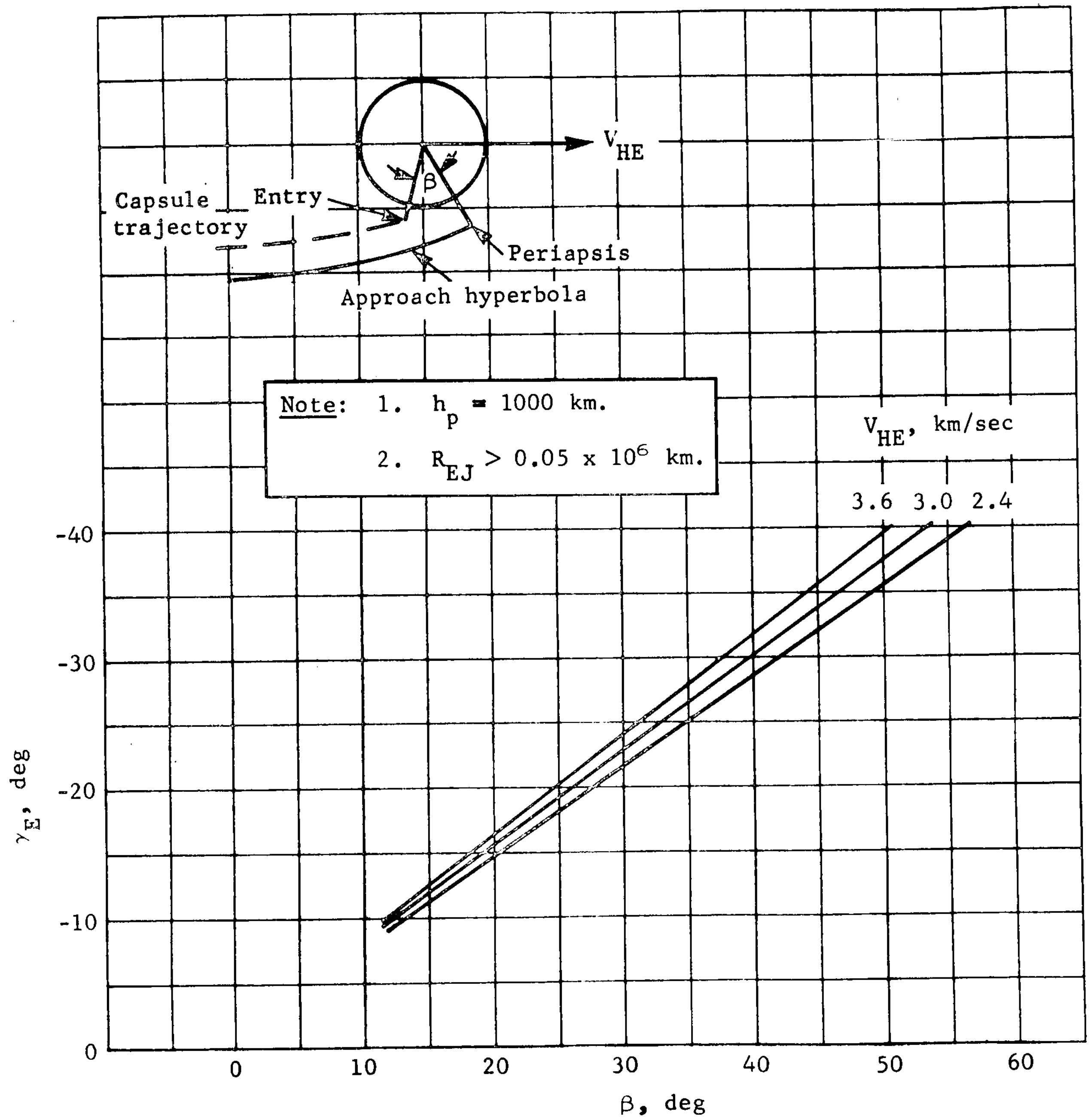

Figure 3.- Entry Location, Direct Mode

Targeting boundaries for the orbit mode are shown in figures 4(a) and 4(b) for the two orbits considered (1000x15 000 and 1000x33 070 km, respectively). The communication constraints once again limit the required lead angles to approximately -17.5°. For the orbit mode, the β limits are defined by the deorbit ΔV_D and coast time (deorbit to entry) constraints. The composite β range for these orbits is 28 to 40°. These β, as well as the 27° for the direct mode, ensure satisfying all of the communication link geometry constraints, power (coast time), and ΔV limits.

The second aspect of the targeting analysis is the interpretation of the above β limits in terms of actual landing areas. To do this, the geometry illustrated in figure 5 must be considered. The location of the approach trajectory periapsis position relative to the V_{HE} vector (approach hyperbola asymptotic velocity) is given by the angle τ'. This angle, a function of the magnitude of V_{HE} and periapsis altitude, varies from approximately 52.5 to 57.5°. Using a mean value of 55° for an example, the atmospheric entry point is $\tau' + \beta$ from the V_{HE} vector, or 82° for the direct mode and 83 to 95° for the orbit mode. The downrange angle traveled in the atmosphere is approximately 12° for the direct mode and 16° for the orbit mode, resulting in touchdown points approximately 70° and 67 to 79° from the V_{HE} vector for the direct and orbit modes, respectively.

The potential locations of the V_{HE} vector for the 1973 Type I Mars mission are shown in figure 6 for two values of Earth departure energy (C_3) and Mars approach energy (V_{HE}). Using values of $C_3 = 30\ (\text{km/sec})^2$ and $V_{HE} = 3.5$ km/sec as limiting values, the locus of possible landing areas for the direct mode (i.e., 70° from the V_{HE} vector) is shown in figure 7. Two approach trajectory examples are shown to illustrate that the landing site latitude for the direct mode is a function of approach trajectory (and orbit) inclination.

The range of landing site locations as measured from the V_{HE} vector for the orbit mode is not much different than that for the direct mode. Thus, the possible landing area for the orbit mode would be very similar to that shown in figure 7 except that the locus of inaccessible area on the right (encircling the V_{HE} vector locus) would shrink 3° and that on the left would grow 9°. The differences are negligible.

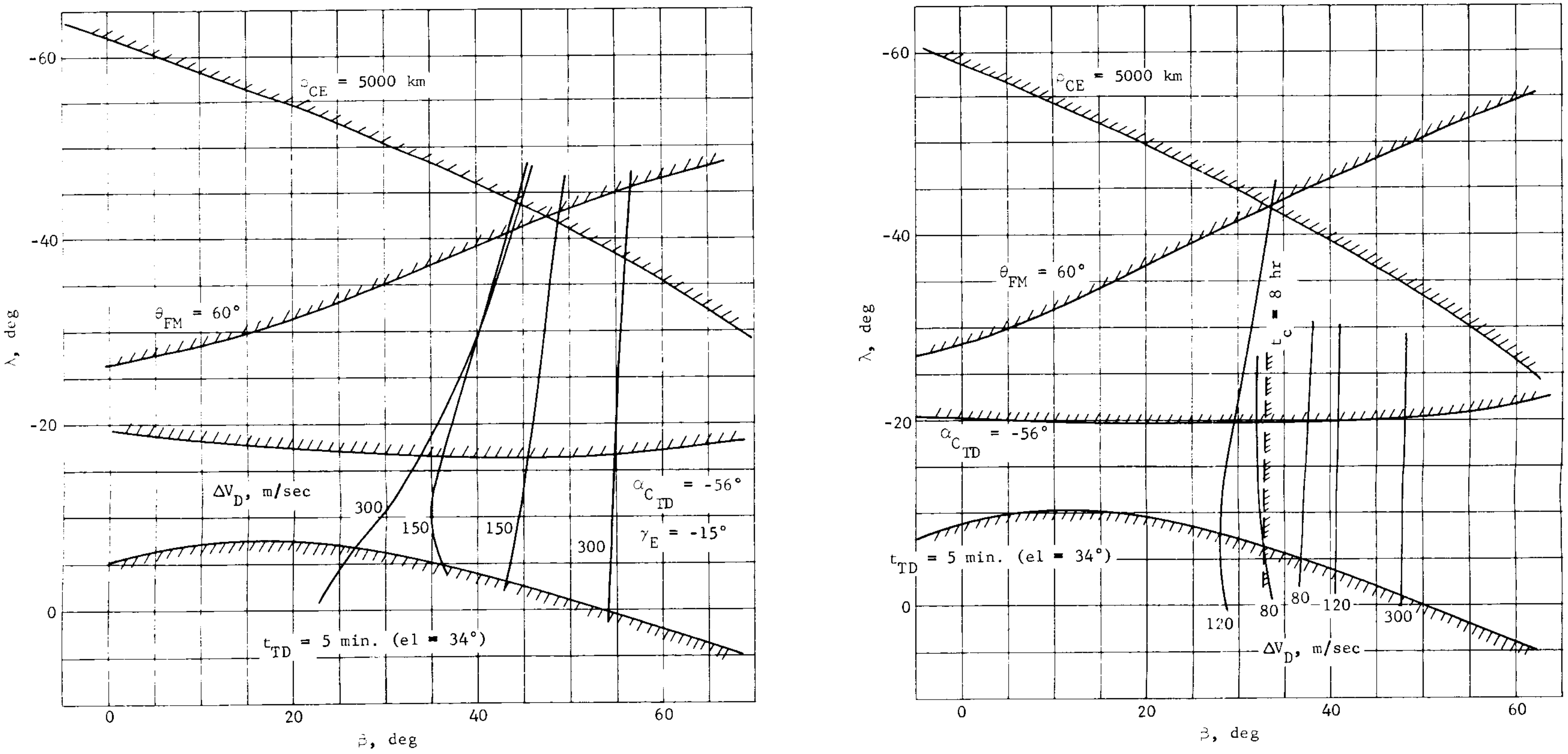

(a) 1000x15 000-km Orbit

(b) 1000x33 070-km Orbit

Figure 4.- Targeting Boundary, Orbit Mode

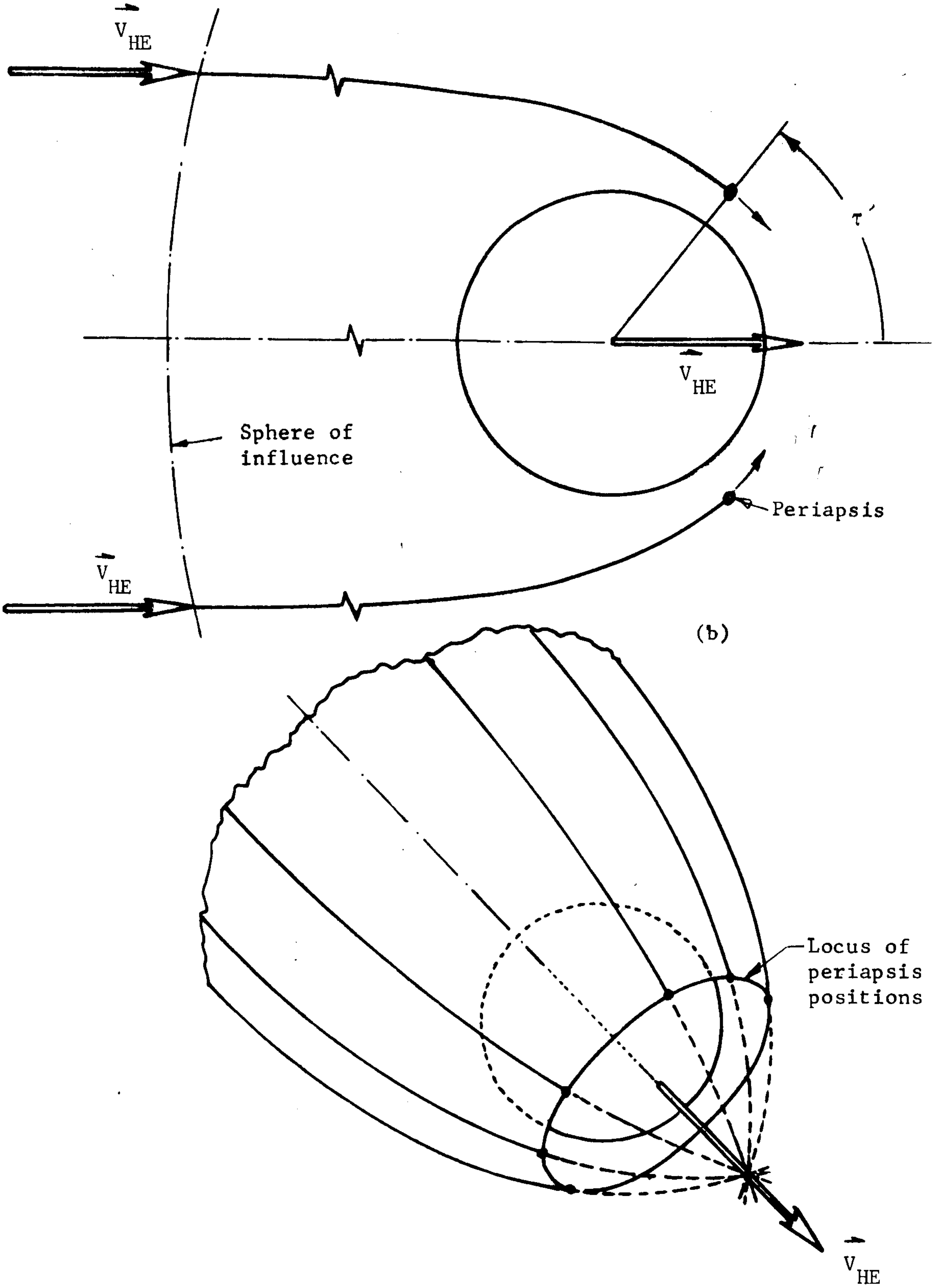
$\vec{V}_{HE}$
τ'
$\vec{V}_{HE}$
Sphere of influence
Periapsis
$\vec{V}_{HE}$
(b)
Locus of periapsis positions
$\vec{V}_{HE}$

Figure 5.- Approach Trajectory Geometry

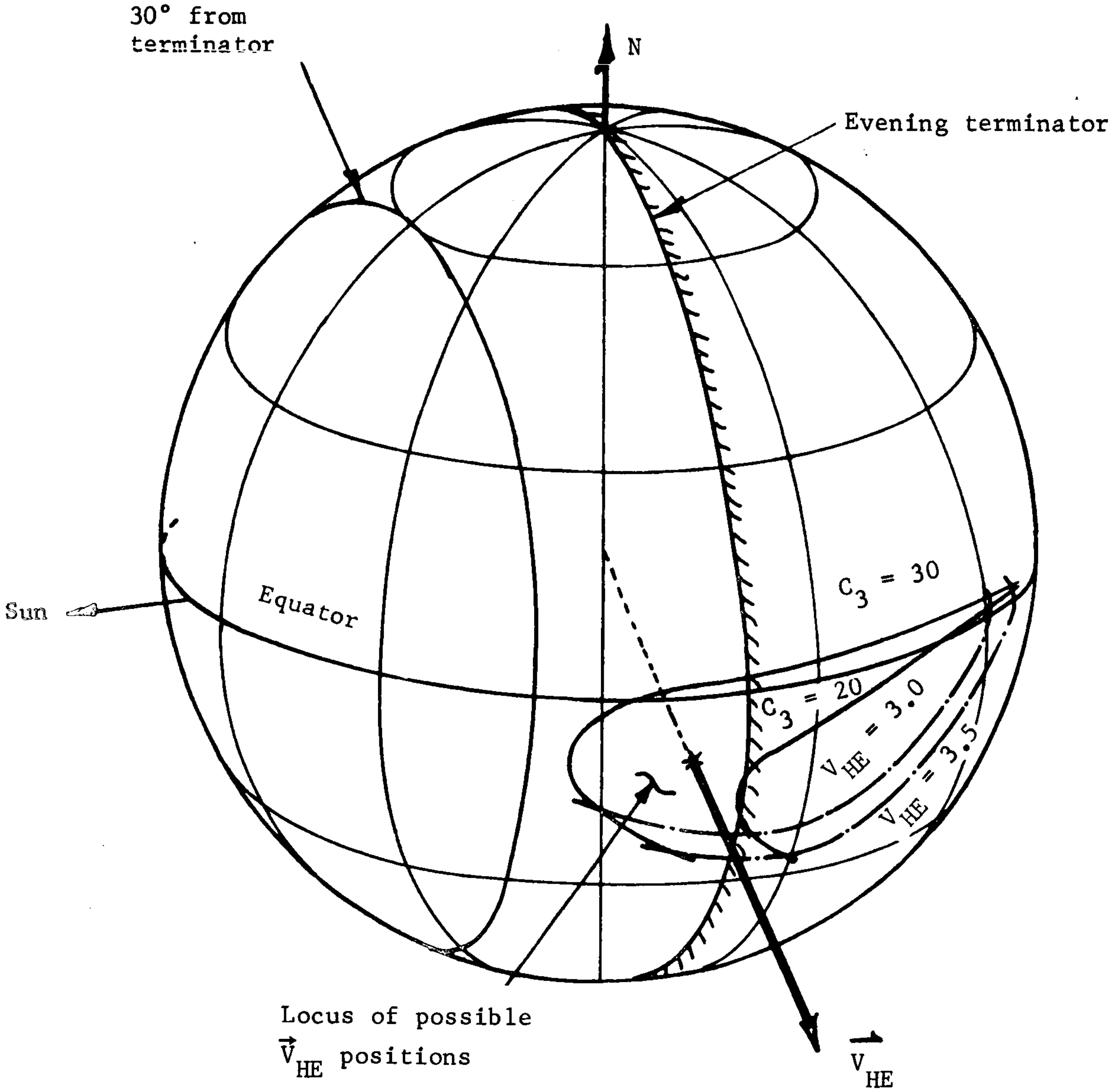
30° from terminator
N
Evening terminator
Sun
Equator
C_3 = 30
C_3 = 20
V_{HE} = 3.0
V_{HE} = 3.5
Locus of possible $\vec{V}_{HE}$ positions
$\vec{V}_{HE}$

Note: C_3 in $(km/sec)^2$;
V_{HE} in km/sec.

Figure 6.- Possible V_{HE} Vector Positions

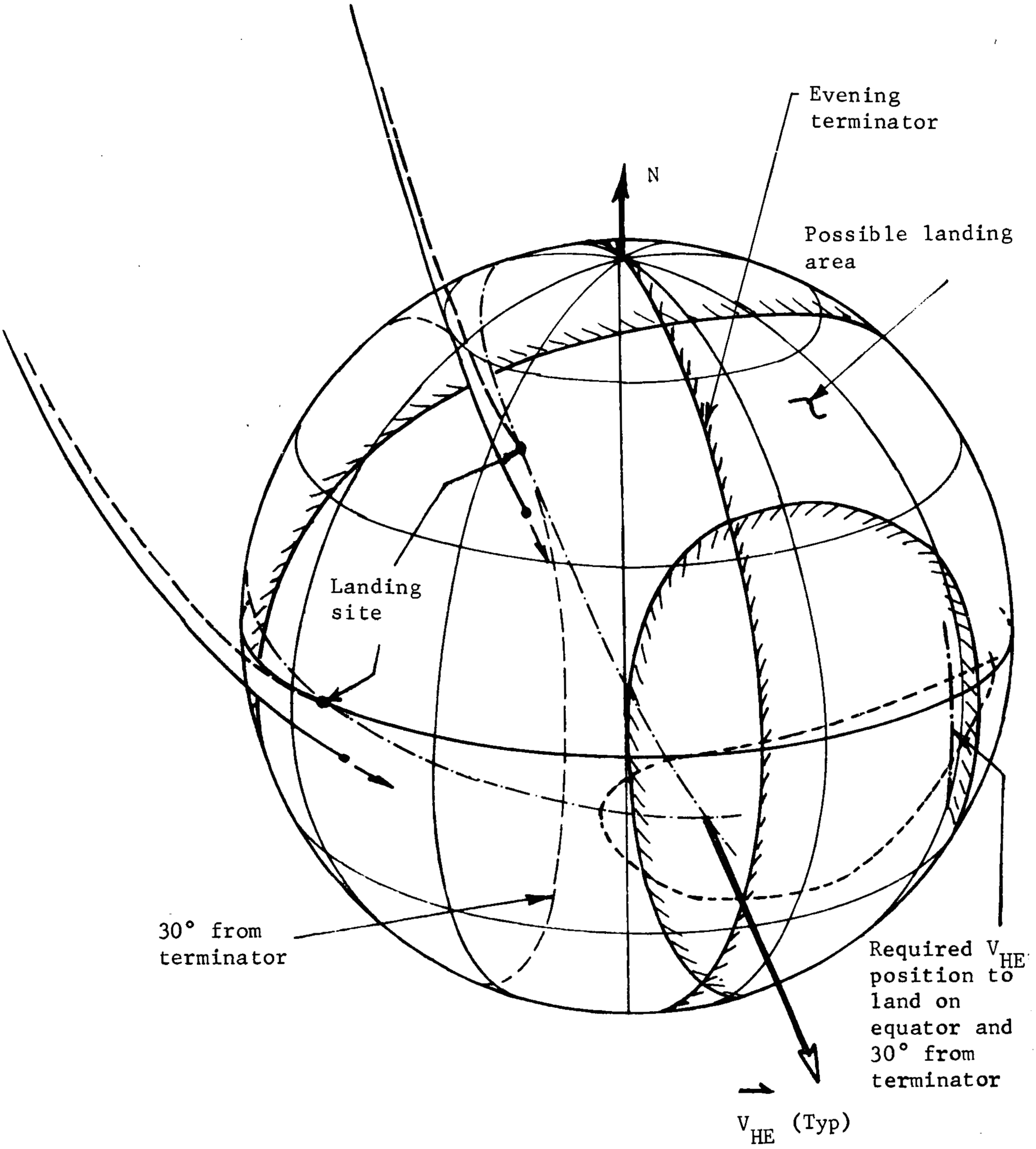
Evening terminator
N
Possible landing area
Landing site
30° from terminator
Required V_{HE} position to land on equator and 30° from terminator
$\vec{V}_{HE}$ (Typ)

Figure 7.- Possible Landing Area, Direct Mode

The principal difference between the targeting capability for the two modes is how they acquire a specific landing site longitude. In the direct mode, this is accomplished by controlling the time of encounter, while the combination of orbital period and time in orbit is used in the orbit mode. The direct mode targeting capability in terms of landing site longitude selection can be seriously compromised by the need for either specific station tracking or simultaneous two-station tracking during the critical preencounter phase of the mission and at orbit insertion. This would fix the encounter time of day to specific times, leading to limited landing site longitudes. The orbit mode sensitivity to this kind of constraint is less severe.

A second major difference between the mode tarteting capability is the ability of the orbit mode targeting to take advantage of orbit periapsis positioning as part of the orbit insertion maneuver. Shifts as great as 45° can be achieved at the expense of an additional 0.4 km/sec added to the nominal orbit insertion ΔV. This makes virtually the entire planet accessible as a potential landing site (fig. 7) and also has advantage of allowing high inclination orbits positioned for good mapping. Under similar conditions, the direct mode landing sites would only be north of approximately 35 to 45°.

The launch date/encounter date combinations satisfying the V_{HE} vector positioning limits presented in figure 6 are shown in figure 8. Without orbit positioning, the V_{HE} vector must be on the right side of the locus for landings near the terminator leading to launch periods in early July 1973, and encounters during late January/early February 1974. The high inclination mapping orbits require launches during late July/early August 1973, and encounter during April 1973. The 30-day launch period, which optimizes launch vehicle performance, is shown for reference.

The entry corridors and landing footprints for the direct and orbit modes are shown in figures 9 and 10, respectively. The direct mode data are presented as a function of b-vector uncertainty where the boundaries on the right, labeled "maximum," are consistent with current DSN capability, and those on the left, labeled "minimum," are expected capability in 1973. The minimum level can also be achieved assuming current capability with the addition of a planet tracker coupled to a sun and Canopus tracker on the orbiter as discussed in the guidance and control section.

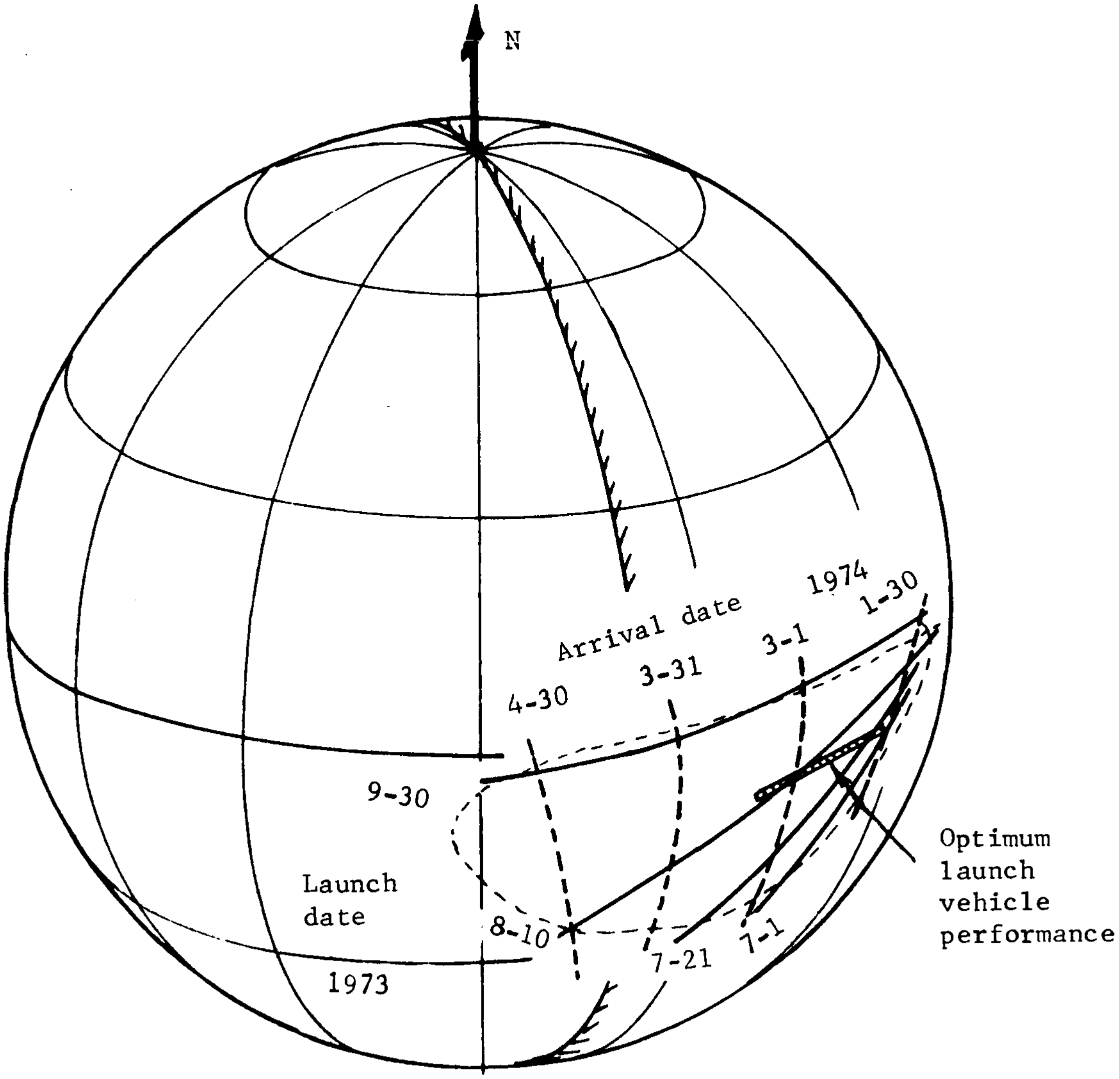
N
Arrival date
1974
1-30
3-1
3-31
4-30
9-30
Launch
date
8-10
7-21
7-1
1973
Optimum
launch
vehicle
performance

Figure 8.- Launch Date/Encounter Date

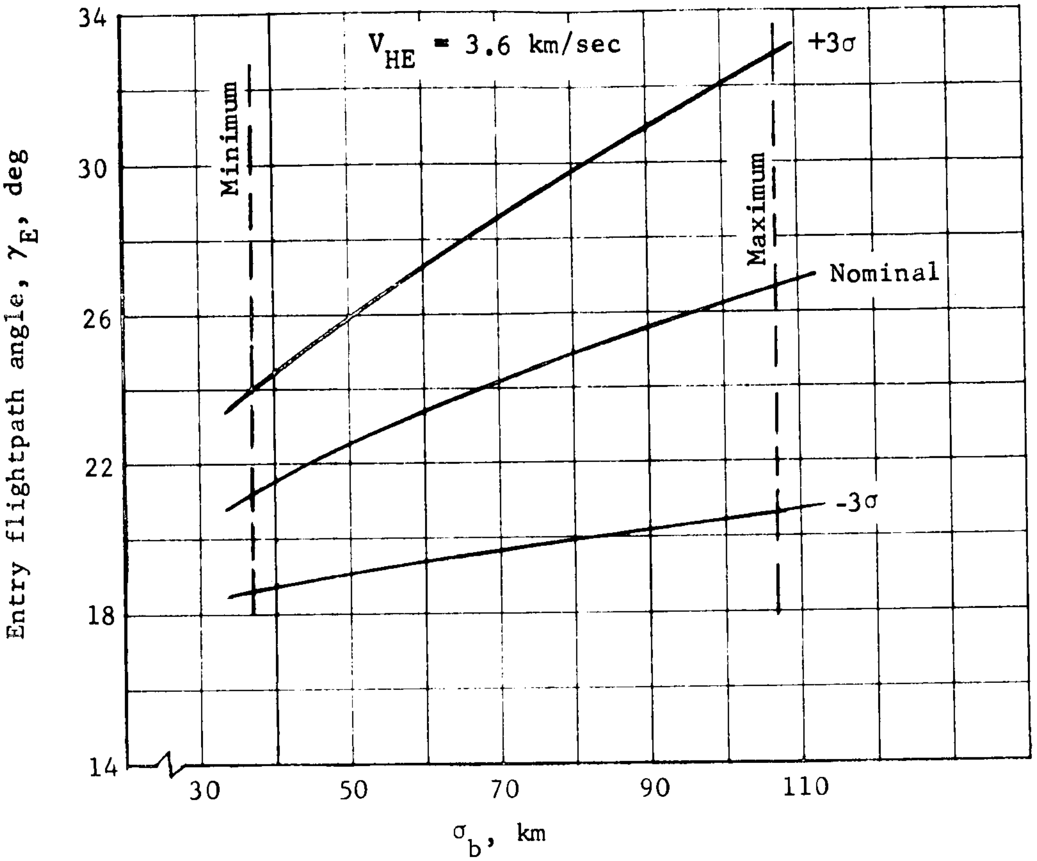

(a) Allowable Entry Corridor

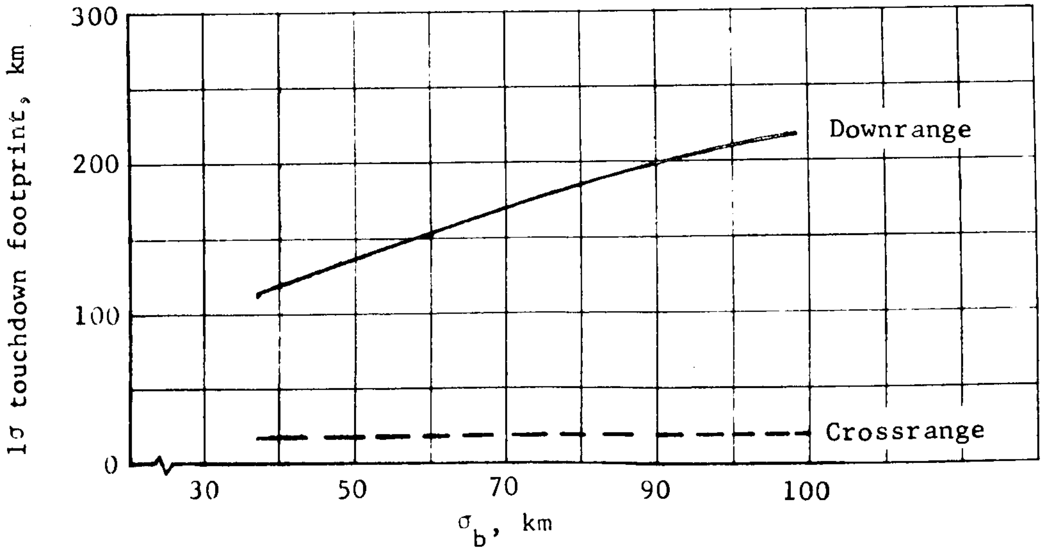

(b) 1σ Touchdown Footprint

Figure 9.- Entry and Touchdown Dispersions, Direct Mode

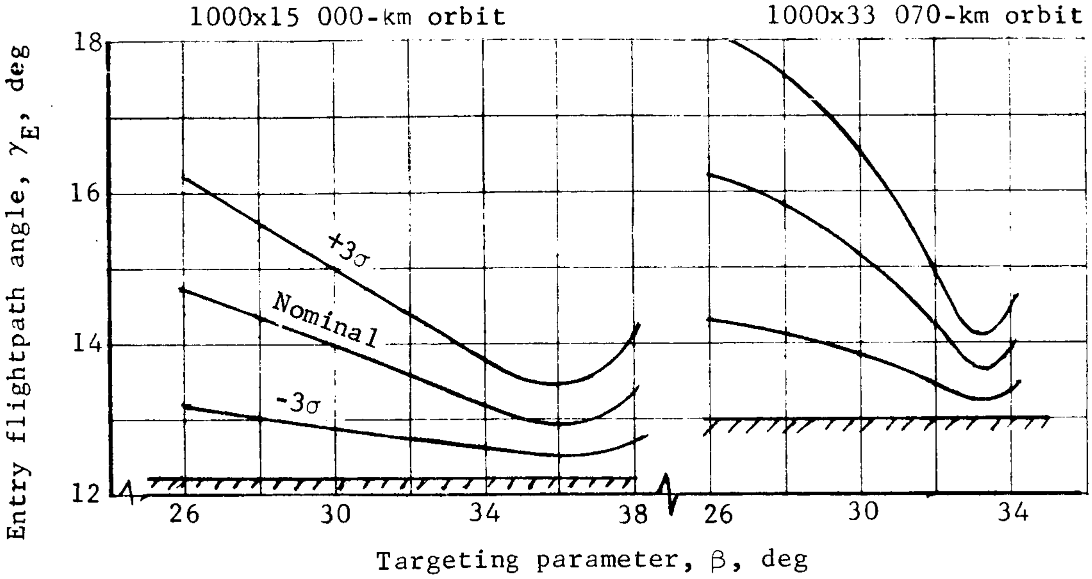

(a) Allowable Entry Corridor

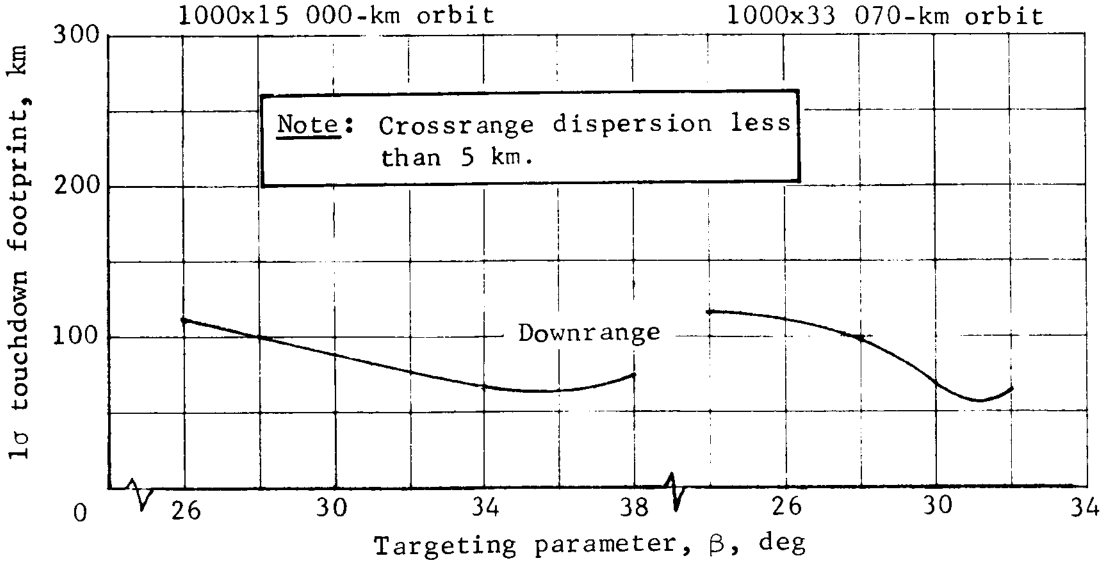

(b) 1σ Touchdown Footprint, km

Figure 10.- Entry and Touchdown Dispersions, Orbit Mode

These sextant readings coupled with the Earth-based doppler data acquired in the 300 000 to 100 000 km from Mars range will reduce the b-vector uncertainties to less than 40 km with current DSN capability. The entry corridors shown in figure 9(a) will result in maximum $-\gamma_E$ of 24 to 33° (3σ) as a function of σ_b. The landing footprint dispersions shown in figure 9(b) vary from 120 to 220 km (1σ) in downrange uncertainty and approximately 18 km crossrange.

The orbit mode entry corridors are shown in figure 10(a) as a function of targeting parameter, β, for both the orbits considered. The corresponding landing footprints are shown in figure 10(b). The maximum $-\gamma_E$ are less than 18° (3σ) and the landing footprints are 60 to 120 km downrange (1σ) and less than 5 km crossrange.

2. ENTRY ENVIRONMENT

The major differences in the entry phase environment as a function of mission mode are the level of peak entry load factor and aerodynamic heating levels. The differences in peak load factor are shown in figure 11 for the combination of entry velocity and atmosphere that maximize and minimize load factor. The peak load factors vary from 5 to 31 (Earth) g for the orbit mode and 11 to 84 g for the direct mode. These differences are not particularly significant.

Representative heating rates and total heat loads for entry velocities covering both modes are shown in figures 12 and 13. These data illustrate that the entry heating environment is relatively mild for either mode and well within current heat shield technology. The heat shield is designed primarily as an insulator against the total heat load. The major difference between the modes is that transition to turbulent flow is more likely for the direct mode, leading to heating rates on the cone edge that are high enough that they become a factor in heat shield material selection. Heating rates above approximately 100 Btu/ft^2-sec will require higher density materials, increasing the heat shield weight. Adoption of the direct mode will require a somewhat more extensive aerothermodynamic test program to evaluate transition, radiative heating, and base heating than would be required for the orbit mode.

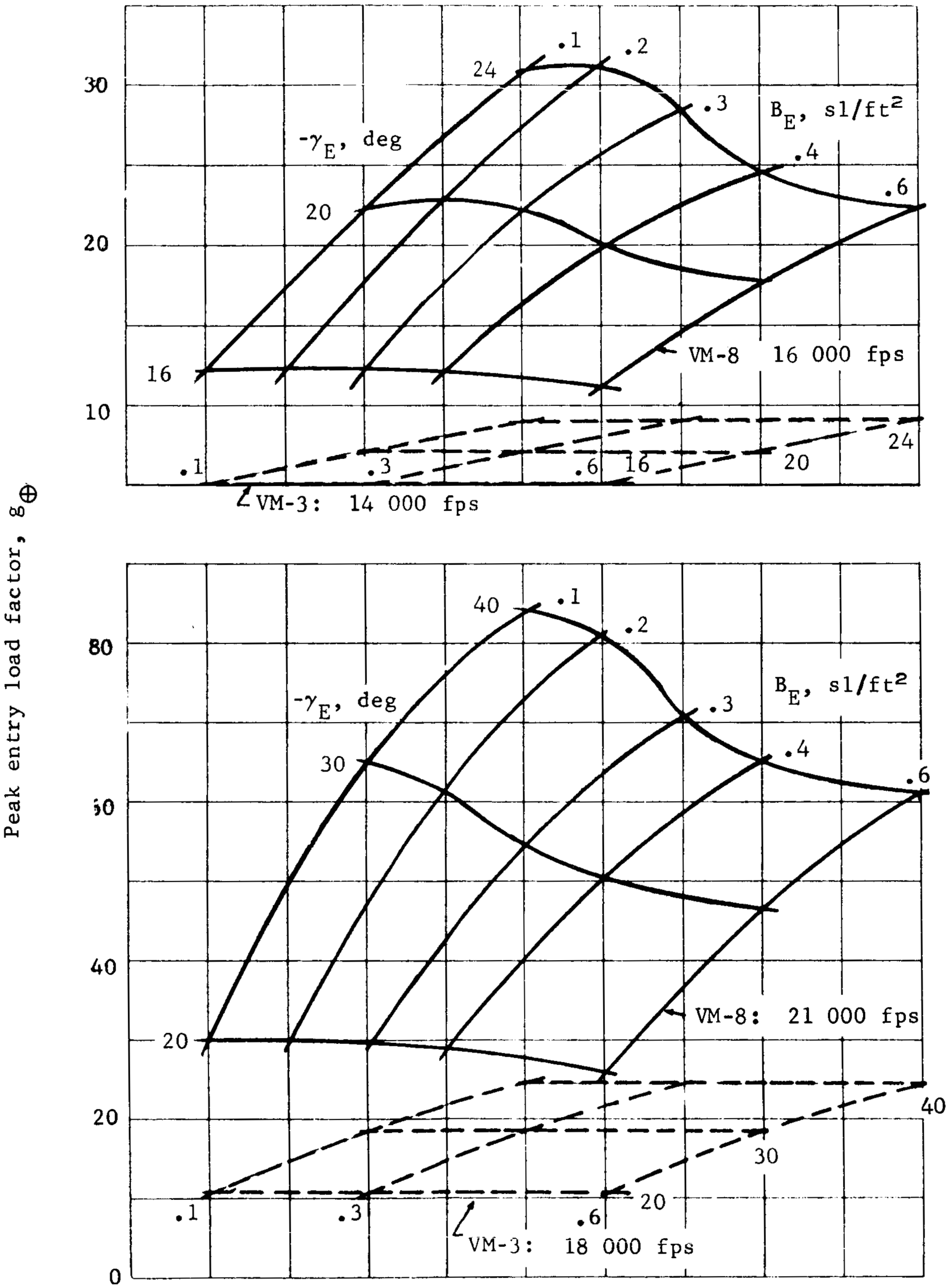

Figure 11.- Peak Load Factor Limits, Orbit and Direct Modes

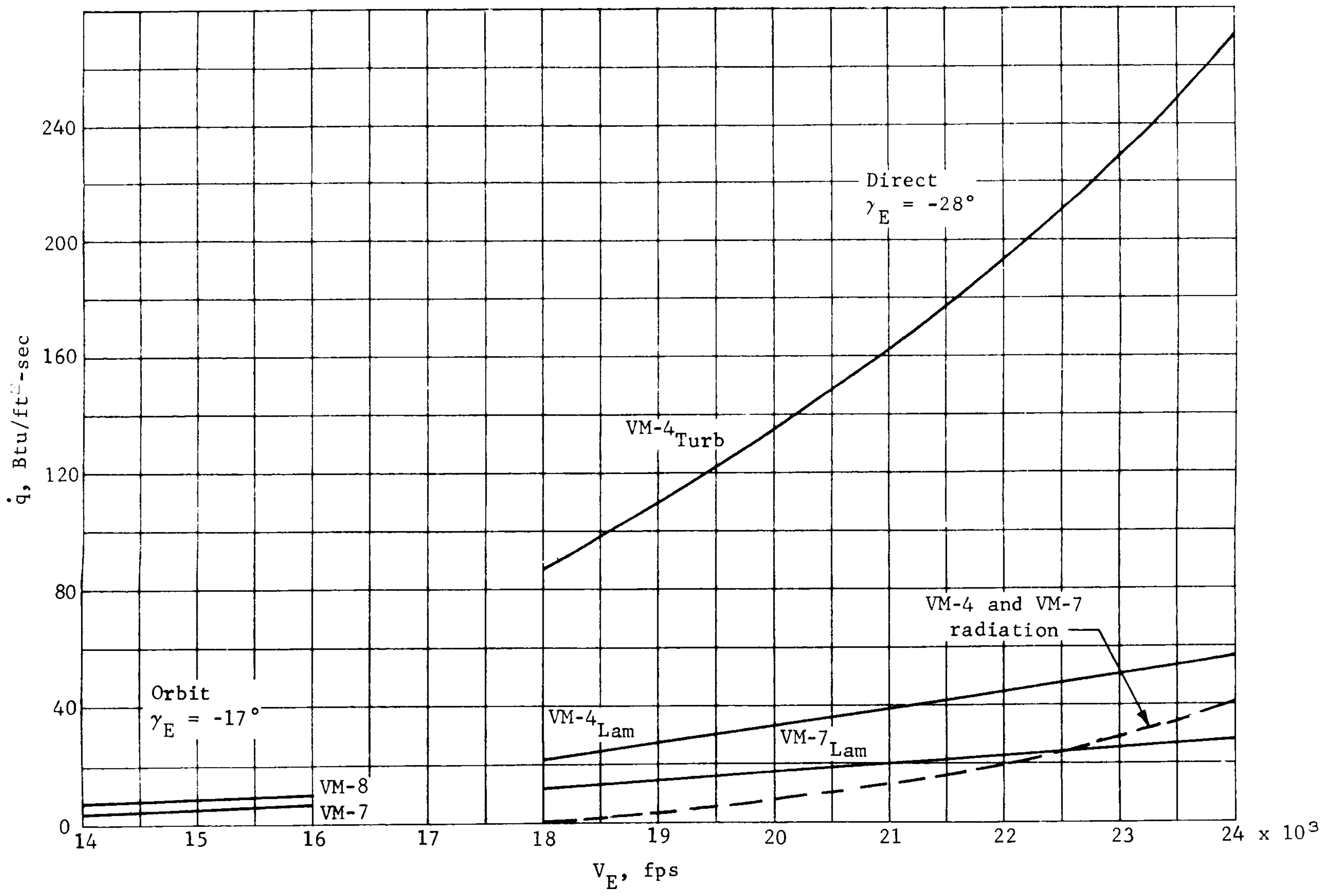

Figure 12.- Maximum Heating Rate Comparison, B = 0.30, Diameter = 15 ft, Cone Edge

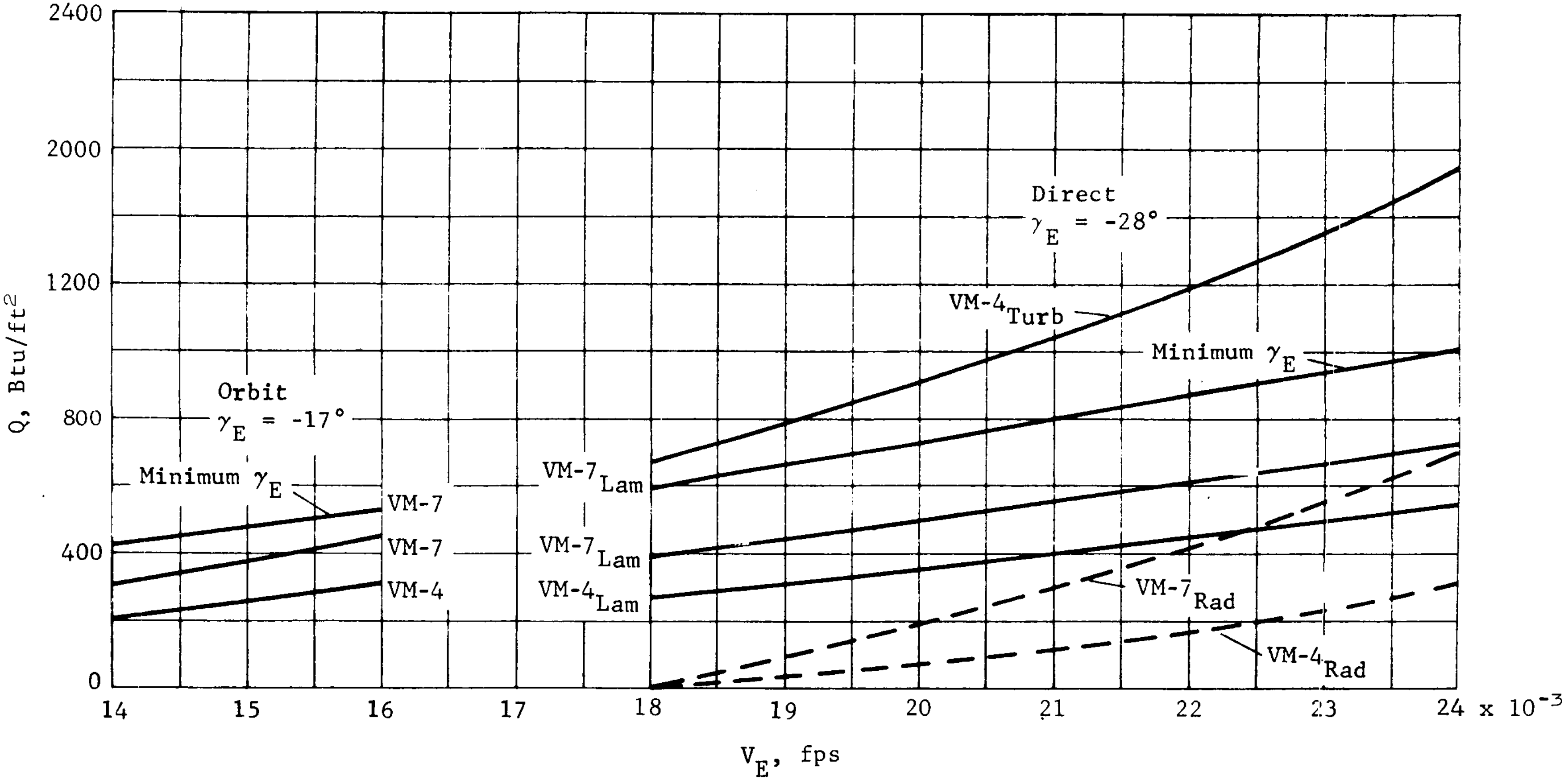

Figure 13.- Total Heating Load Comparison, B = 0.30, Diameter = 15 ft Cone Edge

3. TERMINAL PHASE SYSTEM AND LAUNCH VEHICLES

The terminal phase systems compared in this analysis are:

1) Subsonic type parachute deployed at $M_D = 2$ with vernier rocket landing motors;
2) Tuckback ballutes deployed at $M_D = 3$ and $M_D = 5$ with vernier rocket landing motors;
3) All-retro terminal phase system.

The propulsion systems used in the comparisons given below are three-engine arrangements with monopropellants $\left(I_{sp} = 225 \text{ sec}\right)$ used with aerodecelerators and bipropellants $\left(I_{sp} = 285 \text{ sec}\right)$ used with the all-retro system.

The summary comparison presented here is based on two different criteria. The first is maximum pounds on the ground per foot aeroshell diameter and the second is maximum pounds on the ground per pound entry weight. The data are compared on the basis of useful landed equipment weight, W_{LE}, entry weight, W_E, and total capsule system weight, W_{CS}. Landed equipment, W_{LE}, is defined as entry weight minus aeroshell, total loaded terminal phase system, landing legs and landed structure, diameter sensitive cabling, pyrotechnic subsystem, entry thermal control weights, and attitude control system (ACS) weights. Total capsule system weight, W_{CS}, is defined as entry weight plus deorbit/ejection propulsion module, capsule-to-orbiter adapter and adapter-mounted equipment, and sterilization canister. The comparisons presented below assume a landing at a terrain height of 6000 ft over mean Mars surface level $\left(R_{\male} = 3393 \text{ km}\right)$ and most adverse atmosphere combinations (VM-7 and/or VM-8).

The comparison of terminal phase systems that maximize W_{LE} per foot aeroshell diameter are shown in figure 14 for aeroshell diameters of 8.5 and 15 ft. The data are shown for all systems and indicate variations of both W_{CS} and W_{LE} with entry flight-path angle. The orbit mode data show best W_{LE} for the ballute configurations, but they also have the maximum total capsule system weight. The direct mode data show a similar trend as far as the aerodecelerators are concerned, but the all-retro system provides the greatest W_{LE}.

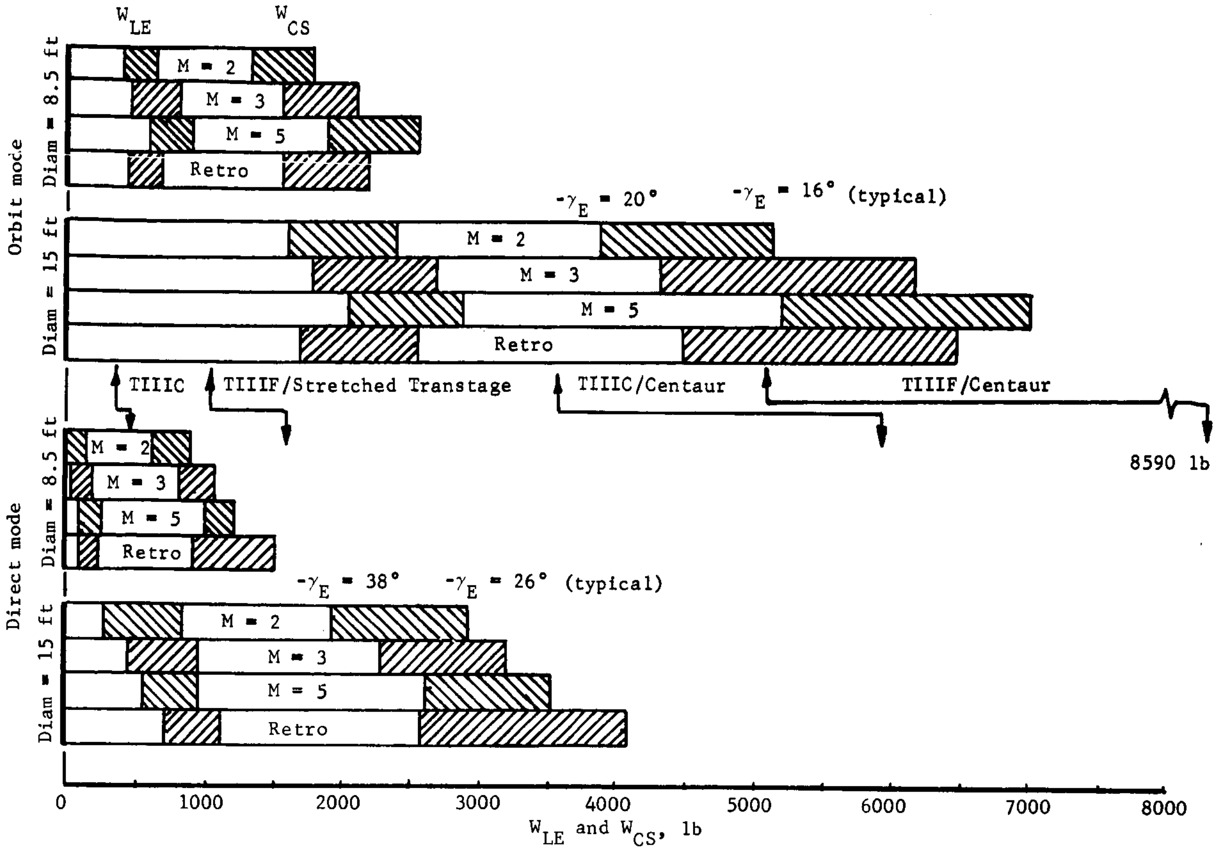

Figure 14.- Terminal Phase System Comparison, Maximum W_{LE} per Diameter

The launch vehicle performance capability (optimum 30-day launch period) is also indicated on the figure. Comparison of orbit mode 8.5 ft diameter, and direct mode 15 ft diameter, shows that both have W_{LE} in the same range and both require the Titan IIIC/Centaur. It is noted here that the variation of indicated weight with diameter are nearly linear.

Two cases are compared for the criterion that maximized W_{LE} per pound entry weight. The first is for a constant W_{LE} = 600 lb, and the second is constant W_E = 1500 lb. These two cases are summarized in figure 15.

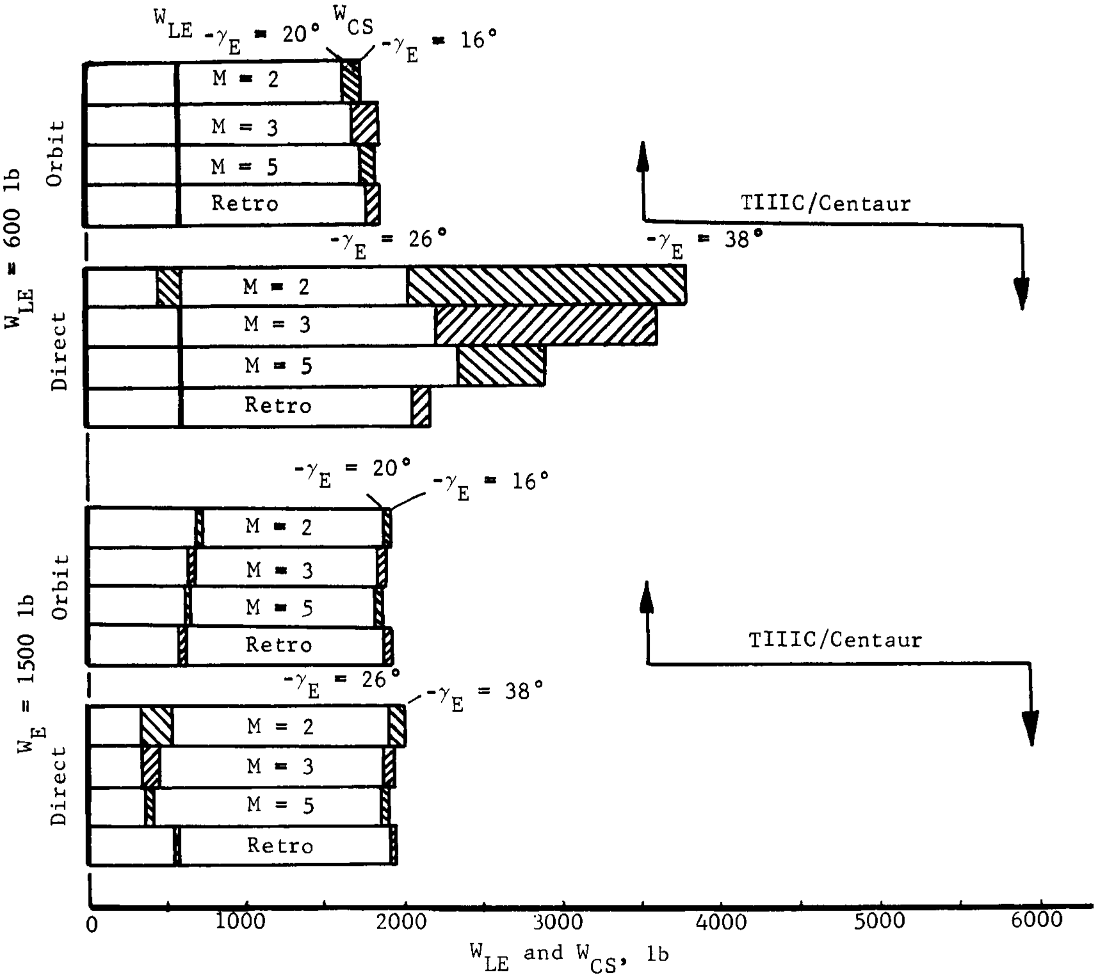

Figure 15.- Terminal Phase System Comparison, Maximum W_{LE} per Pound Entry

The orbit mode comparison of these cases show that the $M_D = 2$ parachute system provides the best overall performance. The direct mode comparison again shows the all-retro system best with the $M_D = 2$ parachute system showing best aerodecelerator performance only at the shallower γ_E. The superimposed launch vehicle capability shows, once again, that the Titan IIIC/Centaur is the only launch vehicle that satisfies these examples. It was noted above that the launch vehicle capability shown is for the optimum 30-day launch period. The Titan IIIC/Centaur capability for the combination of $C_3 = 30$ (km/sec)^2 and $V_{HE} = 3.5$ km/sec used in the targeting analysis in a previous subsection is 2360 lb for the orbit mode and 4360 lb for the direct mode.

This capability is still higher than that required for the examples shown in figure 15. (It is noted here that all of the quoted launch vehicle performance is based on a useful in-orbit orbiter weight, no propulsion system, of 890 lb.) The required aeroshell diameters for the examples shown in figure 15 are shown in figure 16. It is seen that the orbit mode requires diameters less than 12 ft while the direct mode diameters are generally 16 ft or less.

A more detailed summary for the $M_D = 2$ parachute system with monopropellant verniers is shown in figure 17. The basic data is presented as total capsule system weight, W_{CS}, versus entry flight path angle, γ_E, at constant values of landed equipment weight, W_{LE}. These characteristics are shown for both the Orbit and Direct Modes. These data show the sensitivity to design entry flight path angle that exists for the Direct Mode. The required aeroshell diameters $\left(\text{maximum } W_{LE} \text{ envelope}\right)$ are superimposed for reference as are the optimum 30 day launch period vehicle performance capability for each of the vehicles considered. Also superimposed are two Orbit Mode and one Direct Mode point designs which are discussed in the next section of this report.

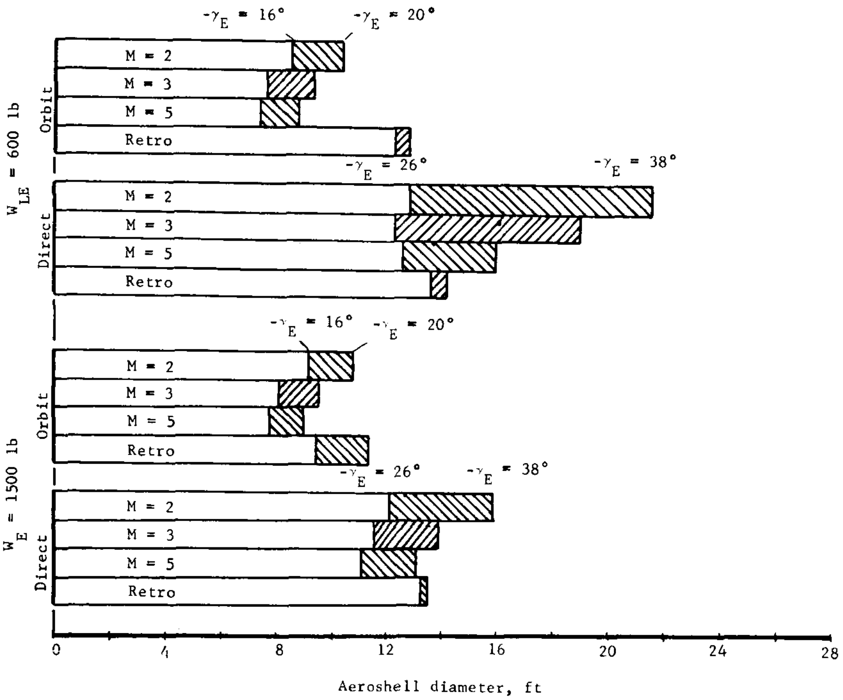

Figure 16.- Required Aeroshell Diameter, Maximum W_{LE} per Pound Entry

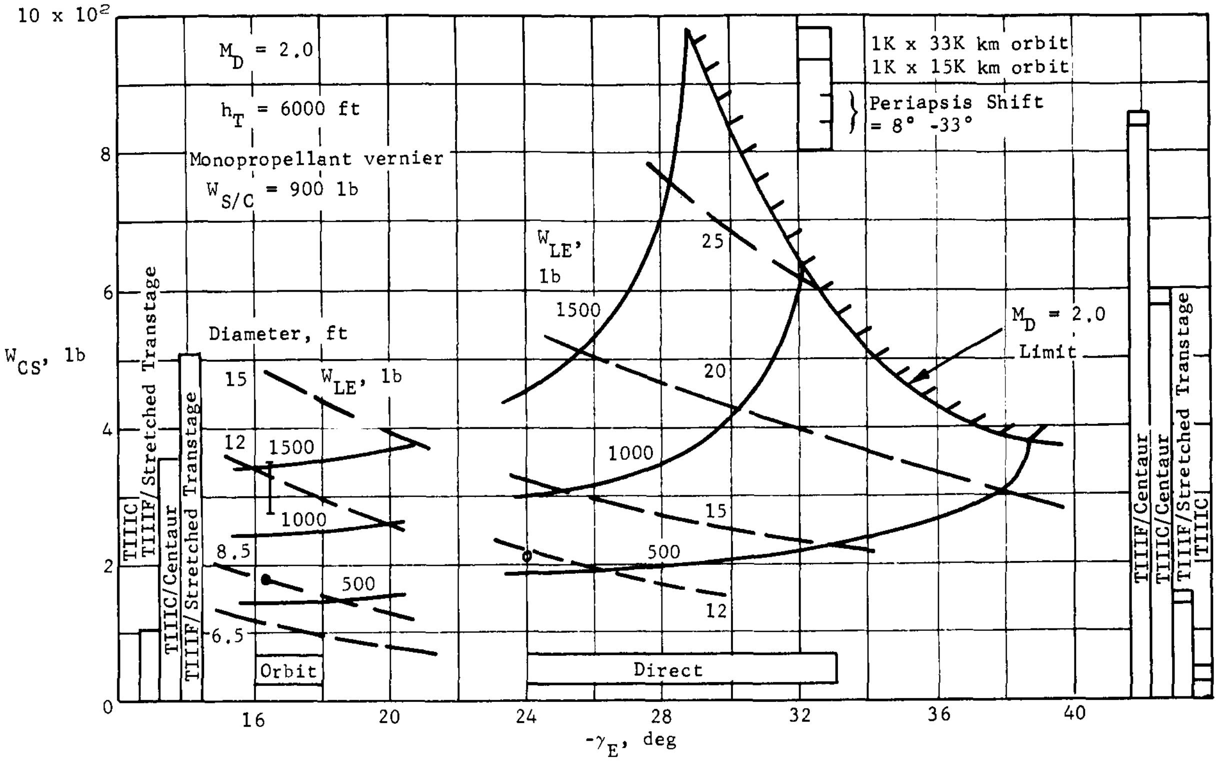

Figure 17.- Aerodecelerator Capsule System Weight Summary

The above comparisons illustrate that the differences between systems and modes are sensitive to the choice of criteria used to make the comparison. Other factors that must be considered are that the packaging and release characteristics for the subsonic type parachute system have to be easier than those for ballutes, particularly when a requirement on the aerodecelerators is that they separate the payload from the aeroshell. The all-retro system performance must be such that it will effect aeroshell separation (not considered in this study) and is sensitive to thrust-to-weight ratio (throttling requirements).

4. CONCLUSIONS

The comparison of the mission modes based on the parametric performance studies discussed above is summarized with the following conclusions:

1) Both modes require the Titan IIIC/Centaur to deliver useful payloads of 600 lb and still have a useful orbiting science mission;
2) Idealized targeting capability of both modes is virtually identical. However, the additional flexibility of the orbit mode allows it to maintain landing site selection flexibility while still satisfying rigorous DSN tracking requirements and orbiting science desires;
3) The orbit mode entry corridors are less sensitive to uncertainties in the astronomical and physical constants (notably planet ephemeris) and have smaller touchdown point disperions;
4) Differences in entry environment are negligible, but will require more extensive aerothermodynamic testing for the direct mode to obtain the same confidence in the entry vehicle design;
5) Required aeroshell diameters are sufficiently close to maximum allowable within current 10-ft shroud to probably require some hammerheading. If this is done, the $M_D = 2$ parachute system is the best overall terminal phase system for the orbit mode. Use of the direct mode suggest an all-retro system, but this requires more detailed analysis of thrust-to-weight ratios as it relates to aeroshell separation, performance sensitivity, and engine throttling requirements.

The overall performance analysis suggests the orbit mode with the $M_D = 2$ parachute/vernier terminal phase system as the combination that provides both total system weight efficiency and has the greatest potential for successful delivery of the landed science.

CONFIGURATION STUDIES

1. PREFERRED APPROACH

The preferred configuration of those examined in this study is based on a 10½-ft aeroshell diameter $\left(B_E = 0.35\right)$ and enters from orbit. This configuration is shown in figure 18. The landed equipment weight of 627 lb includes a 10% margin and provides for all of the entry and landed science specified for this study. The total system capsule weight of 1982 lb also includes a 10% margin on all systems. The entry ballistic coefficient of 0.35 permits deploying a Mach 2 parachute 20 000 ft above the mean surface level when operating in the worst of the VM atmospheres (VM-8). This combination of performance provides sufficient time on the parachute to permit landing on the maximum terrain height examined in this study -- 6000 ft.

The goal of several weeks lifetime on the surface is met with the combination solar array/battery power system. Entry and the first two days of operation on the surface is guaranteed by silver-zinc batteries. During the first two diurnal cycles, imaging experiments are conducted and require the transmission of 10^7 bits of data via a relay link through the orbiter. Experiments beyond the second day are limited to weather-type information. The solar array and a nickel-cadmium battery are used as the extended-mission power source. These data are transmitted via a M'ary noncoherent S-band link directly to Earth.

The 5½-ft wide octagon landed configuration permits overall packaging densities as low as 32 lb/ft^3. The volume within the aeroshell is such that the lander and its legs can be easily stowed.

This configuration, used in conjunction with the 950-lb orbital spacecraft requires the Titan IIIC/Centaur launch vehicle. A 10½-ft diameter aeroshell requires a 12-ft diameter bulbous shroud on the launch vehicle. The capsule, orbiter, and shroud are shown integrated with the Centaur stage of the launch vehicle in figure 19.

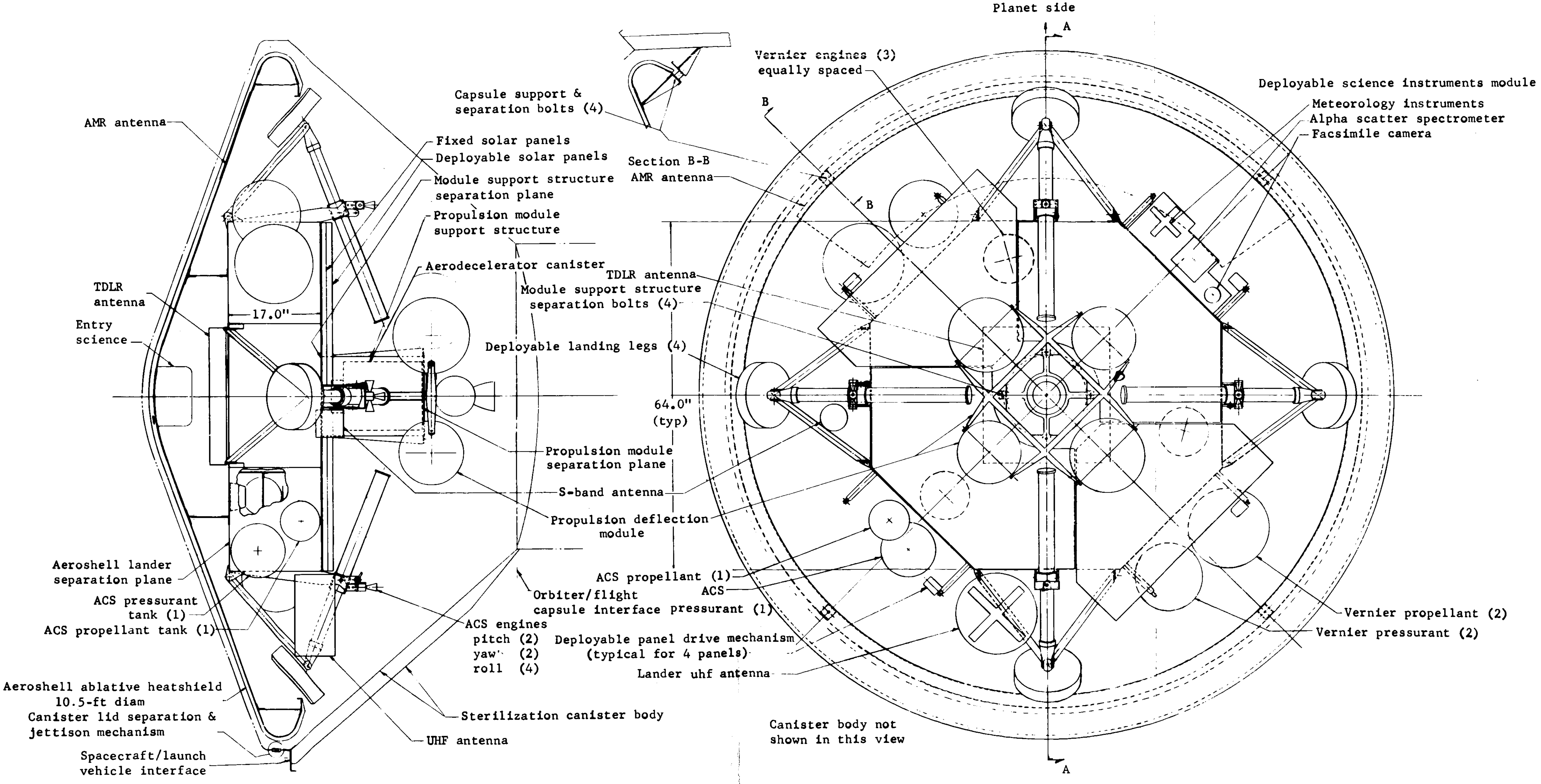
Planet side
A
A
Vernier engines (3)
equally spaced
Deployable science instruments module
Meteorology instruments
Alpha scatter spectrometer
Facsimile camera
Capsule support &
separation bolts (4)
B
B
Section B-B
AMR antenna
AMR antenna
Fixed solar panels
Deployable solar panels
Module support structure
separation plane
Propulsion module
support structure
Aerodecelerator canister
TDLR antenna
Module support structure
separation bolts (4)
TDLR
antenna
Entry
science
17.0"
Deployable landing legs (4)
64.0"
(typ)
Propulsion module
separation plane
S-band antenna
Propulsion deflection
module
Aeroshell lander
separation plane
ACS pressurant
tank (1)
ACS propellant tank (1)
ACS propellant (1)
ACS
Orbiter/flight
capsule interface
pressurant (1)
ACS engines
pitch (2)
yaw (2)
roll (4)
Deployable panel drive mechanism
(typical for 4 panels)
Lander uhf antenna
Vernier propellant (2)
Vernier pressurant (2)
Aeroshell ablative heatshield
10.5-ft diam
Canister lid separation &
jettison mechanism
Spacecraft/launch
vehicle interface
Sterilization canister body
UHF antenna
Canister body not
shown in this view

Figure 18.- Configuration 1B

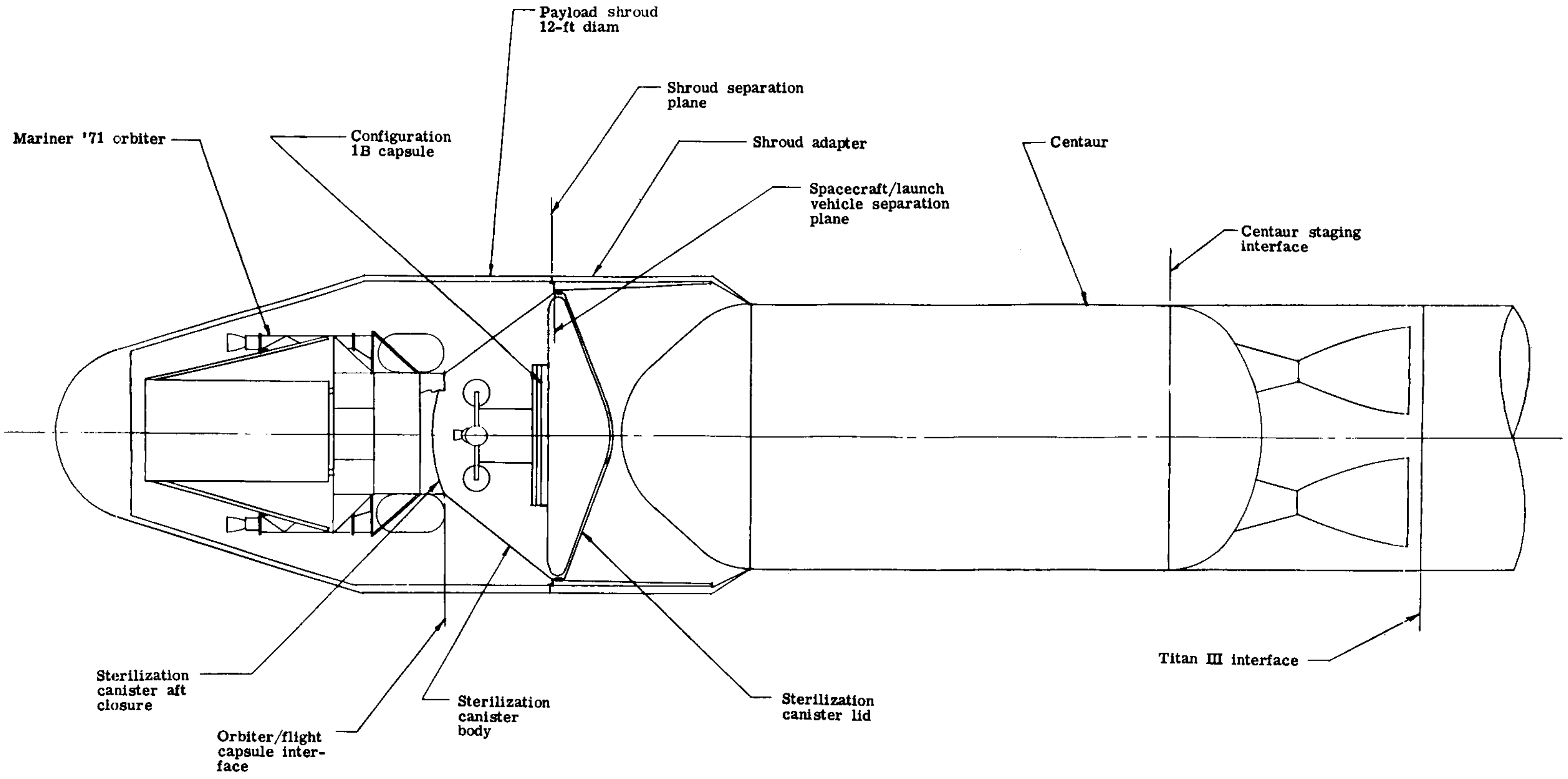
Payload shroud
12-ft diam
Shroud separation
plane
Mariner '71 orbiter
Configuration
1B capsule
Shroud adapter
Centaur
Spacecraft/launch
vehicle separation
plane
Centaur staging
interface
Titan III interface
Sterilization
canister aft
closure
Orbiter/flight
capsule inter-
face
Sterilization
canister
body
Sterilization
canister lid

Figure 19.- Space Vehicle Integration, Configuration 1B

It is pertinent to state that while this is the preferred configuration of those examined in the present study, before this recommendation is accepted for the '73 mission, further consideration should be given to the determination of the maximum diameter aeroshell that will go in the Titan IIIC/Centaur shroud and to the manner in which all design crieteria are supplied. In the present study, worst cases were added linearily, which is extremely conservative.

2. ALTERNATIVE CONFIGURATIONS CONSIDERED

The alternative configurations examined as point designs in the present study are shown in table 1. The preferred configuration described above is Configuration 1B. Configuration 1 options all enter from orbit, while Configuration 2 options enter directly from the approach trajectory. These sets of configurations were intended to represent capsule design associated with the first landings on Mars. All of them provide the stipulated science equipment and have a basic landed equipment weight of 570 lb. As noted earlier, Configuration 1B provides for a 10% margin above the present requirements. Configuration 3 was intended to represent a growth version for later missions. The landed equipment weight is almost 2½ times that of the other configurations.

Configuration 1A was developed to be identical in concept with Configuration 1B, but was constrained to fit within an 8½-ft diameter aeroshell. The basic systems without any margin for reliability considerations resulted in an entry ballistic coefficient of 0.47. In all other respects, the systems approach described for the preferred configuration is the same for this configuration.

The principal factors against this configuration are the packaging density requirements, and the landing gear stowage, and engine location problems. While this configuration was rejected as being too small in physical dimensions, particularly at this stage of the program, no attempt was made to examine slightly larger configurations that would also fit within the Titan IIIC/Centaur shroud. This should be examined as noted earlier.

TABLE 1.- PART II POINT DESIGNS

	1A	1B	2A	2B	2C	3
Landed equipment weight, lb	570	627	570	570	570	1345
Useful landed weight	845	970	914	914	950	1737
Capsule system weight	1723	1982	2077	2077	2281	3403
Mission mode	Orbital	Orbital	Direct	Direct	Direct	Orbital
Aeroshell diameter, ft	8.5	10.5	10.75	10.75	11.5	12.5
Entry flightpath/ angle, deg	18	18	24	24	24	18
Orbiter	950-lb Mariner	950-lb Mariner	950-lb Mariner	600 lb	Autonomous capsule	950 lb Mariner
Launch vehicle	TIII/C Centaur	TIII/C Centaur	TIII/C Centaur	TIIIF/ Stretched Transtage	TIIIC	TIIIC/ Centaur
Surface lifetome	$\geq$ 2 days	$\geq$ 2 days	$\geq$ 2 days	$\geq$ 2 days	$\geq$ 2 days	$\geq$ 6 months

Three configurations were examined for the direct entry case. Direct entry does, in fact, offer the potential of a smaller launch vehicle than the Titan IIIC/Centaur, but at the expense of orbital science. Configuration 2 options are all based on the same 570-lb landed equipment weight as Configuration 1A. Configurations 2A and 2B are identical insofar as the capsule design approach is concerned. The only difference between the two configurations lies in the orbiter. With Configuration 2A, the 950-lb Mariner spacecraft is used as the orbiter and provides the same orbital science that was used in the out-of-orbit configuration. Configuration 2B uses the same spacecraft, but with all of the orbital science and its support equipment removed. This reduction in weight permits the use of a smaller launch vehicle.

The most unique configuration examined in this study was the autonomous capsule approach (Configuration 2C). This approach varies significantly from the other configurations in that the trans-Mars orbiter and capsule functions are combined. That is, power, communications, and guidance functions during trans-Mars cruise that are provided by the orbiter in the other designs are, in this approach, provided by the capsule. This approach has the advantage of matching the performance capability of the existing Titan IIIC launch vehicle. It is the least well understood of the approaches, the most complex of the capsule designs, and the weights must be considered optimistic. Significant weight growth would undoubtably come with further study, in fact, the ability to stay within the Titan III capability would require more extensive examination before it could be assured.

3. CONCLUSIONS

The configurations that seem to merit the most consideration for the '73 opportunity are those including the capability for orbiter science, i.e., Configurations 1A, 1B, and 2A. A performance comparison of these configurations is presented in table 2, and a summary weight comparison is shown in table 3. The landed system approach in these three are identical, although a weight margin has been provided in the preferred approach. Either the direct mode or the out-of-orbit mission mode is feasible. The effects on capsule systems are slight in that the entry environments are not significantly different. As the Titan IIIC/Centaur is required for all of these configurations, and the capsules system are not significantly affected by the mission mode, the choice of the orbital mode was based on the mission flexibility considerations that are described in the previous section of the report. While the 10½-ft configuration is the preferred approach of those examined in this study, a statistical approach of the application of the design requirements and environments, and a more detailed examination of the shroud capsule interface may, in fact, provide the basis whereby the out-of-orbit mode can be accomplished within the existing Titan III shroud.

TABLE 2 - MISSION, SEQUENTIAL WEIGHT, AND SUBSYSTEM PARAMETERS, CONFIGURATIONS 1A, 1B, AND 2A

Parameter	Orbital		Direct
	1A	1B	2A
Mission			
Landing site survey before separation	Yes	Yes	No
ΔV deorbit/deflection, m/sec	120	120	75
Coast time (max.), hr	8	8	8
Targeting, deg			
β_{nom}	$^a31$ $^b34$	$^a31$ $^b34$	None
β_{min}	27 26.5	27 26.5	
β_{max}	35 43	35 43	
V_E, fps	$^a15\ 100$ to 14 400	$^a15\ 100$ to 14 400	19 900
q_{max}, lb/ft^2	250	180	380
g_{max}, ft/sec^2	18	18	34
Q, Btu/ft^2	1300	1000	1700
$\dot{q}$, Btu/ft^2 sec	20	15.5	42
q, parachute deployment, lb/ft^2	16	13	20
Time on parachute, sec	40	65	25
Vernier ignition altitude, ft	4000	4000	4000
$\gamma_{E\ max.}$, deg	-18 -16	-18 -18	-24 -21
Altitude of Mach 2, ft (above MSL)	13 000 16 000	20 000 20 000	11 000 15 000
Terrain elevation, ft	0 6000	0 6000	0 6000
Weight, lb			
Landed equipment	570	627	570
Useful landed	845	970	914
Landed	959	1095	1031
Verniered	1068	1209	1148
Entry	1383	1541	1699
Separated	1558	1741	1853
Capsule system	1723	1982	2077
Launch vehicle	TIIIC/Centaur	TIIIC/Centaur	TIIIC/Centaur
Structures			
Aeroshell			
Diameter, ft	8.5	10.5	10.75
Ballistic coefficient, sl/ft^2	.466	.35	.35
Structure weight, lb	72	102	163
Ablator weight, lb	44.5	56	83
Ablator thickness, in.	.68	.68	.82

TABLE 2. - MISSION, SEQUENTIAL WEIGHT, AND SUBSYSTEM PARAMETERS, CONFIGURATIONS 1A, 1B, and 2A - Concluded

Parameter	Orbital		Direct
	1A	1B	2A
Parachute			
Diameter, ft	65	48	71
Weight, lb	169	90	228
Base cover required	No	No	Yes
Landing slope capability, deg	32	32	32
Shroud diameter	10	12	12
Bulbous	No	Yes	Yes
Science	Entry atmospheric Surface atmospheric Surface imaging Surface composition		
Thermal control	Isotope heaters, insulation, phase change		
Propulsion - Deorbit	One 510-lb thrust, monopropellant engine, fixed thrust, 3:1 blowdown pressurization	One 635 lb[c]	One 540 lb
- Vernier	Three 510-lb thrust, monopropellant engines, 5:1 throttle ratio, 3:1 blowdown pressurization	Three 635 lb	Three 540 lb
ACS	3.7-lb pitch and yaw, monopropellant 2.2-lb roll, monopropellant		
Guidance and Control	IMU, TDLR, AMR, computer, sequencer		(d)
Telecommunications	UHF relay link Direct M'ary Command		
Power	Ag-Zn (2 days) Ni-Cd/solar array (2 days)		

[a] 1000 x 33 070-km orbit.

[b] 1000 x 15000-km orbit.

[e] Other than the propulsion thrust levels, all other subsystem parameters are the same.

[d] Additional and more sophisticated equipment on orbiter for approach guidance.

TABLE 3.- SUMMARY WEIGHT COMPARISON

	1A		1B		2A	
Total flight capsule	(1723)		(1982)		(2077)	
Canister	165		219		224	
Margin	----		22		----	
Separated weight	(1558)		(1741)		(1853)	
Propulsion and Structure	91		97		91	
Propellant and ACS	84		93		63	
Margin	----		10		----	
Entry weight	(1383)		(1541)		(1699)	
Aeroshell and ACS	128		197		258	
Science in aeroshell	18		18		18	
Parachute	169		90		228	
Base cover	----		----		47	
Margin	----		27		----	
Vernier weight	(1068)		(1209)		(1148)	
Propellant and ACS	109		114		117	
Landed weight	(959)		(1095)		(1031)	
Propulsion	114		125		117	
Useful landed weight	(845)		(970)		(914)	
Structure	156		168		222	
ACS	33		33		32	
Power	211	211	211	211	211	211
Guidance and control	131	131	131	131	131	131
Telecommunications	93	76	97	76	97	76
Thermal control	87	67	91	67	82	67
Pyrotechnic	49		54		54	
Science	85	85	85	85	85	85
Margin	----		100	57	----	
Weight of landed equipment		(570)		(627)		(570)

SUBSYSTEM STUDIES

Subsystem concepts and designs have been investigated by Martin Marietta for a Mars soft lander beginning with the Voyager Phase B studies and continuing with in-house studies through March 1968. These studies have been reexamined to identify the impact of the entry mode alternatives and the mission requirements imposed in this study. This section summarizes the results of the parametric analyses performed, the point designs investigated, and the preferred design. In general, only those elements that are affected by the entry mode or are new concepts dictated by the mission objectives are discussed in this summary.

1. SCIENCE SUBSYSTEM

Activity in design of the science subsystem covered three main areas. These were the selection of entry instruments using a statistical error analysis; a survey of the status of instrument technology to discover the critical development problems; and a review of work in sterilizable tape recorders to determine the feasibility of planning for this equipment within the Mars '73 mission schedule. Results of this work are summarized in this section.

Subsystem Description

A functional description of the preferred science subsystem is shown in figure 20. Equipment is arranged in blocks on the basis of logical grouping for planning purposes.

Instruments carried on the aeroshell include an open ion source mass spectrometer, a dynamic pressure sensor, and a total temperature sensor. These are mounted on a special plate carried at the apex of the aeroshell. These three instruments together with the accelerometer triad yield most of the data to satisfy the mission objective of obtaining atmosphere structure profiles.

During terminal descent there is an opportunity to measure atmosphere quantities by direct measurement. A group of three sensors comes into play to give temperature, pressure, and humidity readings over the lower few thousand feet of descent. These are important measurements since they provide an anchor point for the vertical structure profiles.

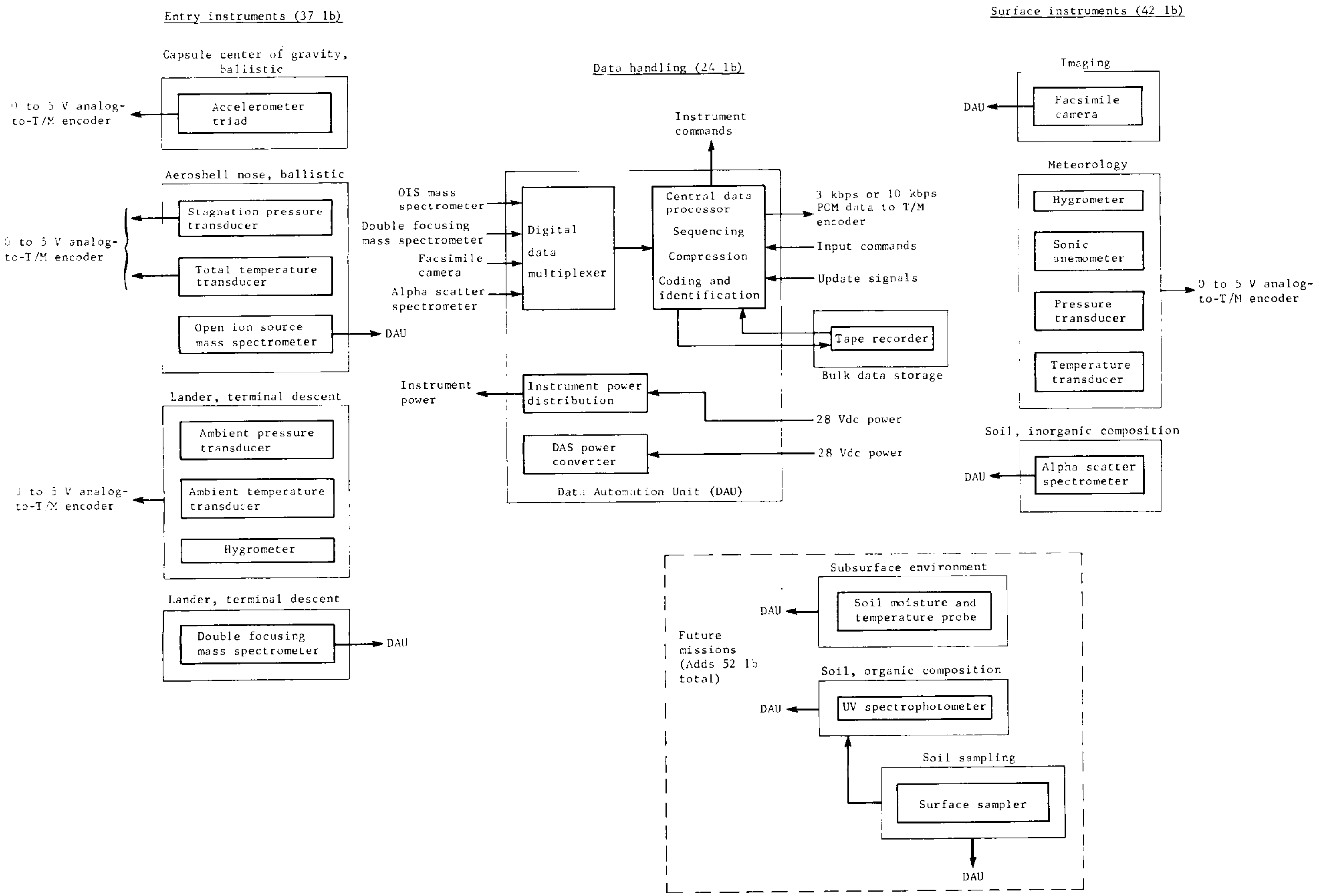
Entry instruments (37 lb)
Capsule center of gravity, ballistic
Accelerometer triad
0 to 5 V analog-to-T/M encoder
Aeroshell nose, ballistic
Stagnation pressure transducer
Total temperature transducer
0 to 5 V analog-to-T/M encoder
Open ion source mass spectrometer
DAU
Lander, terminal descent
Ambient pressure transducer
Ambient temperature transducer
Hygrometer
0 to 5 V analog-to-T/M encoder
Lander, terminal descent
Double focusing mass spectrometer
DAU
Data handling (24 lb)
Instrument commands
OIS mass spectrometer
Double focusing mass spectrometer
Facsimile camera
Alpha scatter spectrometer
Digital data multiplexer
Central data processor
Sequencing
Compression
Coding and identification
3 kbps or 10 kbps PCM data to T/M encoder
Input commands
Update signals
Tape recorder
Bulk data storage
Instrument power
Instrument power distribution
DAS power converter
28 Vdc power
28 Vdc power
Data Automation Unit (DAU)
Surface instruments (42 lb)
Imaging
Facsimile camera
DAU
Meteorology
Hygrometer
Sonic anemometer
Pressure transducer
Temperature transducer
0 to 5 V analog-to-T/M encoder
Soil, inorganic composition
Alpha scatter spectrometer
DAU
Future missions (Adds 52 lb total)
Subsurface environment
Soil moisture and temperature probe
DAU
Soil, organic composition
UV spectrophotometer
DAU
Soil sampling
Surface sampler
DAU

Figure 20.- Science Subsystem

Another approach to getting these data would be to use the instruments in the surface meteorology package. This is not done because of the complication introduced in mounting the surface assembly. Proper measurements during terminal descent require that sensors be located to sense free stream atmosphere. (This is most essential in the case of humidity measurements since very low frost points are expected.) If meteorology instruments are used during terminal descent they will have to be positioned for free stream measurements, thereby entailing extra mechanism and placing additional risk on successful deployment of the meteorology package after landing. By contrast, special sensors for the terminal descent measurements add little in cost and weight since they will be available from development of the surface instruments.

Composition is measured with a double focusing mass spectrometer after aeroshell separation. This instrument has been under development at JPL over the past two years. Composition readings during terminal descent together with data from high altitude measurement of neutral number density using the open ion source instrument provide the data necessary to construct a composition profile of the atmosphere.

After landing, a facsimile camera is extended for surface imaging. Meteorology instruments are deployed to measure atmosphere temperatures, pressure, humidity, and wind velocity and direction. Table 4 shows the data return from the surface instruments for a synchronous orbit.

Immediately after landing, one imaging wedge of 25° azimuth by 70° elevation will be transmitted in real time to the orbiter. This is a low-resolution picture (0.1°/line) and consists of about one million bits of data. Also, about 1000 bits of meteorology data will be transmitted at this time. During the following 24-hr period, three more low-resolution panoramic pictures and two high-resolution examinations are made and stored in the tape recorder. Also, the soil composition experiment will be completed and its data stored on tape. Meteorology instruments will be sampled periodically, their data being collected by solid core storage in the main telemetry subsystem. All stored science data will be relayed to the spacecraft at the end of the 24-hr period. The second diurnal period nets five more image scenes together with continuously recorded meteorology data. Total imaging from the two-day mission will be approximately 1.38×10^7 bits. This exceeds appreciably the required minimum return of 10^7 bits of imagery.

TABLE 4.- SUMMARY OF SCIENCE DATA RETURN

Data transmission period	Data transmission duration (min.)	Data transmission rate, bps	Data bits transmitted	Type of data
Entry, ballistic	150 sec	3000	150 000	Entry science
Entry, terminal descent	100 sec	3000	83 000	Entry science
Lander touchdown	6 min	3000	1 060 000	Imagery and meteorology
Touchdown + 24.6 hr	12 min	10 000	6 300 000	Imagery, meteorology and alpha scatter
Touchdown + 49.2 hr	12 min	10 000	6 600 000	Imagery and meteorology
Total imaging data = 1.38×10^7 bits				

All data from instruments having 0 to 5 V analog output are routed to the telemetry subsystem main data encoder. This includes data from most of the instruments (excepting the two mass spectrometers) in the entry science subsystem and the data from the meteorology package in the surface science subsystem. Those instruments that require sequencing commands, clock pulses, data conditioning, or other specialized signal interfaces are routed to the data automation system and are either put into storage in the magnetic tape recorder or may be routed directly to the main data encoder.

Error analysis. - The Kalman-Bucy minimum variance technique used by Martin Marietta in the USAF/PRIME program has been modified into a Mars entry atmospheric determination error analysis program. This program was used in the mission mode work to compare direct and orbital modes of entry for the effect on accuracy in determining the atmosphere structure profiles. It has also been used to study various combinations of sensors to determine the relative importance of different types of data and the sensitivity of structure determinations to instrument accuracies. A typical result is shown in figure 21.

Three combinations of sensors are compared on the basis of error in value of structure parameters at known altitudes. In one combination, the accelerometer triad and the altitude marking radar are used.

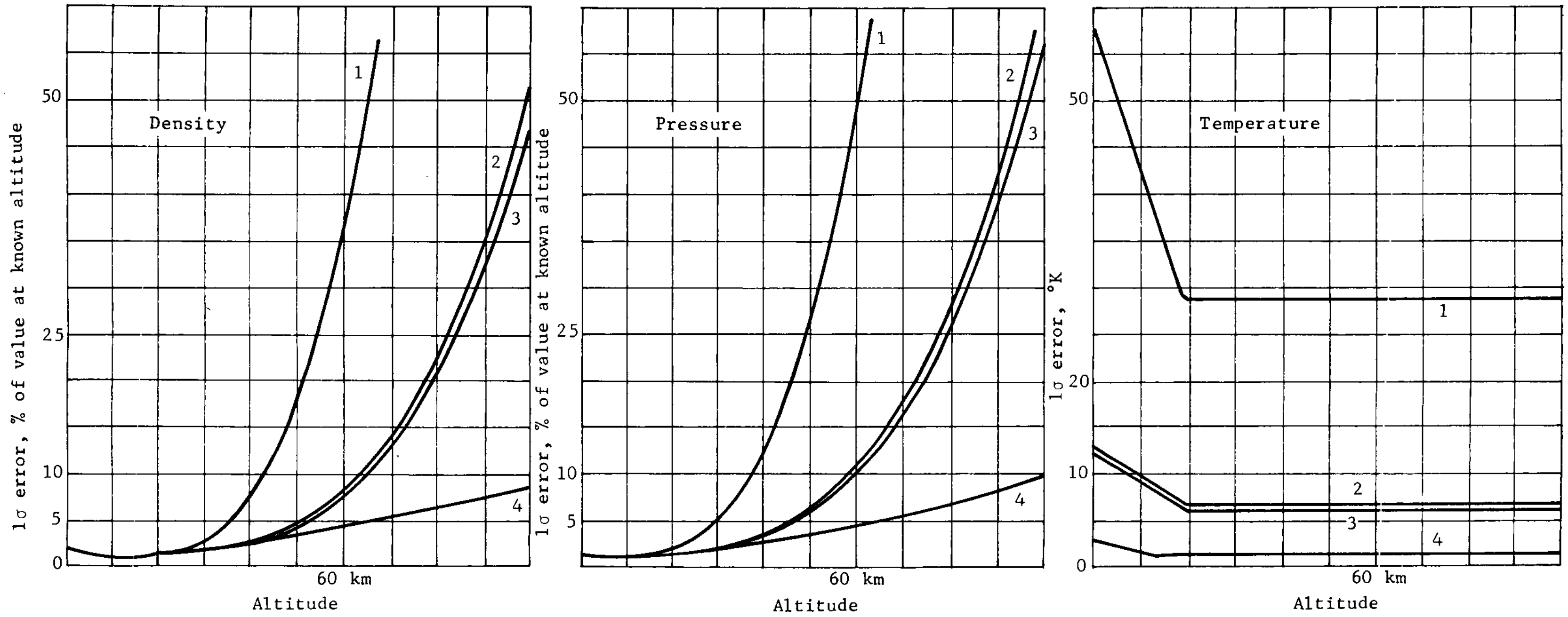

Legend:	
1	AMR, accelerometers
2,3*	AMR, accelerometers, dynamic pressure
4	AMR, accelerometers, OIS mass spectrometer

*Entry from orbit.

Measurement	Accuracy, %	Sampling rate, per sec	Availability, km
Accelerometers	3	1	60 to 8
AMR	2	1	60 to 8
Dynamic pressure	2	1	60 to 8
OIS mass spectrometer	10	5	140 to 70

Figure 21.- Results of Entry Error Analysis, VM-8 Atmosphere

A second grouping includes accelerometers, dynamic pressure, and altitude marking radar. In the third combination an open ion source mass spectrometer is used with accelerometers and radar to add a direct measurement of density from 100 km down to 70 km. Curves in one case are shown for both direct entry and for entry out of orbit.

Results given in figure 21 lead to the following conclusions: (1) the mode of entry does not have a significant effect on the accuracy of atmosphere structure determination; (2) direct measurement of density at high altitudes makes a significant contribution to obtaining accurate structure profiles from entry data; and (3) a total temperature sensor does not play an important role in providing data for atmosphere reconstruction. The open ion source mass spectrometer has a sensitivity threshold far below those of acceleration and dynamic pressure sensors. This accounts for the flattening of the error curve when this instrument is included in the payload.

Instrument technology survey. - During 1968, Martin Marietta engineers have made over 35 visits to national laboratories, commercial organizations, and university groups to determine the technology status of candidate instruments for the '73 Mars lander. The general conclusion of this survey is that a payload of science instruments to meet the mission objectives can be qualified within the '73 mission schedule period. The prominent development problem is designing to withstand dry heat sterilization.

Three outstanding long-lead items are identified. These are the instruments for humidity and wind measurements and the open ion source mass spectrometers. Special attention was given to surveying the background technology from which the humidity and wind instruments will evolve. An aluminum oxide humidity sensor and a sonic anemometer were selected for two main reasons. First, they are mechanically simple; no moving parts are involved. This is a significant advantage considering the importance of inherent ruggedness and ability to withstand unexpected environmental extremes. Second, the sensor materials are stable at dry heat sterilization temperatures and exposure times. Thus, no serious problem in meeting sterilization requirements is expected.

Figure 22 shows the performance range required for a Mars surface hygrometer. This figure shows frostpoint as a function of specific humidity for the two extremes of surface atmospheric pressure given in the new nomograph models (NASA SP-8010). The range of present predictions was obtained from the Handbook of the Physical Properties of the Planet Mars (NASA SP-3030).

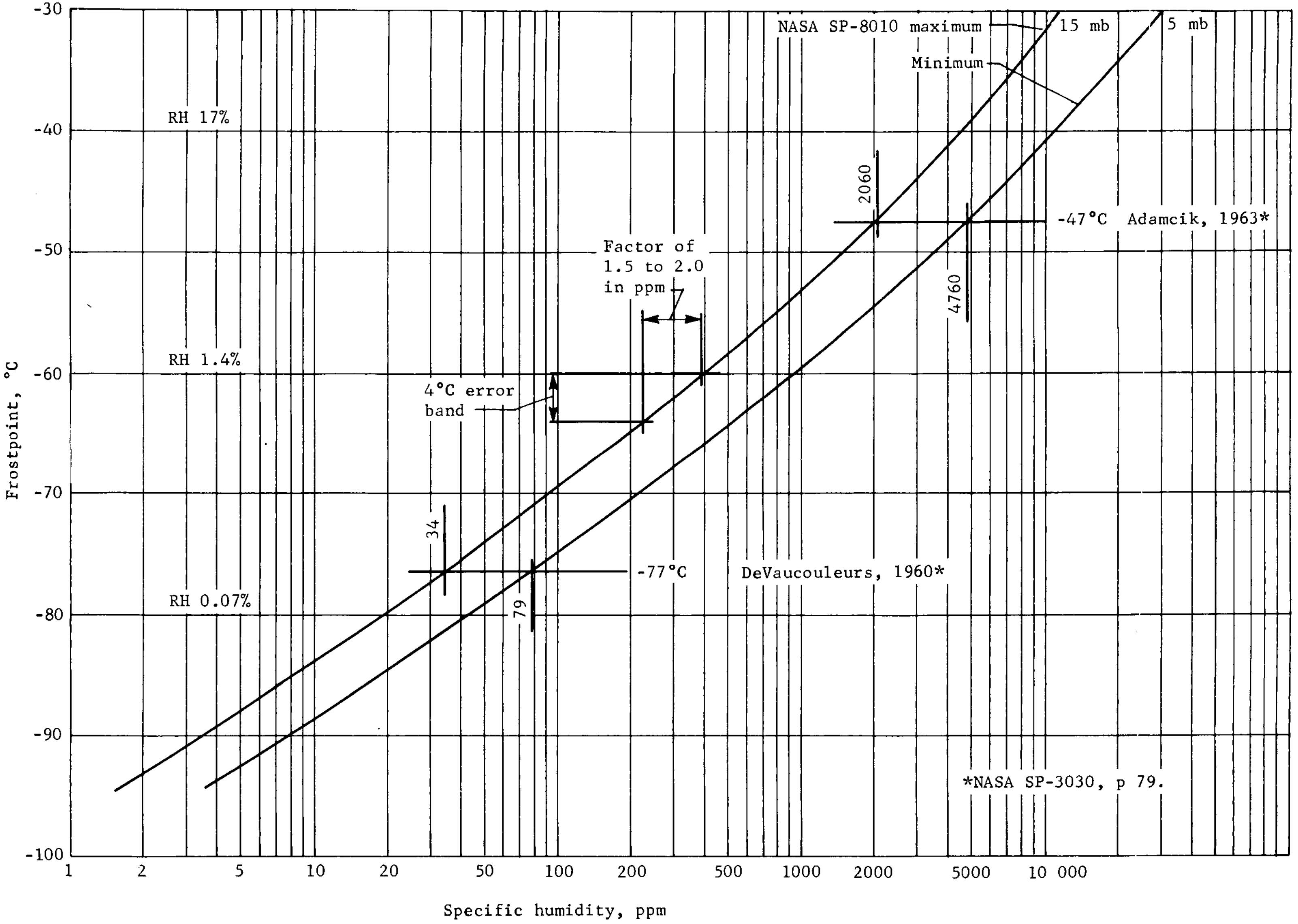

Figure 22.- Humidity on Mars

Frostpoint temperatures over this range are equivalent to those found in the Earth's atmosphere from balloonsonde measurements through the stratosphere. The aluminum oxide hygrometer has a record of successful performance in this application.

For purposes of this study, a facsimile camera was selected as the imaging instrument. This device is in an advanced stage of development due to NASA work carried out over the past seven years. The most significant advantages of a facsimile camera over a vidicon instrument for Mars surface imaging are: (1) small size, light weight, low power, and inherent ruggedness because the system looks at only one resolution element at a time and the sensor is a small solid-state device; (2) no distortion of the image near extremes of the format since optical geometry is identical for each resolution element; (3) no field of view restriction, making it possible to reproduce a panoramic scan without the need for mosaic overlay of adjacent images; and (4) the instrument is not damaged by direct viewing of sunlight. One disadvantage of the facsimile camera is loss of resolution if there is motion of the lander during imaging. Work now being planned for a variable parameter camera aims toward frame times as low as 1 sec to help reduce this problem.

Requirement for a tape recorder. - The need for a tape recorder in the data handling system was given special consideration. Under favorable conditions of landing and orbiting it is possible to accomplish the '73 Mars mission objectives and meet the science requirements without bulk storage of imaging data. However, this approach to mission design leaves little margin for recovery from an unplanned event that would place the landing site in a position of darkness relative to the relay communication link. A tape recorder is included in the science subsystem concept. The need is established because of the loss of flexibility in mission planning and operations imposed by the constraint of real-time transmission of imaging data.

To illustrate the point, figure 23 shows the relay link opportunities occurring for two possible orbits. For the synchronous case the planned landing point is 30° from the evening terminator. The spacecraft passes within relay link range of the lander at the same time each day. All imaging data taken and transmitted in real time will, therefore, be obtained with the same sun angle. Time separation of images during the day will require a tape recorder. Also, a recorder will ensure recovery of images in the event of a landing beyond the evening terminator.

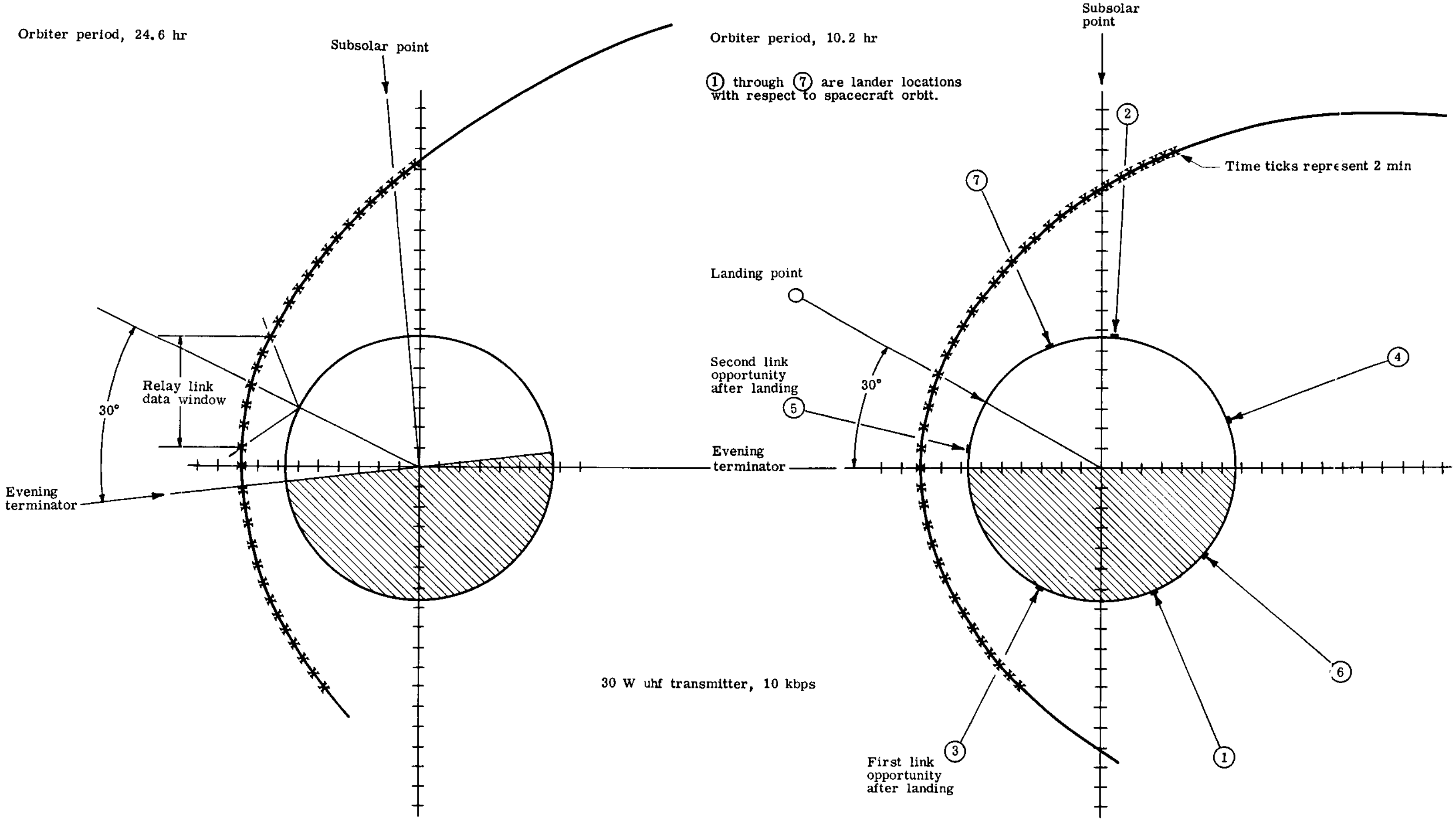
Orbiter period, 24.6 hr
Subsolar point
Relay link data window
30°
Evening terminator
Orbiter period, 10.2 hr
① through ⑦ are lander locations with respect to spacecraft orbit.
Subsolar point
②
⑦
Time ticks represent 2 min
Landing point
Second link opportunity after landing
⑤
30°
④
Evening terminator
⑥
③
First link opportunity after landing
①
30 W uhf transmitter, 10 kbps

Synchronous orbit (1000x33 070 km)

Nonsynchronous orbit (1000x15 000 km)

Figure 23. - Opportunities for Relay of Surface Images

For the 10-hr orbit in figure 23, the earliest opportunity to transmit real-time imagery is approximately 51 hr after landing. Contact may be made with the spacecraft on the third orbit but this occurs with the lander in the dark when no imaging is possible.

Based on information obtained from a survey of the tape recorder industry -- particularly from the contacts with Lash Laboratories, Memorex Corporation, and Leach Corporation -- it is our conclusion that a sterilizable tape recorder can be developed and procured for the '73 Mars mission.

The most important reason for this conclusion is that a required operating lifetime for the '73 lander recorder is only approximately 500 hr. This compares with operating lifetimes up to 10 000 hr, which are more representative for space tape recorders. The short operating time will work to advantage in many ways in developing a sterilizable unit. For example, the problem of excessive head wear from a metal-coated tape would not be expected to arise if only 500 hr of operation were required. The tape recorder is in the category of long-lead equipment.

Conclusions

The following are believed to be the most significant conclusions resulting from science subsystem work for the mission mode study:

1) Mission mode has no significant effect on accuracy of atmosphere determination from entry measurements;
2) Measurement of density and composition at high altitudes has been identified as essential in reconstructing atmosphere structure profiles from entry science data;
3) An adequate base of technology exists for instruments to meet the science requirements for a '73 Mars mission;
4) The capability for bulk storage of imaging data is required to provide flexibility for mission planning and operations without the constraint of real-time transmission during imaging. A sterilizable tape recorder can be developed within the '73 mission schedule to serve this function;
5) Science items identified as long-lead are the open ion source mass spectrometer, aluminum oxide hygrometer, sonic anemometer, and tape recorder.

2. STRUCTURES AND MECHANISMS

Preferred Configuration

Sterilization canister. - The sterilization canister is an all-aluminum pressuretight container enclosing the separable capsule. The entire spacecraft is supported through the canister by the shroud at the maximum canister diameter. The canister is opened at its maximum diameter to permit capsule separation.

Deorbit module. - The deorbit module structure consists of a beam assembly supporting the deorbit motor, the propellant tanks, and gas pressurant tanks. The module is attached at four points to an aluminum structural cylinder that also houses the aerodynamic decelerator system. The deorbit module is jettisoned immediately after the deorbit maneuver by separation springs following ignition of pyrotechnic release devices (fig. 18).

Aeroshell structure. - The aeroshell for this configuration is 10.5 ft in diameter and is constructed of aluminum skin and aluminum frames (fig. 18). This structural approach is heavier than one using beryllium or magnesium of the same geometry, but lighter than a fiberglas honeycomb. An 8.5-ft aeroshell diameter was also examined. However, at this diameter packaging densities required are marginal and there is a lander stowage problem. The landing leg foot pad is stowed much closer to the edge of the aeroshell for this configuration and results in the need for thermal protection, such as ablator to the bottom of the foot pad. fig. 24(a). This problem can be eased either by incorporating a more complex leg stowage mechanism, or by increasing the aeroshell diameter as was done for the preferred configuration.

An added problem of small diameter aeroshells is illustrated by the engine locations of the Configuration 1A lander, figure 24(b). The 8.5-ft-diameter aeroshell makes the lander octagon smaller (56-in. wide) for Configuration 1A compared to 64 in. for Configuration 1B. To keep the packaging density within the octagon reasonably low, the engines are located external to the octagon periphery. Spacing the three engines 120° apart brings one of them close to one of the leg assemblies, thus requiring thermal protection on the leg struts. This is also alleviated by going to a larger aeroshell diameter.

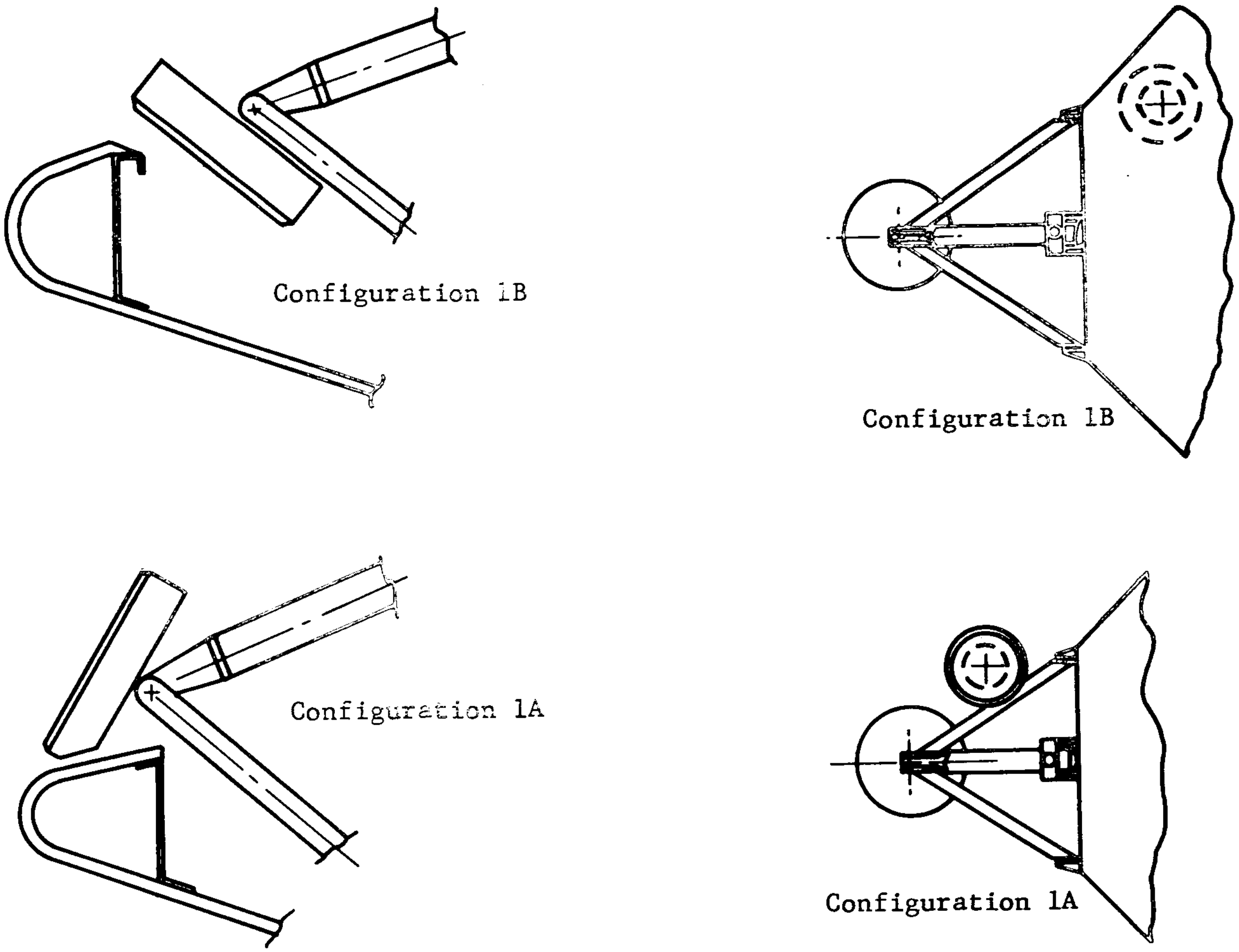
Configuration 1B
Configuration 1A
Configuration 1B
Configuration 1A

(a) Leg Stowage

(b) Engine Installation

Figure 24.- Leg Stowage and Engine Installation

Aerodynamic decelerator. - The 48-ft-diameter parachute and deployment mortar are housed in an aluminum cylindrical container inside the deorbit module support structure. A ring of shock-attenuating crushable honeycomb material installed between the mortar and the lander structure reduces the mortar reaction loads on the lander structure.

A harness assembly, consisting of four straps, attaches the aerodecelerator to the lander structure at the leg assembly support fittings. When the aerodecelerator is separated from the lander, the deorbit module support and spent mortar are also separated from the lander and carried away with the aerodecelerator.

Lander structure. - The lander body is an all-aluminum octagonal welded truss structure (fig. 25). More recent detail design studies have indicated the possibility of using titanium welded trusses to reduce heat losses through the insulation blanket.

Four Surveyor-type leg assemblies are used to attenuate the landing shock. A preliminary analysis shows this configuration will land stably on slopes to 32° with landing velocities of 25 fps vertically and 10 fps horizontally. The Surveyor fluid spring attenuator system was selected to assure that all foot pads would be in contact with the surface following landing, thus minimizing motion of the lander from wind loads on the deployed solar panels. The solar panels in this study were configured as aluminum honeycomb hinged to permit 70° upward and 40° downward rotation by stepping motors to improve exposure to solar radiation.

Parametric Studies

Parametric investigations in support of the study objectives included: (1) for direct entry, a study of methods for extending the aeroshell beyond the fixed 15 ft diameter imposed by the 16-ft booster shroud; and (2) a study of heat shield requirements for a range of V_E, γ_E, B_E, for both orbital and direct entry cases.

Aeroshell extension beyond 15-ft diameter. - Two concepts were investigated for extending the effective diameter of the aeroshell prior to entry: deployable rigid panels (flaps), and a continuous inflatable "airmat" extension. Figure 26 illustrates the percent of entry weight required for the basic aeroshell alone, or with either the flap or airmat extensions.

The basic aeroshell is an all-aluminum frame stabilized monocoque structure. The rigid flaps are aluminum honeycomb panels attached to two spars supported by links and hinges at the aeroshell periphery. A major problem associated with these flaps, other than the weight penalty illustrated in figure 26, is the increased length of the sterilization canister required to stow the rigid flaps.

The airmat is a textile product configured into a conical shape, internally pressurized to assure dimensional stability on entry. In addition to the inflatable cloth cone, the system uses gas, gas tanks, and plumbing. The inflatable airmat requires a flexible ablator such as Martin Marietta's PPA 1078 to permit folding and stowage of the mat in the aeroshell. Stowage of the mat with its ablator will be difficult and hard to control from a quality control aspect.

Heat shields for orbital and direct entry. - The primary characteristic required of the heat shield for a Mars out-of-orbit entry is that of a low density insulation. The SLA 561 ablator developed by Martin Marietta for Mars entry was analyzed as typical of such materials.

This analysis covered a range of entry velocities of 14 000 to 21 000 fps, entry flight path angles of -13 to -38°, and entry ballistic coefficients from 0.1 to 0.6 slug/ft^2. The unit ablator weight for the orbit mode is shown in figure 27 with the design entry parameters superimposed. Similar data are shown in figure 28 for the direct mode. The range of entry parameters for the direct mode is close to the design limits of the SLA 561. The limitation is the potential peak heating rate in excess of 100 Btu/ft^2-sec. The direct mode entry conditions are such that the criteria used for transition to turbulent flow is approached, giving rise to potential peak radiative heating rates greater than 100 Btu/ft^2-sec with the VM-4 atmosphere composition. Should this be verified by test, the heat shield material would have to be changed from the low density SLA 561 (14.7 lb/ft^3) to a higher density ablator such as ESA 5500M (58 lb/ft^3) to protect against the higher heating rates. The orbit mode entry environment is such that the SLA 561 ablator can be used with wide margins.

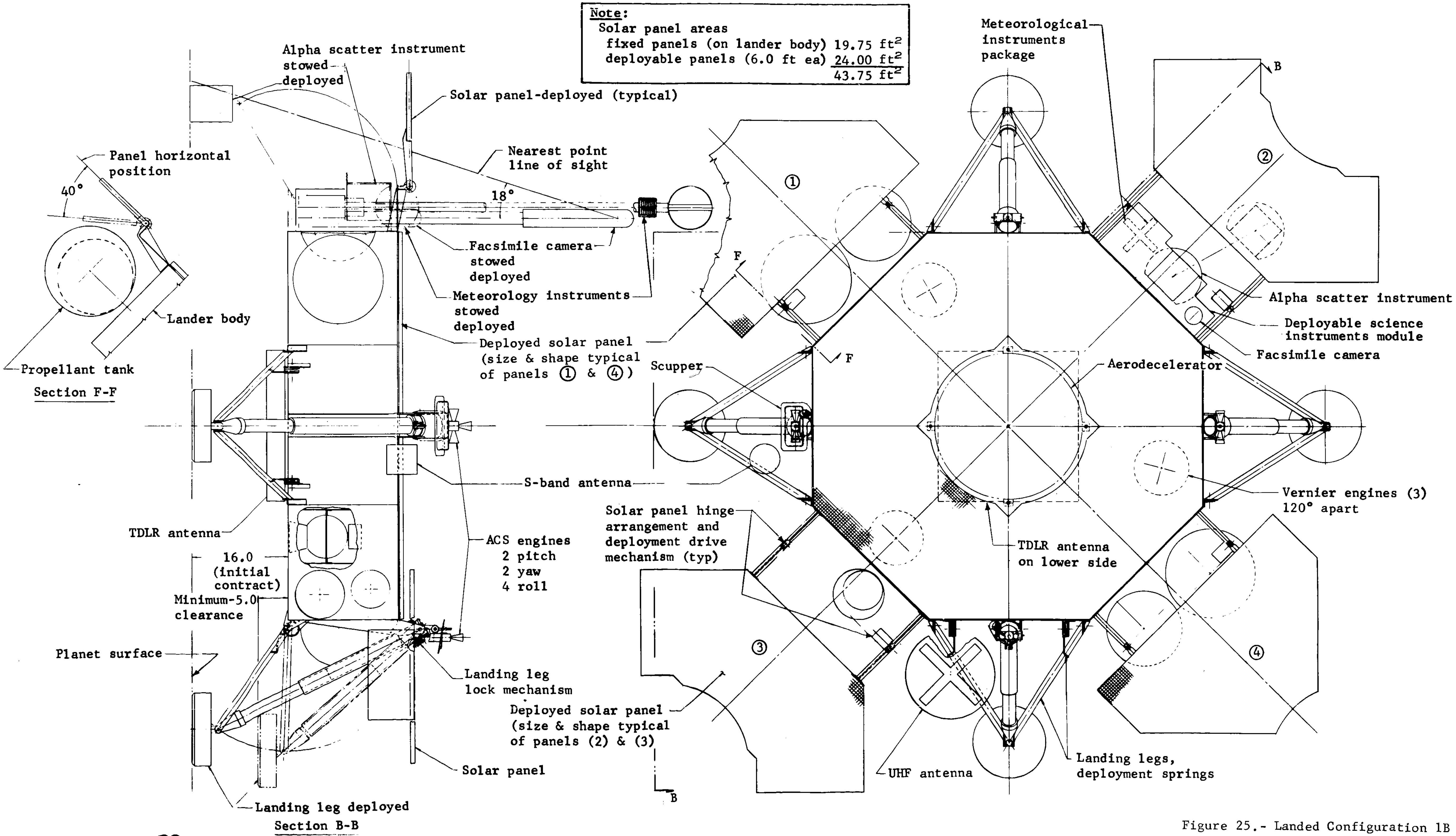

Note:
Solar panel areas
fixed panels (on lander body) 19.75 ft²
deployable panels (6.0 ft ea) 24.00 ft²
43.75 ft²
Alpha scatter instrument
stowed
deployed
Solar panel-deployed (typical)
Panel horizontal position
40°
Nearest point line of sight
18°
Lander body
Propellant tank
Section F-F
Facsimile camera
stowed
deployed
Meteorology instruments
stowed
deployed
Deployed solar panel (size & shape typical of panels ① & ④)
Scupper
S-band antenna
TDLR antenna
16.0 (initial contract)
Minimum-5.0 clearance
Planet surface
ACS engines
2 pitch
2 yaw
4 roll
Landing leg lock mechanism
Deployed solar panel (size & shape typical of panels (2) & (3)
Solar panel
Landing leg deployed
Section B-B
Solar panel hinge arrangement and deployment drive mechanism (typ)
Meteorological instruments package
B
F
F
①
②
③
④
Alpha scatter instrument
Deployable science instruments module
Facsimile camera
Aerodecelerator
Vernier engines (3) 120° apart
TDLR antenna on lower side
UHF antenna
Landing legs, deployment springs
B

Figure 25.- Landed Configuration 1B

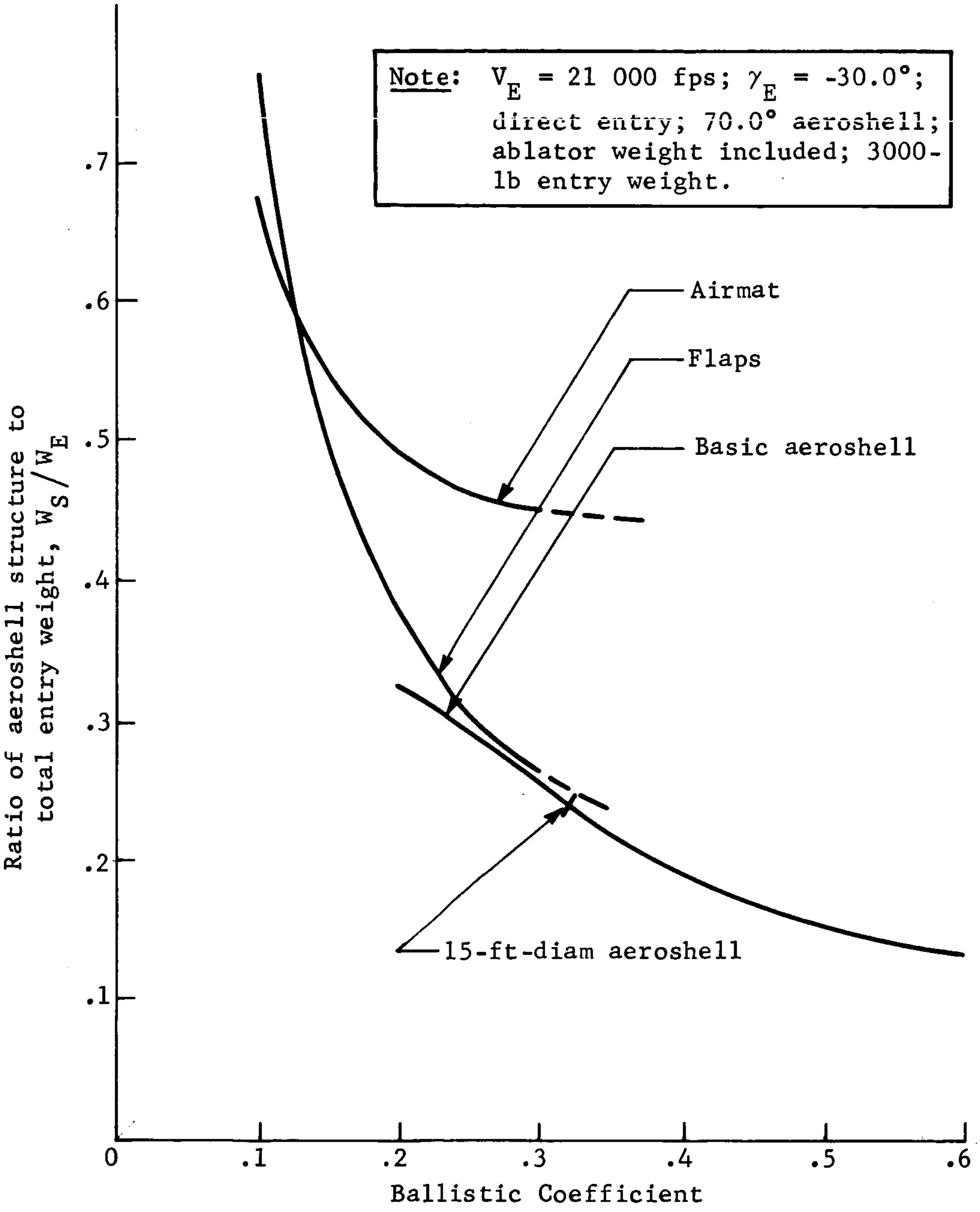

Figure 26.- Ratio of Aeroshell Structure to Entry Weight as a Function of Ballistic Coefficient

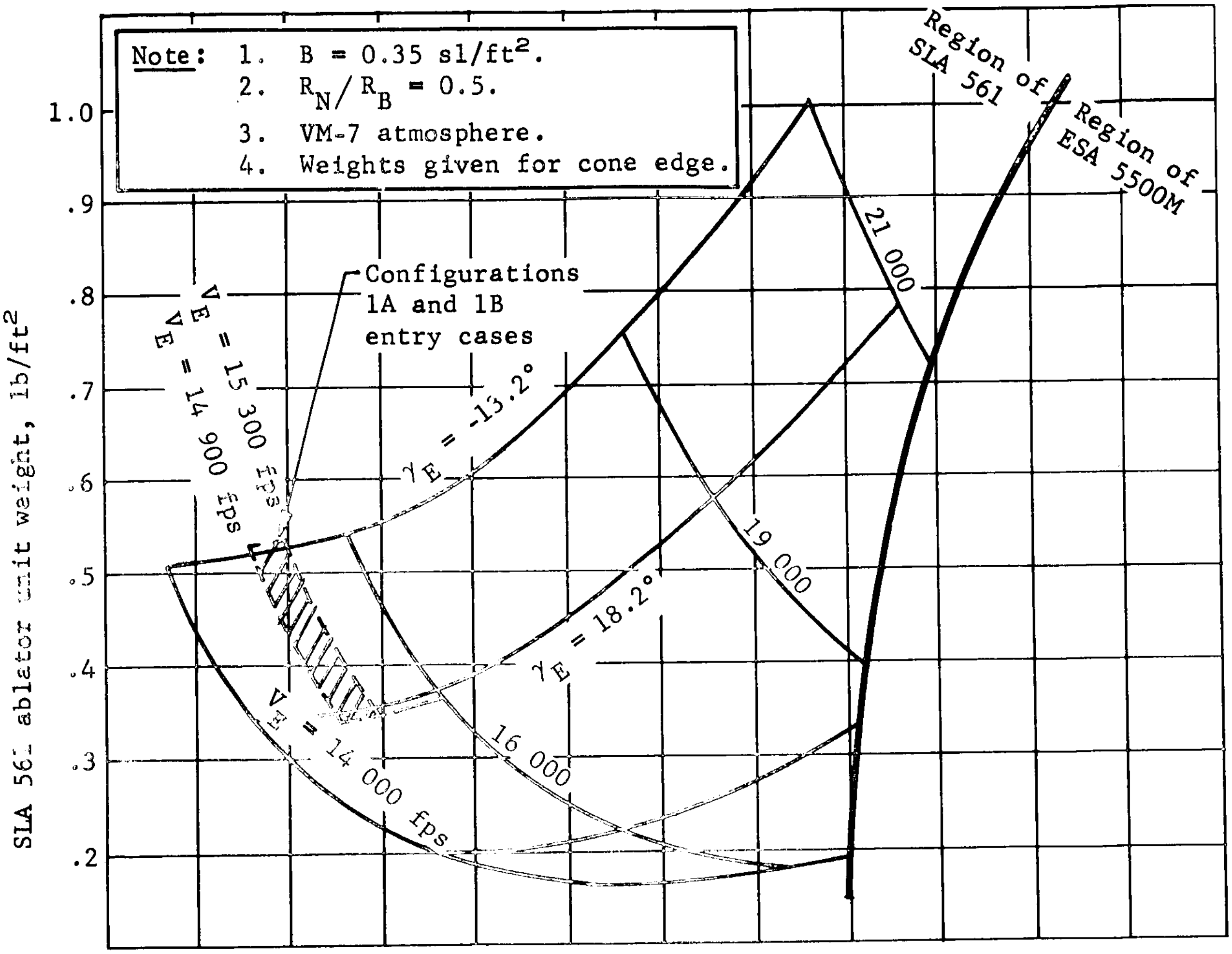

Figure 27.- SLA 561 Ablator Weight Variations, Orbit Mode

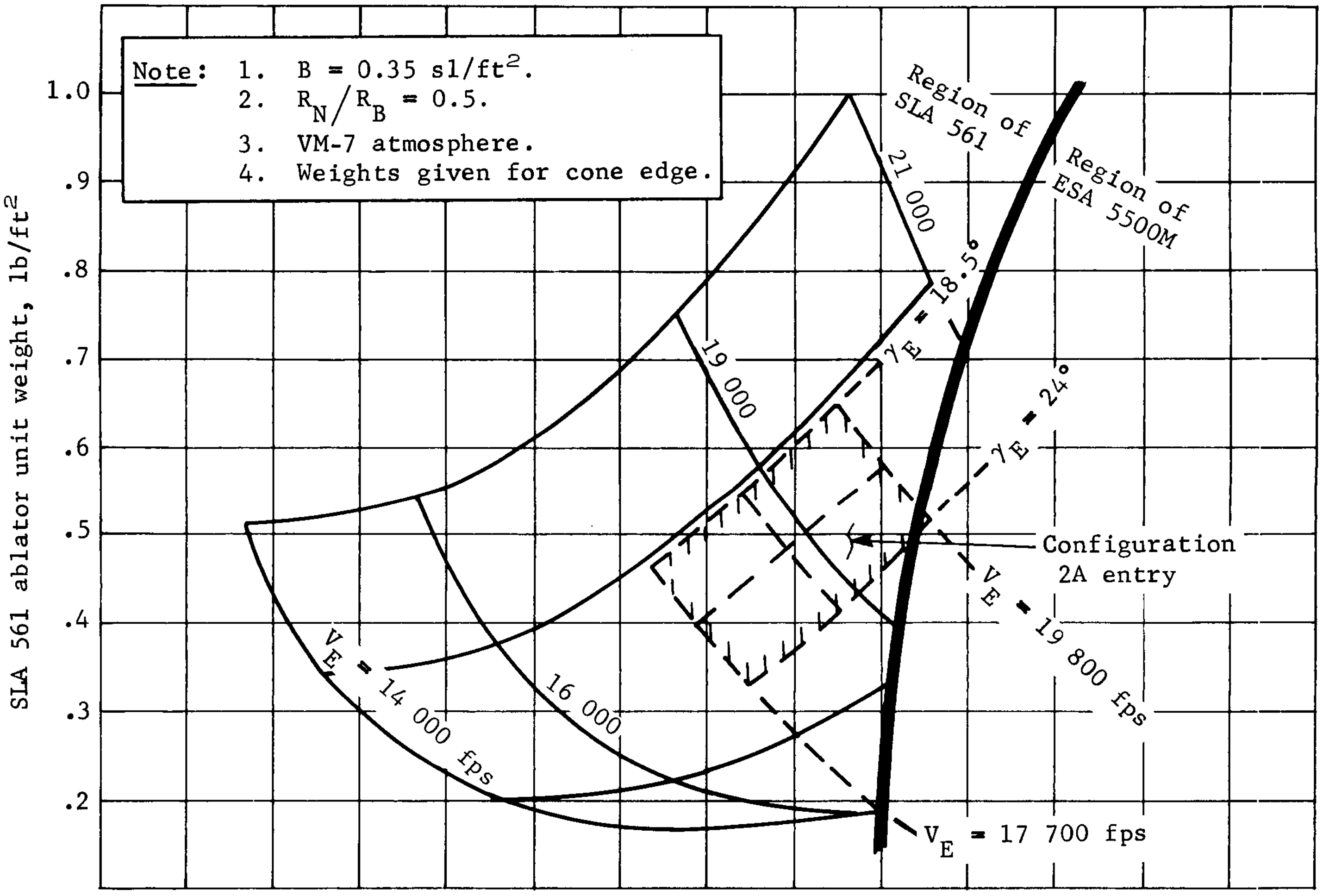

Figure 28.- SLA 561 Ablator Weight Variations, Direct Mode

Conclusions

The significant conclusions regarding structures and mechanisms are:

1) Either mission mode is within the state of the art;
2) The more severe environment of the direct entry mode is not a major consideration;
3) The 8.5-ft aeroshell is marginal from a packaging point of view;
4) More attention should be given to the packaging problem and to the capsule/orbiter/launch vehicle shroud problem to see if a bulbous shroud development can be avoided for the out-of-orbit mission mode;
5) Only small reductions in ballistic coefficient can be achieved with aeroshell extensions without paying a severe weight penalty. If extensions are required, rigid flaps are preferred.

3. PROPULSION SUBSYSTEM

Preferred Approach

The preferred propulsion configuration, shown in figure 29, features the following design choices:

1) Monopropellant systems were chosen over bipropellants for design simplicity;
2) Monopropellant systems are used for both deorbit and landing, thus only one engine development is required;
3) Sterile propellant loading simplifying operational problems with terminal sterilization;
4) Blowdown pressurization avoids the regulator reliability problems;
5) Nitrogen gas pressurant avoids the helium leakage problems.

Parametric Analysis

The preferred design is based on a series of trade studies; the weight results of these studies are summarized in figure 30. As figure 30 shows the selection of the type of entry mode has only a small effect on the weight of the propulsion subsystem (3 to 12%) and has no effect on the basic design of either the landing system or deflection system. However, design choices internal to the system have important effects.

Monopropellant and solid motor deorbit and deflection systems were compared; as shown in figure 30, the solid motor systems have a useful system payload weight advantage equivalent to 45 lb of payload; however, the cost of an additional motor development is incurred.

Regulated and blowdown pressurization subsystems were compared; blowdown pressurization, at a blowdown ratio of 3:1, is preferred to gas regulation because regulator failure modes are eliminated and a small weight advantage occurs.

Propulsion subsystem weight as a function of total impulse was derived for deorbit, deflection, retro, and vernier operations. The scope of the parametric study is shown in table 5.

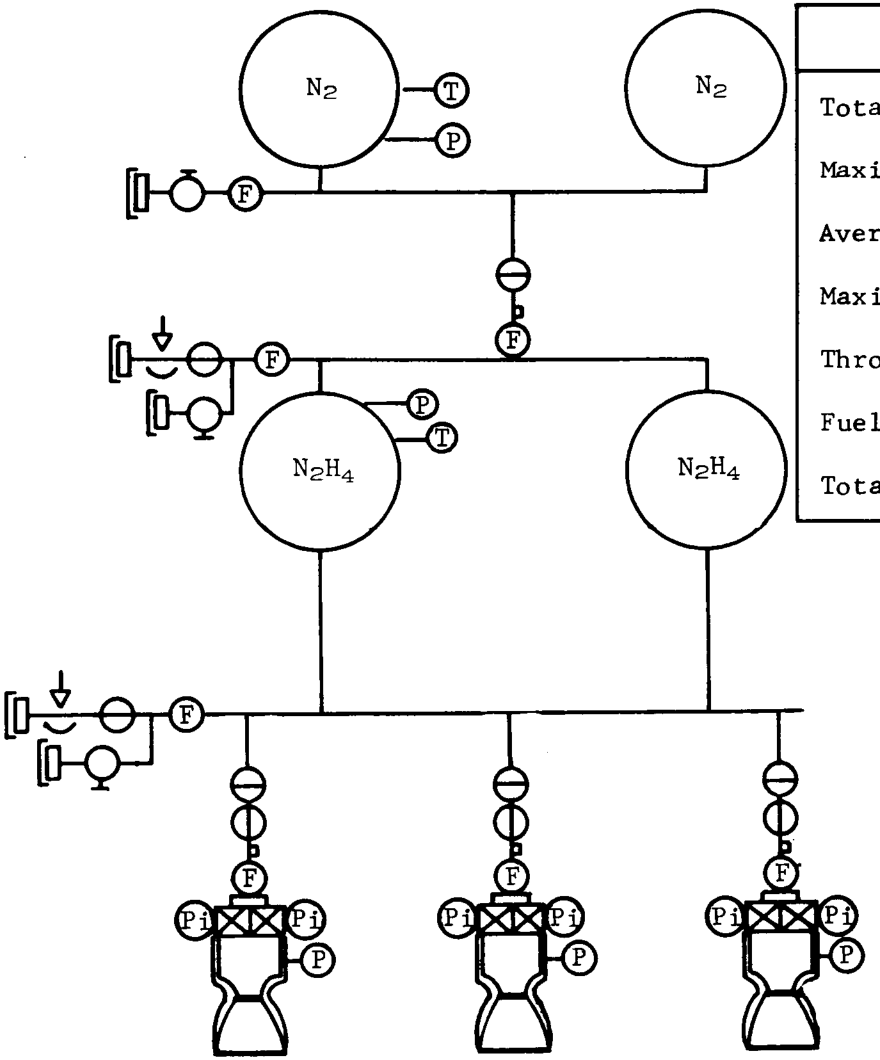

Parameter	Deorbit	Landing
Total impulse available, sec	21 292	25 200
Maximum trust per engine, lb	635	635
Average specific impulse	228	223
Maximum chamber pressure, psi	300	300
Throttling ratio	---	6.3:1
Fuel weight, usable, lb	89.0	113.0
Total weight, lb	152.7	233.8

Legend:

⦶	Ordnance valve (normally closed)
⊖	Ordnance valve (normally open)
⚲	Hand valve
⊠	Throttle valve
Ⓕ	Filter
Ⓟ	Pressure transducer
Ⓣ	Temperature transducer
⊥	Test port
↓	Tube cutter
[	Fill connection
(Pi)	Position indicator

Figure 29.- Landing Propulsion System

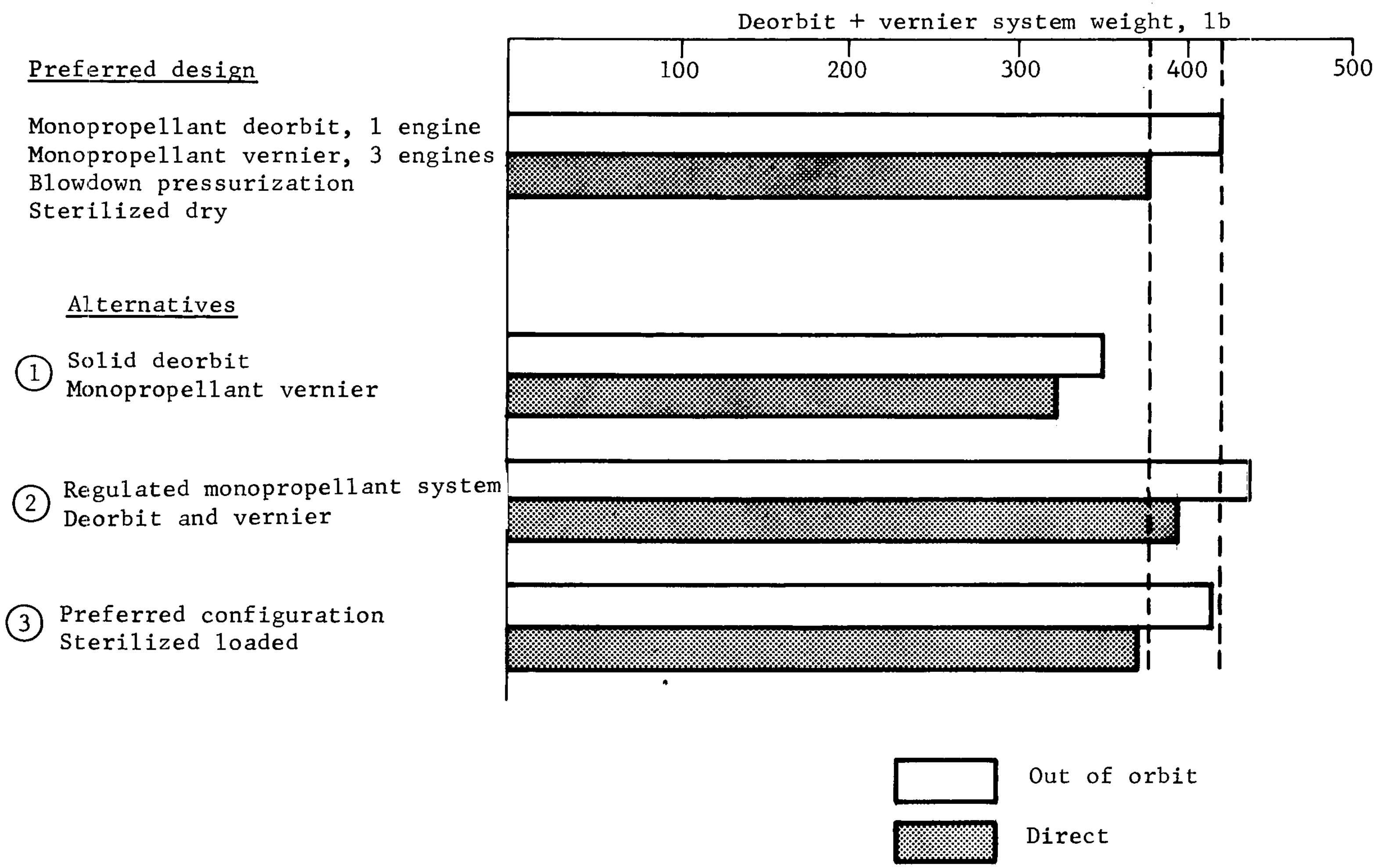

Figure 30.- Summary of Trade Studies

TABLE 5.- SCOPE OF PARAMETRIC PROPULSION STUDY

Function	Type	Total capsule weight, lb	Required velocity change
Deorbit and deflection	Solid, monopropellant, bipropellant	500 to 10 000	50 to 610 m/sec
Retro	Monopropellant, bipropellant	400 to 8 000	150 to 160 m/sec
Landing	Monopropellant	300 to 6 000	600 to 850 fps
Two-burn retro	Solid	1500 to 6 000	910 to 1530 m/sec

Typical study results are shown in figure 31, which shows propulsion system weight as a function of total impulse for the three types of propulsion systems considered. The monopropellant and bipropellant systems are essentially the same weight in the preferred design range and solids are the most efficient system.

Conclusions

The significant conclusions for the propulsion subsystem are:

1) The propulsion subsystem design is virtually unaffected by the choice of mission mode;
2) The preferred design results in weight, cost, and reliability gains;
3) The throttling monopropellant engine is a long lead item.

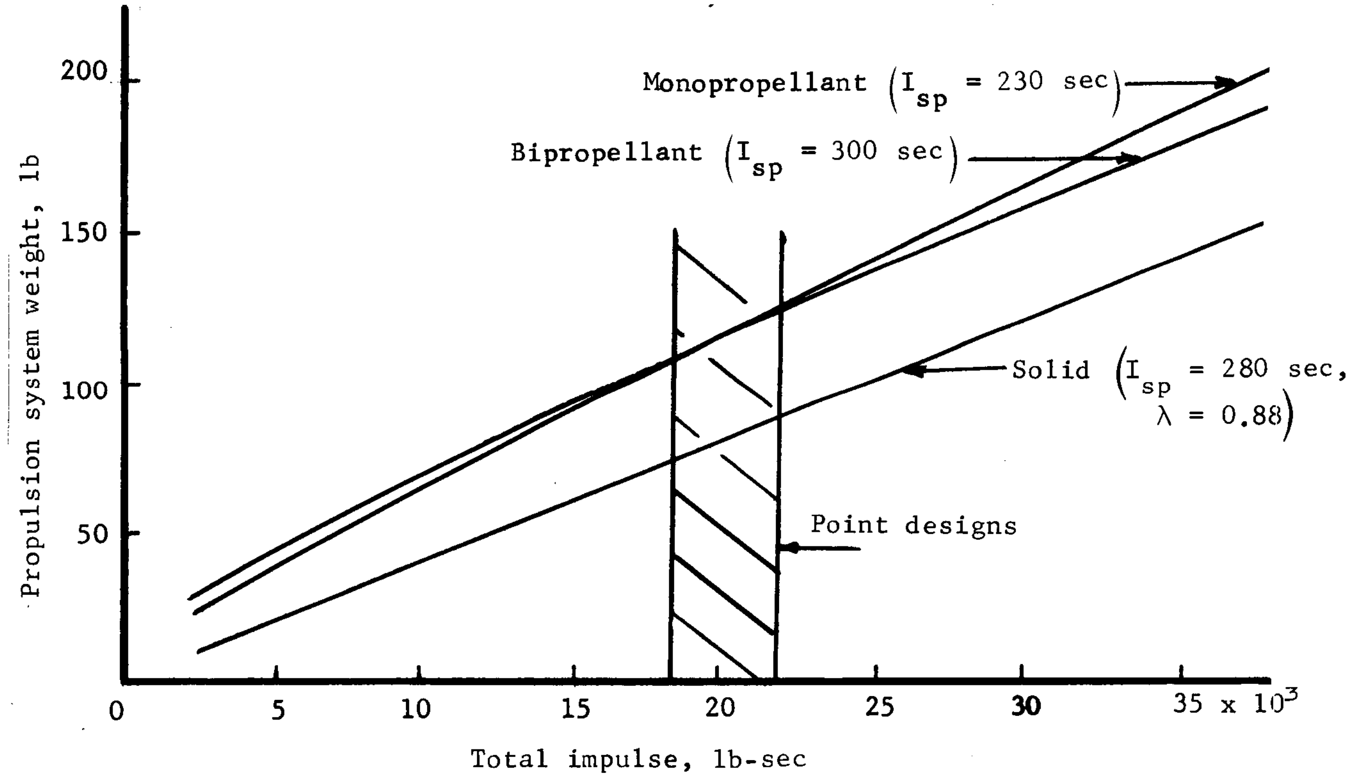

Figure 31.- Propulsion System Weight versus Total Impulse

4. GUIDANCE AND CONTROL SUBSYSTEM

Preferred Approach

The guidance and control subsystem contains equipment that performs three major functions. They are:

1) Inertial guidance and control for orbital coast, deorbit, and entry phases;
2) Velocity, altitude control, and attitude control during the vernier phase;
3) Capsule system and science sequencing.

The subsystem components as shown in figure 32 are the inertial measurment unit (IMU), the guidance and control computer (GCC), the altitude measuring radar (AMR), the terminal descent and landing radar (TDLR), and the Phase II sequencer required to control the long-term weather station experiments. The IMU and GCC provide the inertial attitude and velocity control required before the aerodynamic entry phase. During entry the IMU provides attitude rate for capsule damping control. During the vernier phase the TDLR is used with the GCC to cause the vehicle to follow a preprogramed descent contour, as shown in figure 33. The IMU is again used for control system damping. The GCC provides the primary capsule and entry science sequences. The IMU and the AMR provide acceleration data and altitude data to the GCC. These data are used to initiate the entry phase, the parachute phase, and other discrete capsule events. After landing, the GCC provides the Phase I science sequence and initiates the Phase II sequencer. The Phase I sequence can be started or reprogramed by earth-based command. Table 6 summarizes the performance characteristics of this equipment.

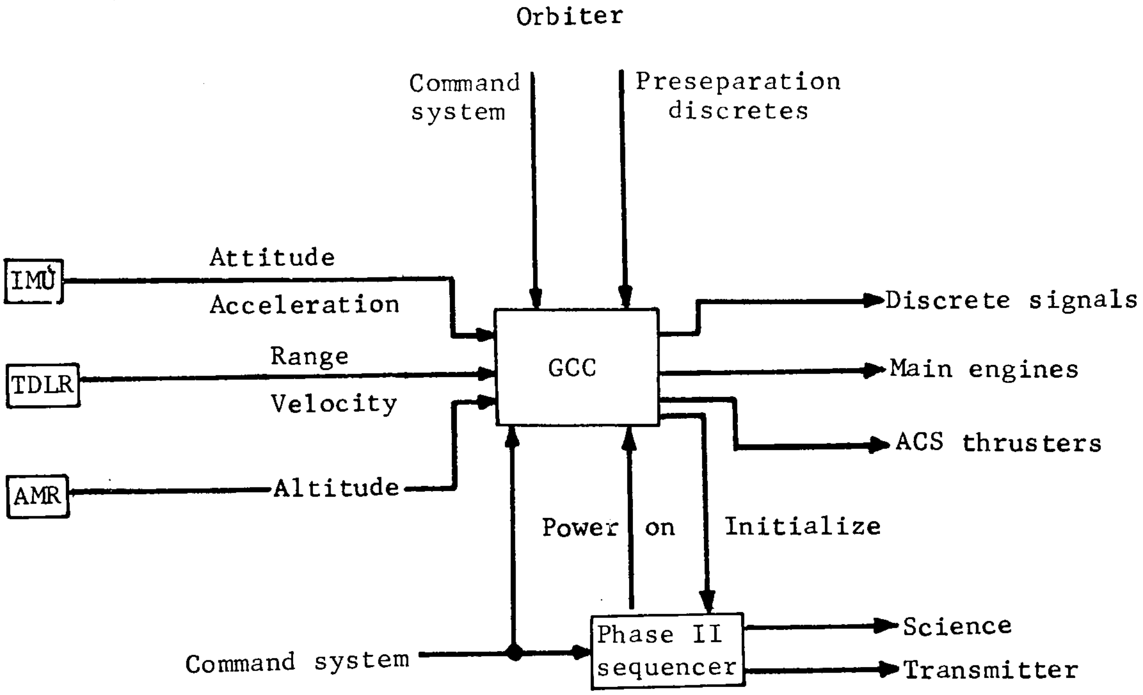
Orbiter
Command system
Preseparation discretes
IMU
Attitude
Acceleration
TDLR
Range
Velocity
AMR
Altitude
GCC
Discrete signals
Main engines
ACS thrusters
Power on
Initialize
Command system
Phase II sequencer
Science
Transmitter

Figure 32.- Guidance and Control Subsystem Block Diagram

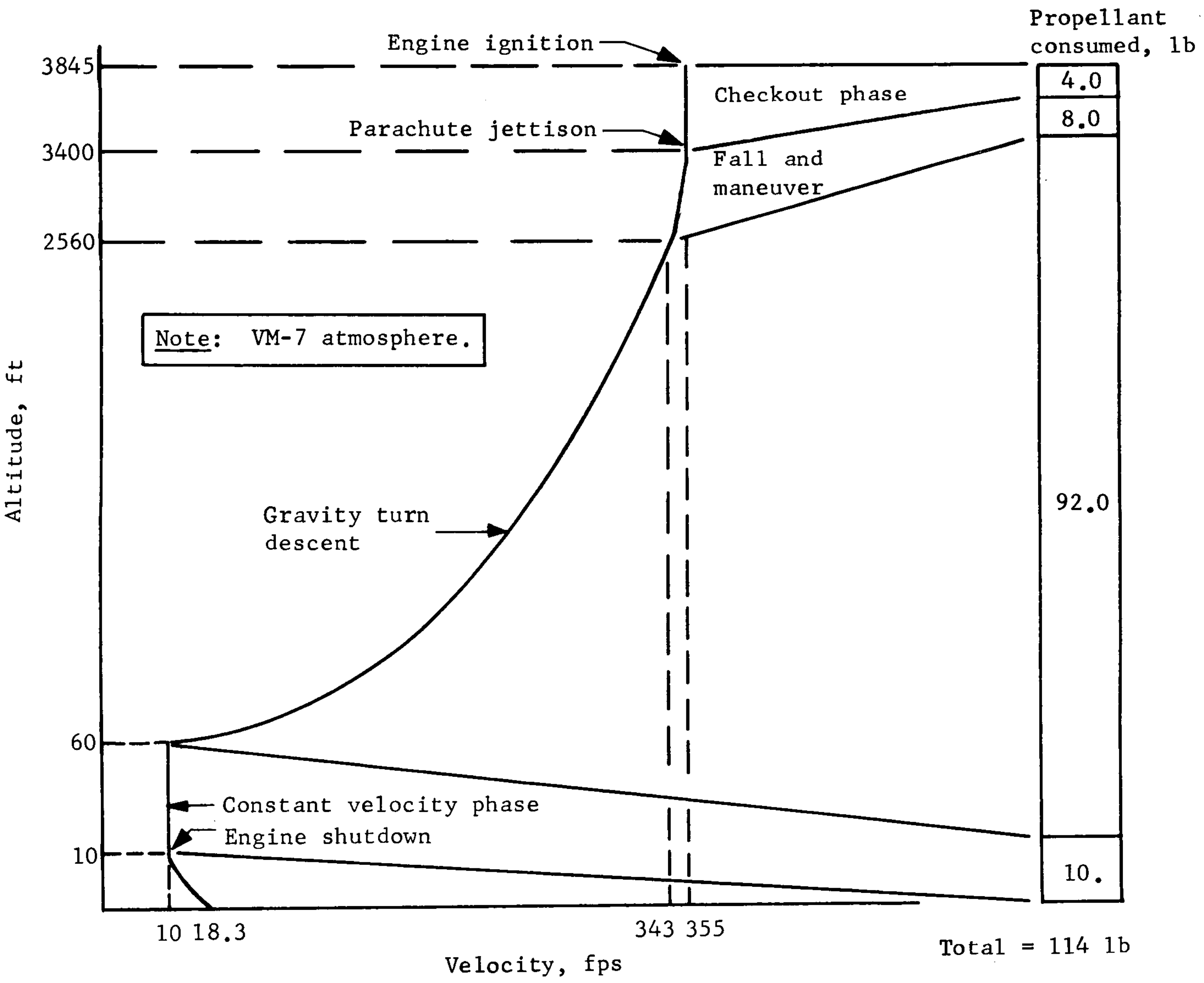

Figure 33.- Terminal Descent Profile and Propellant Utilization (Configuration 1B)

TABLE 6.- GUIDANCE AND CONTROL SUBSYSTEM CHARACTERISTICS

Component	Performance*	Weight, lb	Power, W	Status
IMU	----	22	39	Developmental
Three gyros	±0.22°/hr	----	----	----
Three accelerometers	±400 μ g	----	----	----
GCC	8 μsec add	42	41	Developmental
AMR	±120 ft	12	7	Developmental
TDLR				
Five range beams	3% or 5 ft	33	46	Prototype under contract
Five velocity beams	4.5% or 3 fps	----	----	
Phase II sequencer	----	3	3	State of the art
*Three sigma, where applicable.				

Parametric Analysis

The basic guidance and control equipment was not treated parametrically in this study because it is identical for either the direct or out-of-orbit mission mode. Two exceptional cases were considered: the autonomous capsule and configurations using planetary approach guidance. The autonomous capsule requires the addition of a sun-Canopus attitude reference and additional GCC capability to accommodate the spacecraft functions of the interplanetary mission phase.

For the direct mode, planetary approach guidance was studied to assess the feasibility of using onboard measurements to improve the trajectory uncertainty as the vehicle approaches the vicinity of Mars. If the trajectory uncertainty can be improved to under 37 km (1σ), the corresponding capsule entry angle dispersion will result in a maximum entry angle less than 24° (3σ). A greater entry angle will require larger diameter aeroshells for the direct mode capsules. The onboard system chosen for study consists of a sun tracker, a Canopus tracker, and a Mars tracker. The Mars tracker could also provide range to the planet by measuring the subtended angle of the image. Kalman recursive data filtering was used in the study. The conclusions from the study are:

1) The trajectory dispersion can be reduced to less than 37 km (1σ) in the critical direction without an accurate disc angle measurement. A typical case is shown in figure 33;

2) The sensors required (fig. 34) are within the state of the art;

3) The sensors should be a part of the orbiter equipment rather than the capsule equipment;

4) For the equipment to provide the accuracy data processing must continue to within 4 hr of the final velocity correction.

Conclusions

The guidance and control subsystem conclusions are:

1) The capsule guidance and control preferred approach is not affected by mission mode;

2) For lightweight 1973 capsules using the direct mode, an increase in aeroshell diameter is required unless trajectory uncertainty is less than 37 km (1σ). Weight growth beyond 1973 is not practical without this accuracy;

3) Measurements from a sun, star, and planet tracker mounted on the spacecraft can reduce the trajectory uncertainty to less than 37 km (1σ). These sensors are within the expected state of the art. Both the capsule entry corridor dispersions and the orbiter ephemeris errors can be improved by these measurements;

4) Of the equipment shown in figure 32, the long lead items are the IMU, TDLR, and AMR antenna. The IMU lead time is primarily caused by the sterilization requirement. The TDLR lead time is due to the extensive test program required and sterilization. The AMR antenna fabrication as an integral part of the aeroshell requires early development and testing.

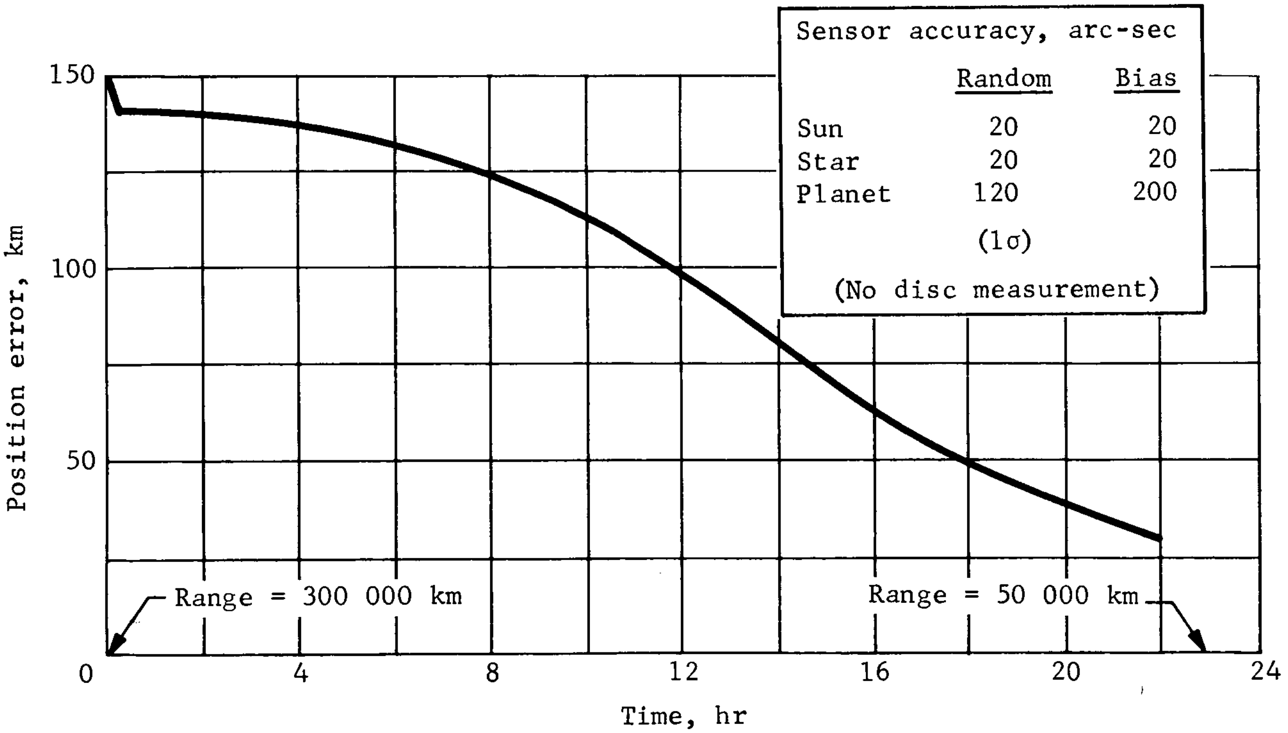

Figure 34.- Position Error (1σ) versus Time

5. TELECOMMUNICATIONS

Preferred Approach

Figure 35 is a block diagram for the point design of the telecommunications subsystems. The weights for the subsystems are 27 lb for telemetry, 11 lb for uhf communications, and 23 lb for S-band communications. During entry, the data rate of the relay link is 3 kbps, using a frequency shift key (FSK) modulated transmitter of 5 W output at 400 MHz. After the initial relay period, the power level of the transmitter is switched to 30 W and the data rate to 10 kbps to permit the return of about 5 x 10^6 bits of data during each subsequent opportunity.

Communications will continue via the relay link for two days, with daily opportunities of about 10 minutes for contact near periapsis. Assuming a change of the orbit to accomplish mapping, communications would continue via the S-band low rate data link at about 1 bps for 2 hr each day, resulting in a daily return of about 6000 bits. The direct link performance is based on a 20 W traveling wave tube amplifier (TWTA) transmitter.

Parametric Analysis

Engineering and science data to be returned to Earth from capsule separation to the point of landing will be handled by a relay link via the orbiter. There is no other reasonable communication choice during that portion of the mission. The performance requirements of this link are greatly simplified since imaging data are not required during terminal descent. Data collection rates for science and engineering are well below 1500 bps and hence, using redundant transmission of data with a time delay to retrieve blackout data, information rates are below 3000 bps.

The communication geometry during entry is limited to a maximun range to 2500 km, and under these conditions a 400 MHz uhf link with FSK modulation can handle 3 kbps of data with rf power levels of 5 W or less. The power required and the weight of the uhf equipment are relatively insensitive to data rate reductions below 3 kbps.

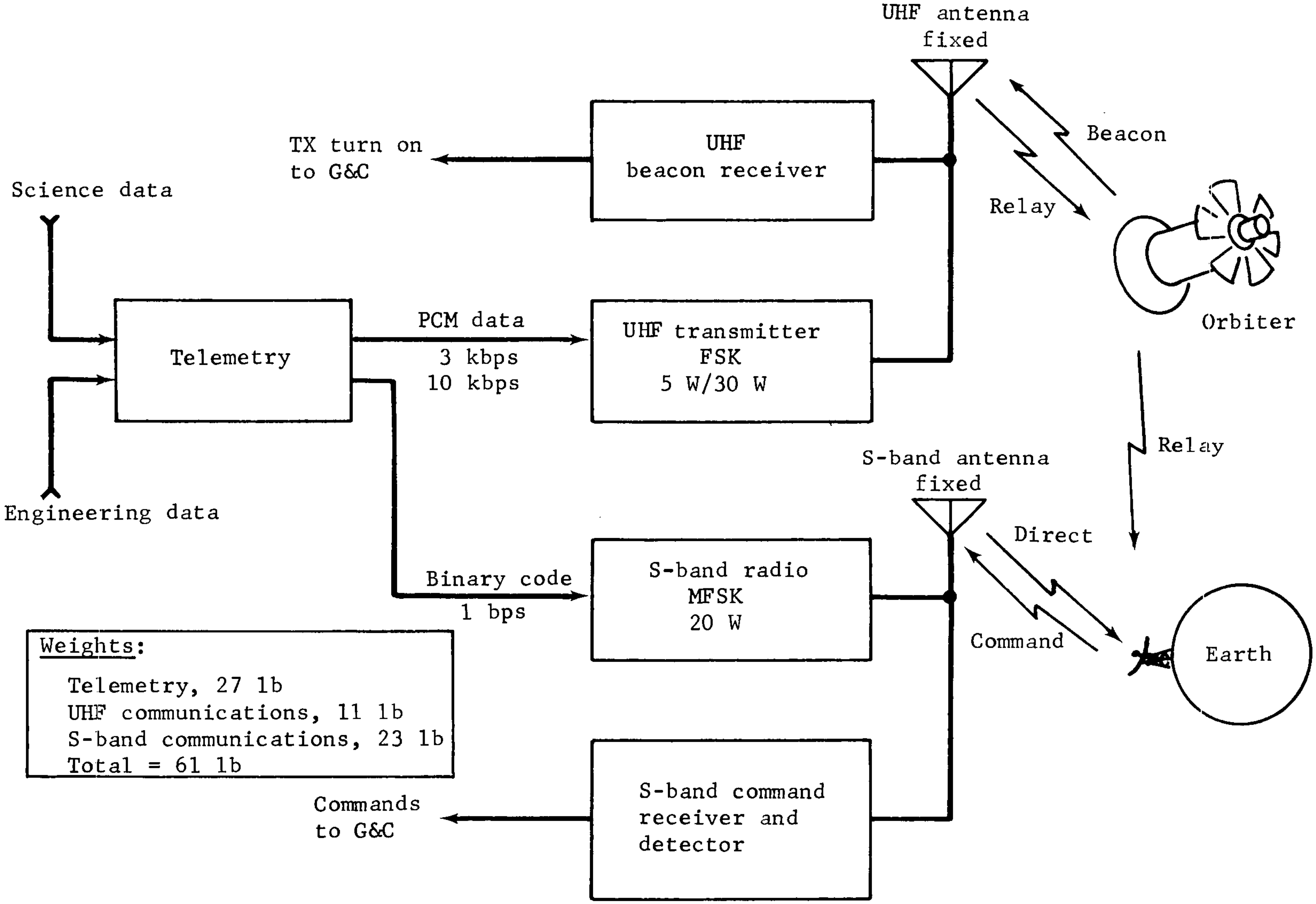
UHF antenna fixed
Beacon
Relay
Orbiter
TX turn on to G&C
UHF beacon receiver
Science data
Telemetry
PCM data
3 kbps
10 kbps
UHF transmitter FSK 5 W/30 W
Relay
S-band antenna fixed
Engineering data
Direct
Command
Binary code
1 bps
S-band radio MFSK 20 W
Earth
Weights:
Telemetry, 27 lb
UHF communications, 11 lb
S-band communications, 23 lb
Total = 61 lb
Commands to G&C
S-band command receiver and detector

Figure 35.- Telecommunications Subsystem

The entry communications are not affected by the mission mode selection because bounds on the deorbit impulse, the line-of-sight requirements, the requirement for about 10 minutes of communications immediately after landing, and multipath considerations result in essentially identical communications geometries for both mission modes.

The communication problem is that of using available weight after landing to meet the mission requirement of 10^7 bits of data return and to achieve the goal of 10^8 bits of data return.

Figure 36 shows the performance of a postland relay link parametrically, relating rf power level and data rates for various communication distances. The data shown make the conservative assumption of isotropic antenna gains at both ends of the link. Data rates in the order of 10 kbps can be obtained for lander-orbiter contacts near periapsis, where communication ranges are typically less than 2500 km and contact times at least 500 sec. Therefore, a data volume of 5×10^6 bits can be returned in a single orbiter pass. Assuming either the synchronous orbit, or the alternative orbit of 1000 by 15 000 km, a satisfactory communication contact will result at least once per day. The requirements for 10^7 bits of data can, therefore, be satisfied in two days of operation and the goal of 10^8 bits can be met in 18 subsequent contacts during the long-term mission.

Relay link communications in the neighborhood of apoapsis is also a possibility, resulting in data rates in the order of 100 bps at ranges of about 25 000 km.

Figure 37 represents typical results of the parametric studies for direct link communications from the lander to Earth, based on the projected DSIF capability of 210-ft antennas.

Two types of modulation are shown, coded coherent PCM/PSK/PM and noncoherent MFSK. Ranges shown are those associated with the last arrival date, 2.6×10^8 km, and the maximum range during the mission of 3.96×10^8 km. The coherent link requires the use of a high-gain articulated antenna for reasonable transmitter power levels. The weight limitations associated with the 1973 mission, as well as the complexities of antenna pointing and steering, led us away from selecting this system. Use of a fixed broad-beam antenna and a transmitter power output of about 20 W results in data rates in the order of 1 to 2 bps with a noncoherent MFSK link. The use of such a link is recommended for long-term surface operations to serve as a means for the return of weather data independent of the presence of the orbiter.

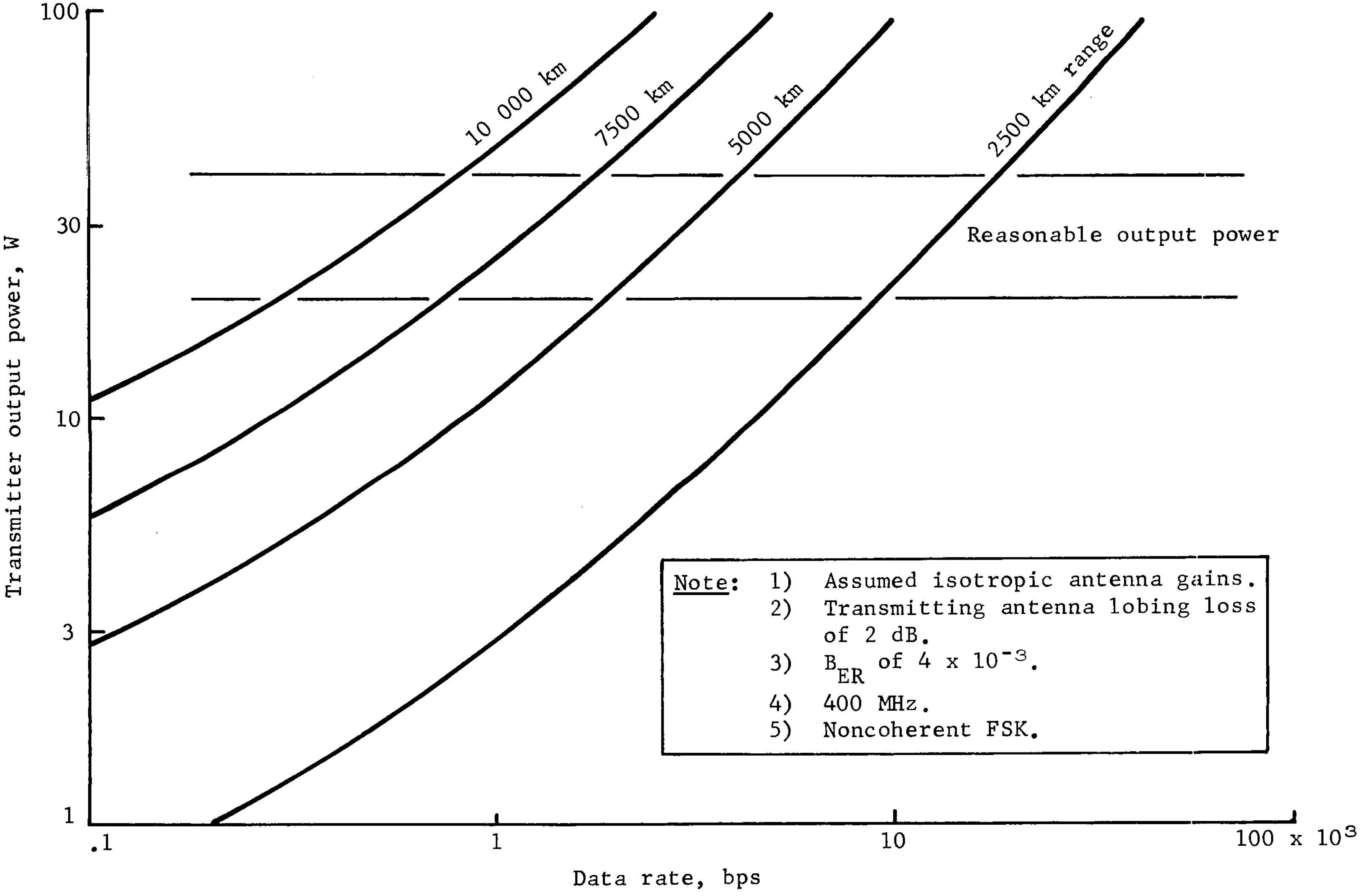

Figure 36.- Postland Relay Link Performance

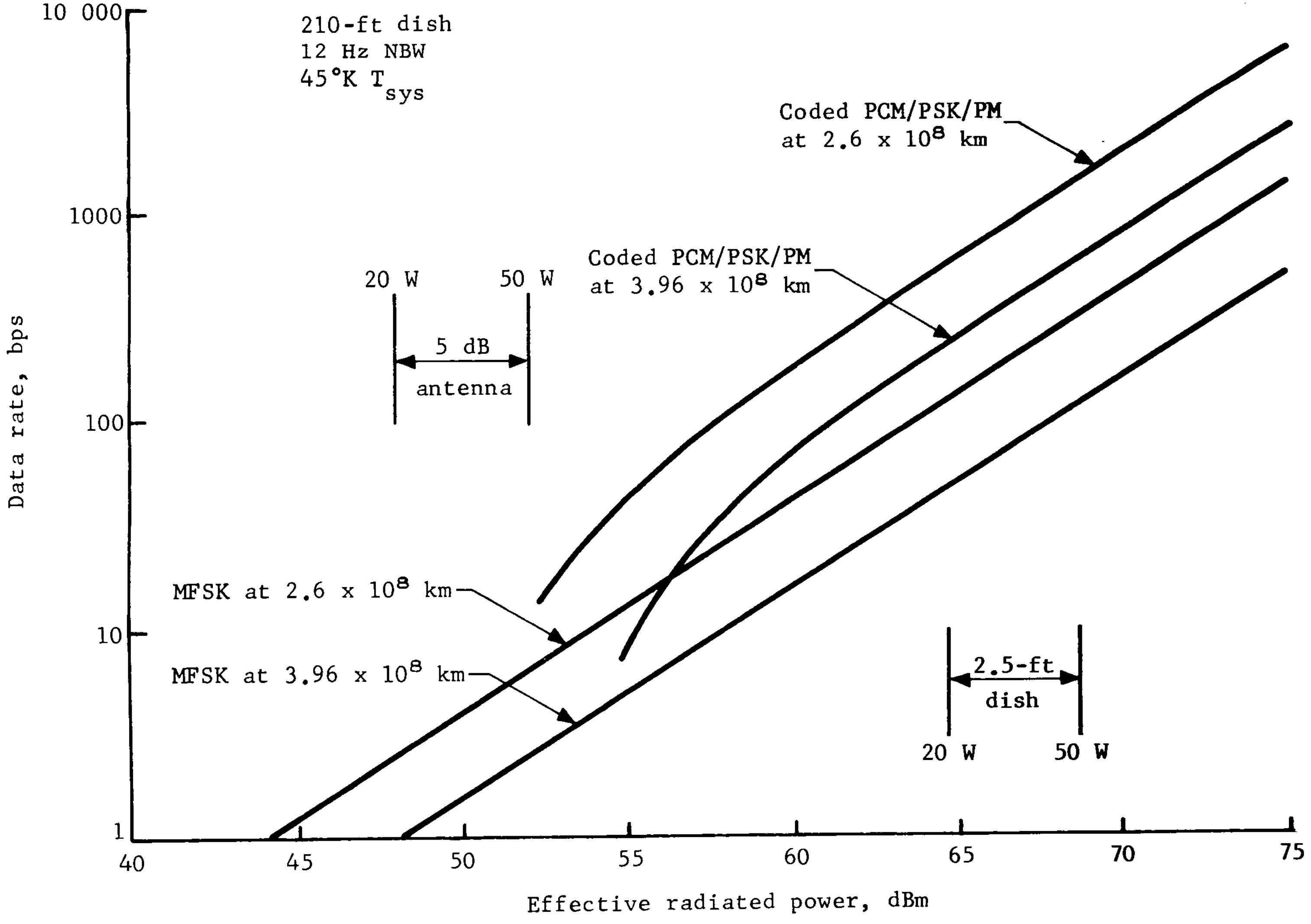

Figure 37.- Direct Link Performance

This downlink is required in any case to aid in the acquisition and lockup of the direct command link. We feel that this is a better technique than using unproven onboard automatic techniques for command lockup or depending on the delayed return of command receiver performance data via the relay link.

Conclusions

The significant telecommunications subsystem conclusions are:

1) The telecommunication subsystem configuration is unaffected by the choice of mission mode;
2) A relay link provides adequate performance from separation to landing and allows return of initial imaging data before onset of the first night;
3) Primary postlanding communications are accomplished by continued use of the relay link to meet the total data return requirements of 10^7 bits within two days.
4) Postland communications can be accomplished independent of the orbiter by a low data rate MFSK link, returning adequate science data for the rest of the mission;
5) Communication via the relay link during satisfactory opportunities can achieve the goal of 10^8 bits in 20 contacts.
6) There are no long lead developments in telecommunications.

6. POWER SUBSYSTEM

Preferred Approach

The preferred design is based on the use of a solar array for long-term surface operations. A usable area of 40 sq ft is available in a configuration consisting of body-mounted cells on a central horizontal panel, and four side panels which are deployed after landing. If the landing site is in near-equatorial northern latitudes, good system margin is available to live through cloudy days. Single drive adjustability of each side panel via command control increases the power output of the array under adverse latitude and slope conditions.

The array is supplemented by a 17 A-h Ni-Cd battery for post-land operations. A 78 A-h Ag-Zn battery is used for entry and for assured operations during the first two days. The potential exists for eliminating one type of battery and the associated development work by either going to Ni-Cd only at a weight penalty of about 173 lb or by using Ag-Zn only, assuming that the development work on secondary sterilizable Ag-Zn batteries has demonstrated adequate cycle life. **The power subsystem design is based on the load profile shown in Figures 86 and 87 of Volume II, which includes only transmission of data direct to earth during extended life.**

Parametric Analysis

Several configurations, differing in the choice of power sources, were studied. Our studies included an all-battery configuration, an RTG/battery configuration, and two solar array/battery configurations. For each configuration, data were developed parametrically, giving weight and performance to meet a broad range of power profiles. Ag-Zn batteries alone can provide the required energy for entry and for a short landed mission of several days. For a mission life of weeks to months as specified, a constant power source is required, with Ni-Cd or Ag-Zn batteries used to supplement that source for peak loads, and for dark-period operation in the case of solar arrays.

Figure 38 shows the energy densities of sterilizable Ag-Zn and Ni-Cd batteries on which the sizing of the power system is based. These data, which represent current predictions for complete batteries, lead to the conclusion that a Ag-Zn battery should be used during entry and for the first two days of landed operation to assure the return of at least 10^7 bits of data at minimum power source weight.

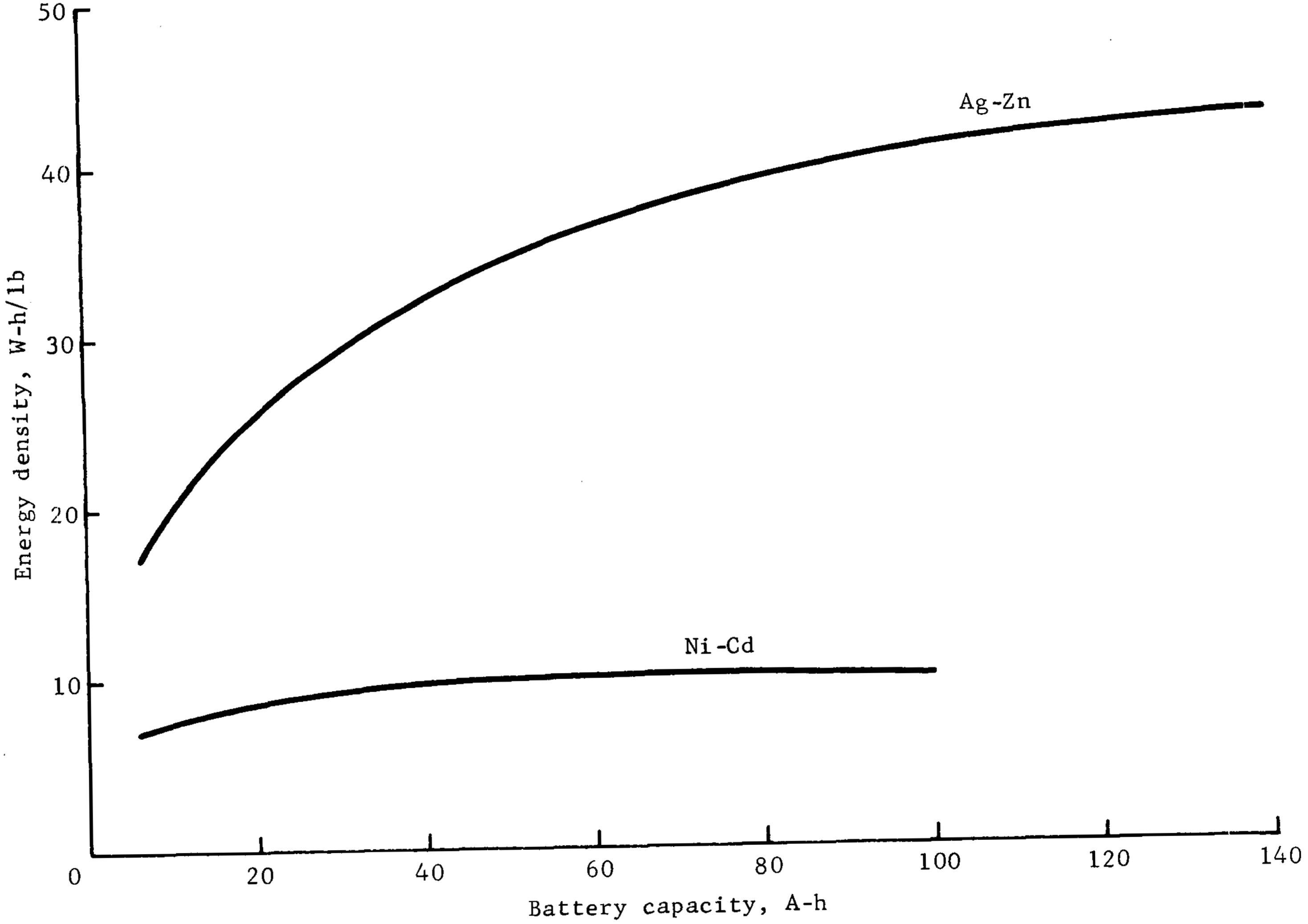

Figure 38.- Energy Densities of Sterilizable Batteries

For long-term operations, the Ni-Cd battery should be used to supplement an RTG or solar array because of its proved high cycle life.

For long life, the choice is between the RTG and the solar array. From a purely technical point of view, the RTG is a good solution to the long-life power problem. It is not only lower in weight, as shown in figure 39 and table 7, but also provides waste heat for thermal control and is insensitive to the Martian environment. The solar array, on the other hand, is sensitive to the unknowns of cloud cover, dust, and abrasive winds.

However, a solar array is recommended in out point design based on the following factors: (1) the power source development, qualification, and hardware costs are lower ($1 to 2 million) than that of a newly designed RTG ($30 to 40 million) as shown in Section 8 of Appendix D; and (2) the solar array weight is acceptable within the constraints of the landed configuration.

Considerably fewer development problems could be expected for the solar array compared to the RTG. Those problems are limited essentially to compatibility of adhesives with decontamination processes and to the development of an antidust coating.

The parametric studies for the solar array resulted in the development of specific energy data as shown in figure 40. The data are for two solar array configurations, a group of horizontal fixed panels, and another configuration consisting of a body-mounted horizontal panel and four adjustable side panels. The latter configuration was chosen for our point design, with an adjustment made through command control after deployment to orient the panels in a optimum manner relative to the ephemeris of the sun. Based on 40 sq ft of useful solar array area and 20° landing latitude, the weather station postland mission requires from 15 to 18 W-h/ft^2/day. The data emphasizes two points:

1) Adjusting the side panels for optimum power improves the energy available from the array by as much as 45% for the case of landing at 20° S latitude with 17° adverse slope;
2) Landing at northern latitudes provides a larger solar array output for the 1973 mission and provides a margin to accommodate clouds.

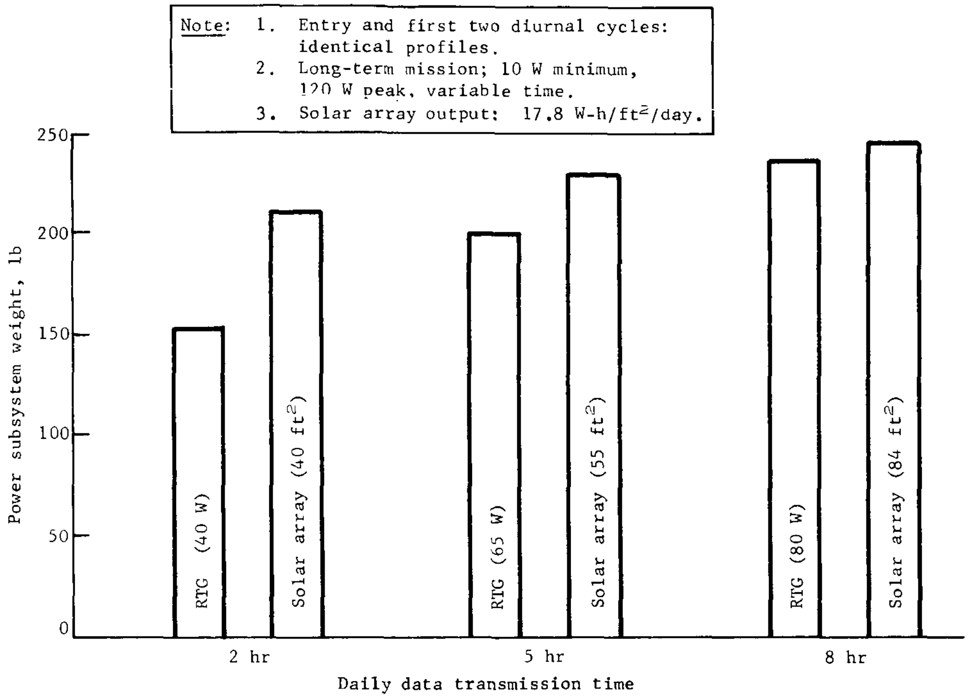

Note: 1. Entry and first two diurnal cycles: identical profiles.
2. Long-term mission; 10 W minimum, 120 W peak, variable time.
3. Solar array output: 17.8 W-h/ft²/day.

Figure 39.- Weight Comparison of RTG and Solar Array Power Subsystems

Table 7.- Comparison of RTG and Solar Array Power Subsystem Characteristics

	Daily transmission time					
	2 hr		5 hr		8 hr	
	RTG	Solar Array[b]	RTG	Solar Array[b]	RTG	Solar Array[b]
Source Power, W Density Weight, lb	 40 .86 W/lb 46.5	 81 avg 1 lb/ft² 48[a]	 65 .86 W/lb 75.5	 113 avg 1 lb/ft² 63[a]	 80 .86 W/lb 93	 170 avg 1 lb/ft² 88[a]
Ag-Zn battery Capacity, A-h Weight, lb	 10 15	 76 60	 0 0	 76 60	 0 0	 76 60
Ni-Cd battery Capacity, A-h Weight, lb	 12 48	 17 62	 23 78	 17 62	 29 94	 11 44
Converter regulator Maximum Power, W Weight, lb	 40 3.5	 160 7	 65 4	 160 7	 80 4.5	 160 7
Battery charger, lb	5	5	3	5	3	5
Other, lb	39	39	39	39	39	39
Total, lb	157	221	199.5	236	233.5	243

[a] **Includes 12 lb of panel actuator**

[b] **Thermal Control uses isotope heaters (weight not included in this tabulation).**

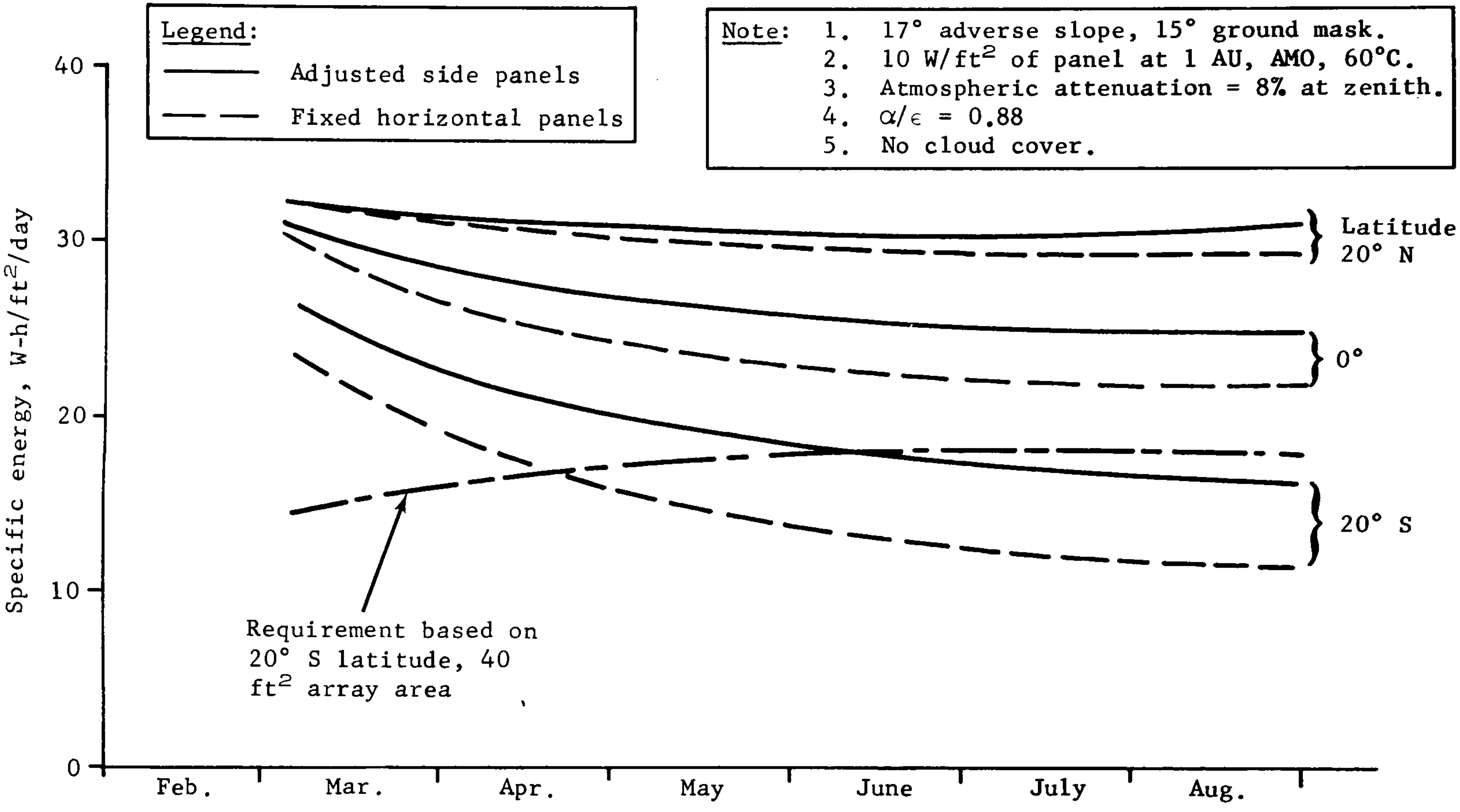

Figure 40.- Solar Array Performance Data

Conclusions

The power subsystem conclusions are:

1) The power subsystem configuration is unaffected by the choice of mission mode (for constant separation to entry time);
2) The solar array is the best program approach to achieving surface operational life beyond 2 days for the 1973 mission;
3) Use of a Ag-Zn battery for entry and for the first two days after landing, and a Ni-Cd battery for extended life provides the lightest power subsystem for the 1973 capsule (unless a secondary sterilizable Ag-Zn battery is developed);
4) Long-lead items for 1973 are the development of a sterilizable Ag-Zn battery, the development of solar cell adhesives meeting decontamination requirements, and the development of an antidust coating for the solar panels.

7. THERMAL CONTROL SUBSYSTEM

Preferred Approach

The preferred approach to cruise mode thermal control consists of multilayer insulation on the outside of the sterilization canister and thermostatically controlled heaters powered from the orbiter solar cells. The key element in the design is the multilayer insulation. The weight and performance of the insulation was confirmed by full-scale cruise-mode tests conducted by Martin Marietta. These tests which showed that a heat leak as low as 0.40 Btu/hr-ft^2 (at 55°F) can be achieved by an insulation design which weighs 0.078 lb/ft^2. These data are in close agreement with the insulation tests conducted later by General Electric under contract to JPL.

The preferred descent mode thermal control is passive and uses multilayer insulation, dense insulators, and coatings distributed on descrete elements of the system.

The preferred approach to Mars surface thermal control is shown in figure 41; it incorporates radioisotope heaters, 3 in. of surface insulation, and phase change material on the S-band transmitter. Radiosotope heaters (200 W) were chosen because they do not require consumables and allow the choice of extreme design environments at a reasonable weight. In addition, the radioisotope heater system is significantly lighter than competing designs. The lander internal temperature is controlled by driving the isotopes in and out of the lander using thermostatically controlled actuators. The preferred system will maintain all surface laboratory equipment within temperature limits for the hot and cold extreme environments; the results of a detailed performance evaluation are given in figure 41.

Parametric Analysis

Table 8 shows the thermal parameters and ranges investigated in the parametric evaluation.

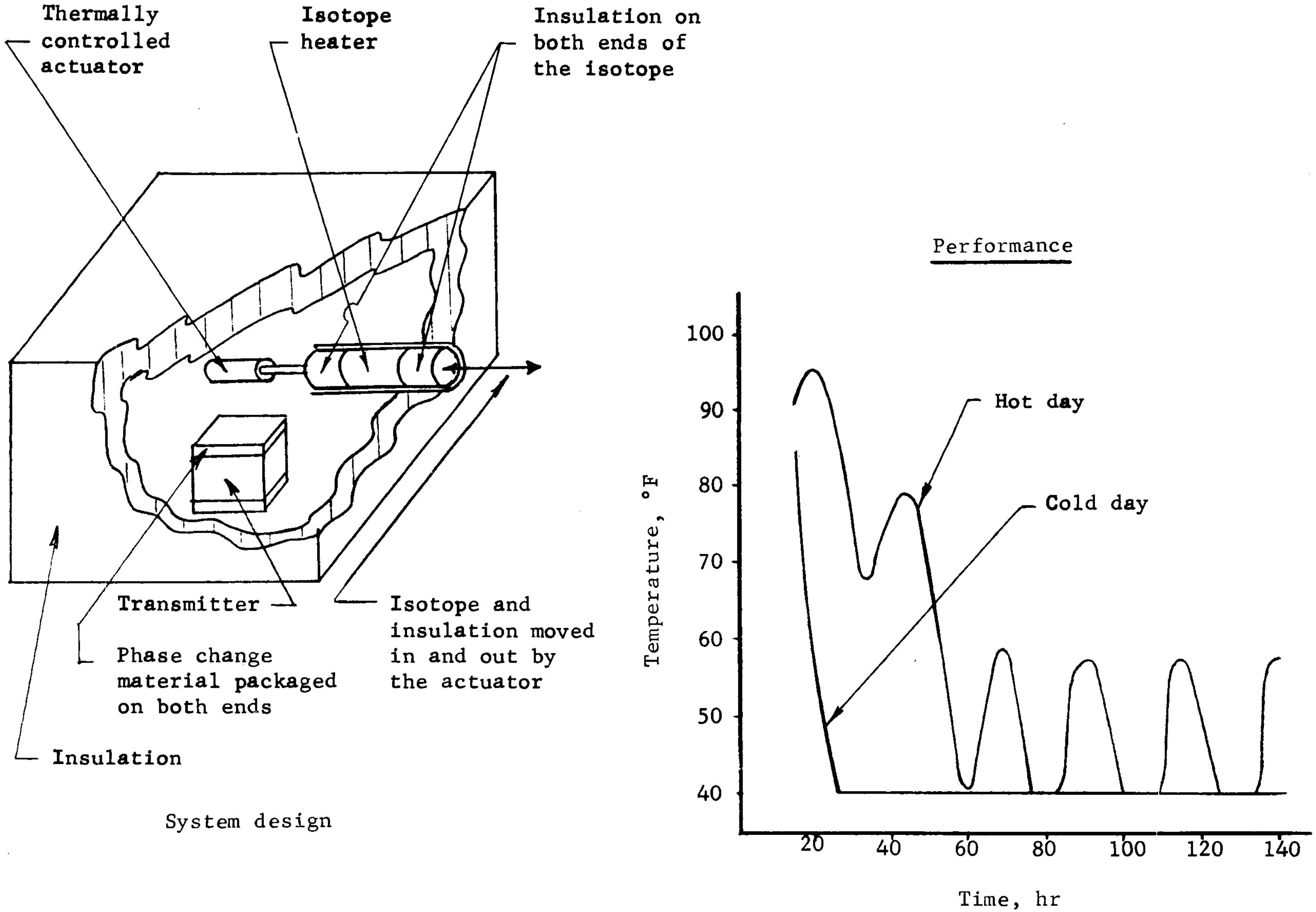
Thermally controlled actuator
Isotope heater
Insulation on both ends of the isotope
Transmitter
Phase change material packaged on both ends
Isotope and insulation moved in and out by the actuator
Insulation
Temperature, °F
100
90
80
70
60
50
40
20
40
60
80
100
120
140
Time, hr
Hot day
Cold day

System design

Performance

Figure 41.- Preferred Mars Surface Thermal Design

TABLE 8.- SCOPE OF PARAMETRIC THERMAL CONTROL STUDY

Parameter	Range
Life	2 days to years
Size, cu ft	10 to 100
Environment	Cold to hot extreme
Insulation performance	
Conductivity, Btu/hr-ft-°R	.007 to .025
Density, lb/cu ft	.5 to 4
Thermal energy sources	Function of size and type
Batteries	
Chemical	
Radioisotope	
Solar collector	
Capillary pumped RTG loop	
Energy storage	
Energy rejection	
Power duty cycle	
Penetration losses	

One of the most significant aspects of the parametric evaluation was the treatment of the Mars surface environment as a parameter. The multiple variables that make up the Mars surface environment (e.g., wind velocity, atmospheric temperature, solar flux at the surface, surface temperature) were grouped into four environments of varying severity. The surface temperatures resuting from these four environments are shown in figure 42 along with the most significant thermal parameters used. The parametric phase results, therefore, show the effect of environmental criteria on system design. In general, the weights of systems that use low specific energy sources for heat (e.g., battery-powered landers) are very sensitive to the severity of the environmental criteria chosen. This weight sensitivity increased directly with lifetime. High specific energy systems (e.g., radioisotope systems) may be designed for very severe, and hence conservative environments with little weight penalty.

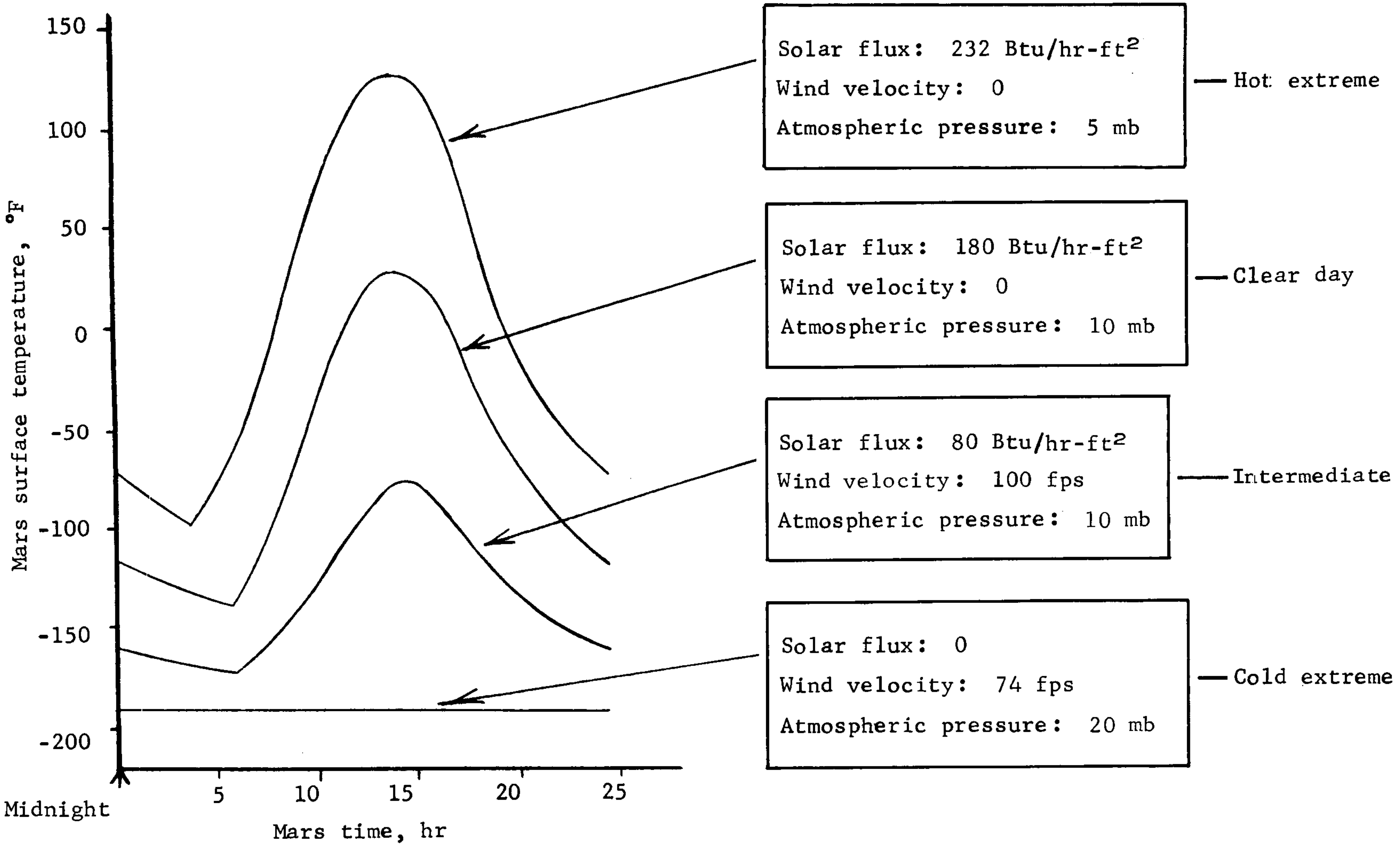

Figure 42.- Environmental Models

Another significant result of the parametric phase is the evaluation of the importance of Mars surface insulation performance on system weight. In low specific energy designs the insulation performance can be a stronger influence on system weight than the surface environmental criteria chosen. A particular Mars surface insulation system, consisting of low density fiberglas mounted between radiation shields, was analyzed. This analysis, figure 43, shows that the insulation conductivity strongly depends on the atmospheric constituents assumed. Figure 44 shows that an insulation conductivity in the range of 0.007 to 0.025 Btu/hr-ft-°F is reasonable. This result is significant because little or no test data exist on insulations at Mars surface conditions.

The energy source chosen has a strong influence on thermal system weight, as shown in figure 44. For lifetimes beyond about 30 days and for the cold extreme environment there is no reasonable alternative to radioisotope heaters.

Conclusions

The thermal control subsystem conclusions are:

1) The mission mode choice has essentially no effect on the thermal system;
2) Isotope heaters are the recommended heat sources because competing sources use consumables and the high specific energy of isotopes provides environmental insensitivity and low system weight;
3) Cold and hot extreme environments are recommended for design. The weight gains afforded by less conservative environmental models are not large;
4) Insulation performance is a strong function of the atmospheric gas assumed ;
5) The isotope heaters are long lead items.

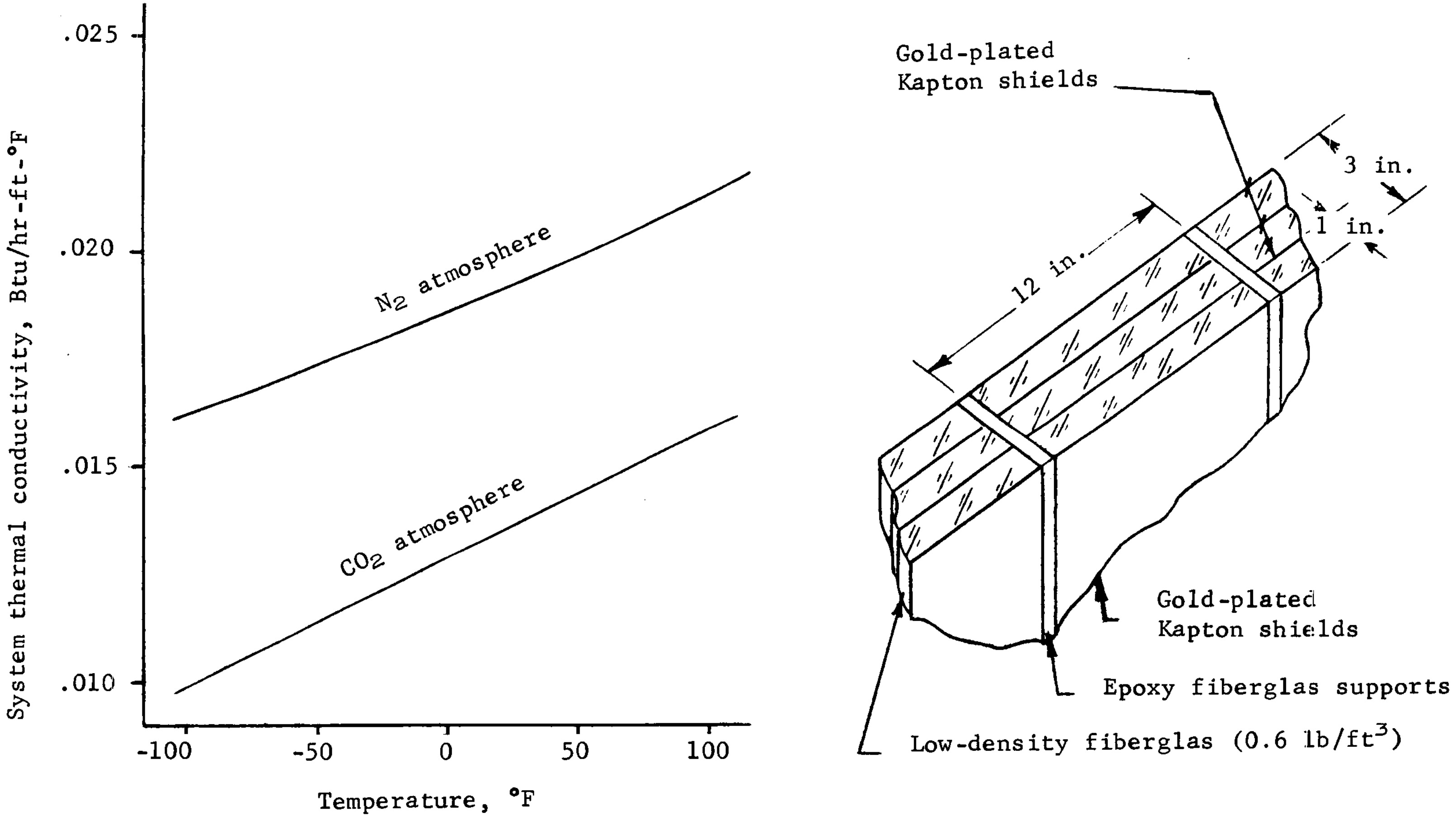

Insulation system

Figure 43.- Insulation System Conductivity

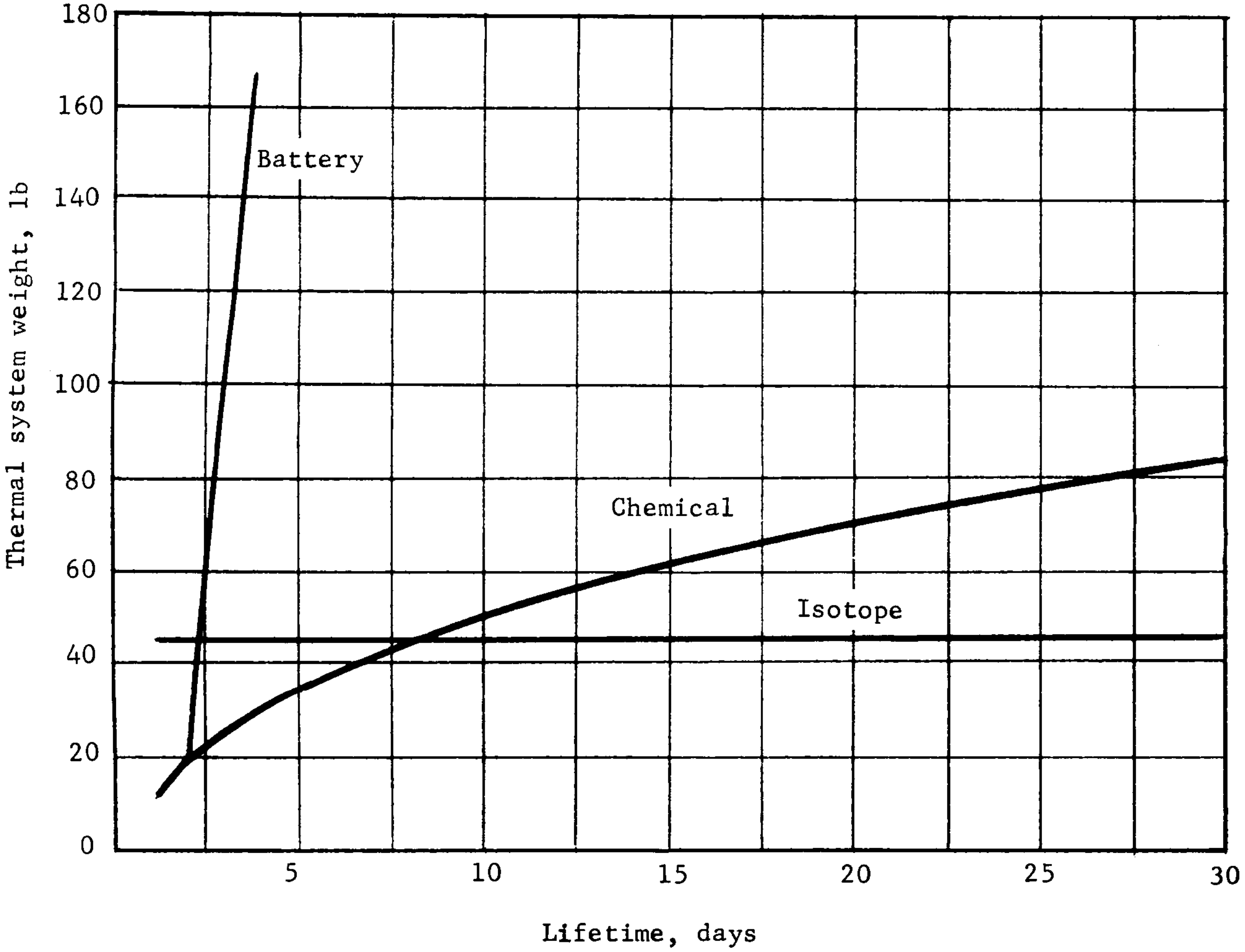

Assumptions:

1. Cold extreme environment.
2. Insulation conductivity, 0.0168 Btu/hr-ft-°F.
3. Area, 38.5 ft^2.

Figure 44.- Energy Sources

CONCLUSIONS

There are no primary flight capsule concept differences resulting from the selection of mission mode. Both the direct and out-of-orbit modes are equally feasible, although the direct mode entry environments are slightly more severe. The main differences between the modes are concentrated in the flexibility and confidence in mission operations. The specific conclusions are tabulated below and on the following page.

Out-of-orbit mode recommended.

Of the point designs studied, Configuration 1B $\left(10.5\text{-ft aeroshell, } B_E = 0.35\right)$ is recommended.

Titan IIIC/Centaur launch vehicle required for either mission mode when orbiter science capability is desired.

Bulbous shroud required for direct mode, and probably required for out-of-orbit mode when using a Mach 2 parachute, VM atmopshere, 6000-ft terrain height, and 10% margins.

Targeting capability is the same in either mission mode when considering only flight profile constraints. However, superimposing any time or orientation constraints decreases the direct mode landing site selection flexibility.

Accuracy of atmosphere structure determination not significantly different between mission modes.

Science, propulsion, telecommunications, power and pyrotechnics, and thermal control (autonomous capsule excepted) subsystems are not affected by mission mode choice.

All subsystem components are either present state-of-the-art technology or can be developed for the 1973 launch opportunity.

Terminal descent and landing radar (TDLR), altitude measuring radar (AMR) antenna, inertial measurement unit (IMU), engines, isotope heaters, sterilizable batteries, sterilizable solar cell adhesives, aerodecelerators, and certain science components are long lead efforts which must start in Phase C.

Out-of-orbit mode	Direct mode
More in-flight mission flexibility Site survey before separation	Can use Mariner Mars '71 orbiter, but at sacrifice of targeting and orbital science objectives
Choose for science objectives Avoid poor capsule surface environment or adverse weather patterns	Slightly larger launch vehicle performance margin More extensive development required
Targeting can be to different site after launch	Higher entry environment More severe base heating
Checkout with time for malfunction correction	Increased aerodynamic sensitivities to tolerances and misalignments
Second lander can benefit from first lander's data return	Larger aeroshell and canister
Can fit within 10-ft shroud; use of a Mach 2 parachute allows for no margins. To provide margins, an 11.5-ft shroud is required	More comprehensive aerothermodynamic test program
Can fit within 10-ft shroud and provide margins by using a Mach 5 ballute	Additional and more sophisticated equipment on orbiter for approach guidance
Requires additional orbit insertion propulsion added to Mariner Mars '71 orbiter	
Requires successful orbit insertion maneuver for successful capsule mission	

Several areas have been identified that appear to merit further investigation as a result of this study effort. Primary among these is a detailed study of the integration with a Titan IIIC/Centaur shroud. Straightforward integration concepts limit the aeroshell diameter to 8.5 ft. With this constraint, there is neither margin nor growth capability, and several packaging problems exist. Preliminary investigation indicates that the allowable diameter must be increased to the order of 9.5 ft, but further analysis is necessary to confirm this and to determine whether this increase in aeroshell diameter can be accommodated in the 10-ft diameter Titan III shroud.

Two other areas relevant to the desire to use a standard 10-ft diameter shroud are:

1) Integration and packaging of potential life-detection experiments;
2) The possibility of statistically combining selected environmental parameters for obtaining design requirements.

The first is needed to identify potential requirements for deployment and separation/isolation considerations between isotope sources and sensitive detection equipment. A statistical combination of environments, as opposed to stacking worst cases, may allow a considerable reduction in the required aeroshell diameter.

Martin Marietta Corporation
Denver, Colorado, August 20, 1968

NASA CR-66659 thru 66664

National Aeronautics and Space Administration
FINAL REPORT, STUDY OF DIRECT VERSUS ORBITAL ENTRY FOR MARS MISSIONS. Raymond S. Wiltshire, Hugh E. Craig, et al. August 1968

(NASA CONTRACTOR REPORT NASA CR-66659 thru 66664)

This is the final report of the work accomplished by Martin Marietta Corporation for the Langley Research Center under Contract NAS1-7976, Study of Direct Versus Orbital Entry for Mars Mission. This effort was conducted from March 26 thru July 1, 1968. The study objectives were (1) to obtain the net science payload for the direct entry mode, and (2) to evaluate the direct and out-of-orbit entry modes for soft landing capsules. The three main tasks defined to fulfill these objectives were (1) conduct mission and subsystem parametric analyses, (2) establish mission design for each capsule mode; and (3) provide conceptual design for three capsule systems.

I. Wiltshire, Raymond S.; Craig, Hugh E.; et al.

II. NASA CR-66659 thru 66664

NASA

NASA CR-66659 thru 66664

National Aeronautics and Space Administration
FINAL REPORT, STUDY OF DIRECT VERSUS ORBITAL ENTRY FOR MARS MISSIONS. Raymond S. Wiltshire, Hugh E. Craig, et al. August 1968

(NASA CONTRACTOR REPORT NASA CR-66659 thru 66664)

This is the final report of the work accomplished by Martin Marietta Corporation for the Langley Research Center under Contract NAS1-7976, Study of Direct Versus Orbital Entry for Mars Mission. This effort was conducted from March 26 thru July 1, 1968. The study objectives were (1) to obtain the net science payload for the direct entry mode, and (2) to evaluate the direct and out-of-orbit entry modes for soft landing capsules. The three main tasks defined to fulfill these objectives were (1) conduct mission and subsystem parametric analyses, (2) establish mission design for each capsule mode; and (3) provide conceptual design for three capsule systems.

I. Wiltshire, Raymond S.; Craig, Hugh E.; et al.

II. NASA CR-66659 thru 66664

NASA

NASA

This final report is presented in the following six volumes:

NASA CR-66659 - Volume I - Summary:
NASA CR-66660 - Volume II - Parametric Studies, Final Analyses, and Conceptual Designs;
NASA CR-66661 - Volume III - Appendix A - Launch Vehicle Performance and Flight Mechanics;
NASA CR-66662 - Volume IV - Appendix B - Entry and Terminal Phase Performance Analysis;
NASA CR-66663 - Volume V - Appendix C - Entry Configuration Analysis;
NASA CR-66664 - Volume VI - Appendix D - Subsystem Studies and Parametric Data.

NASA

This final report is presented in the following six volumes:

NASA CR-66659 - Volume I - Summary;
NASA CR-66660 - Volume II - Parametric Studies, Final Analyses, and Conceptual Designs;
NASA CR-66661 - Volume III - Appendix A - Launch Vehicle Performance and Flight Mechanics;
NASA CR-66662 - Volume IV - Appendix B - Entry and Terminal Phase Performance Analysis;
NASA CR-66663 - Volume V - Appendix C - Entry Configuration Analysis;
NASA CR-66664 - Volume VI - Appendix D - Subsystem Studies and Parametric Data.